Department of Precision and Microsystems Engineering

The design of a monolithic, compliant, resonant running robot at insect scale

J. K. Schonebaum

Report no : 2019.018
Coaches : Dr.ir. F. Alijani and Dr.ir. G. Radaelli
Professor : Dr.ir. F. Alijani
Specialisation : Engineering Dynamics
Type of report : Master of Science Thesis
Date : 19 July 2019

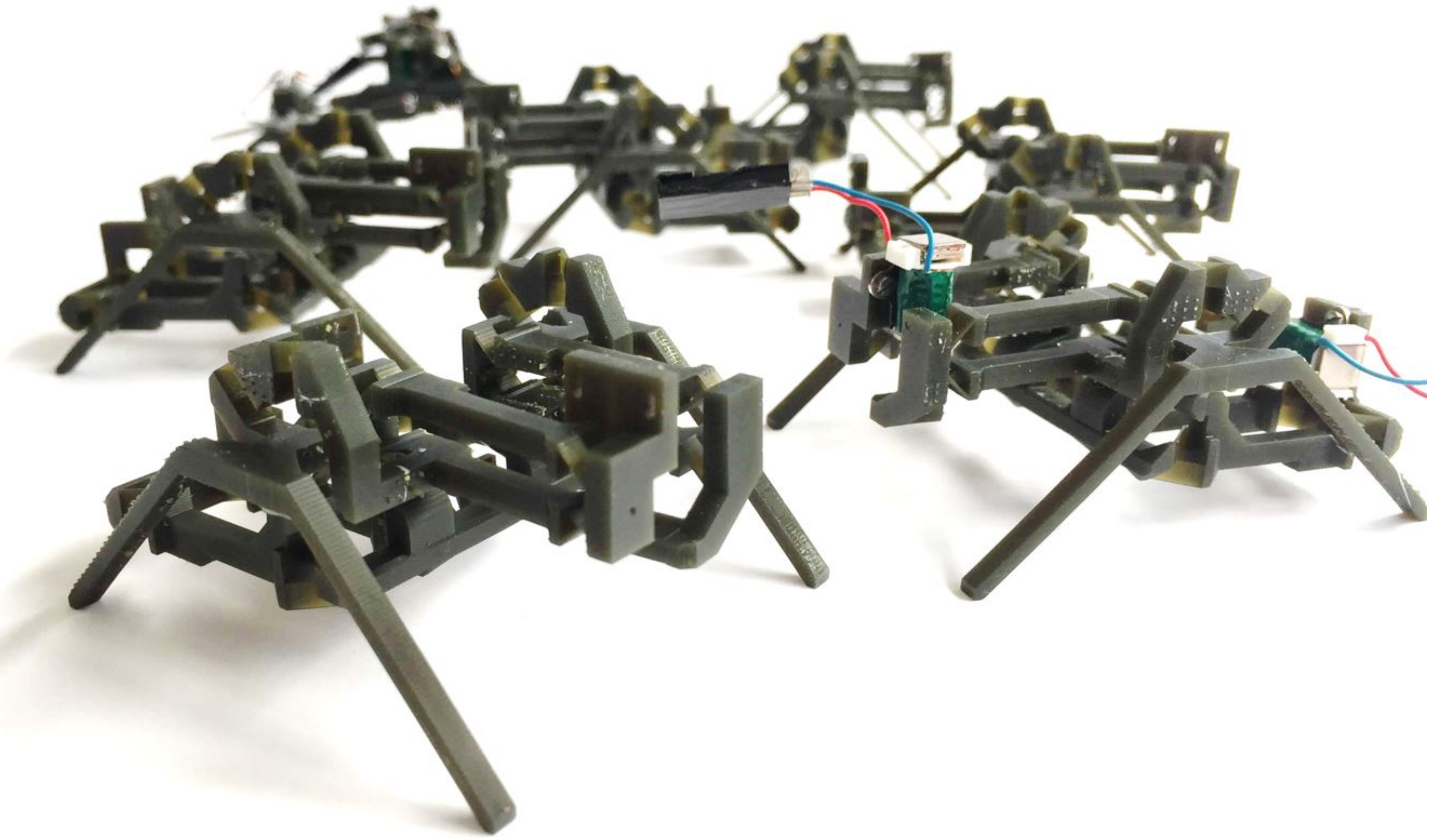

Delft University of Technology

Challenge the future

The design of a monolithic, compliant, resonant running robot at insect scale

MASTER OF SCIENCE THESIS

by

J. K. Schonebaum

to obtain the degree of Master of Science
in Mechanical Engineering
at Delft University of Technology,
to be defended publicly on Friday July 19, 2019 at 12:15

Student number:	4166302	
Thesis committee:	Dr.ir. F. Alijani	Chair and supervisor
	Dr.ir. G. Radaelli	Supervisor
	Prof.dr. P.G. Steeneken	
	Dr.ir. J.F.L. Goosen	
	Dr.ir. M.A. Bessa	External committee member

Faculty of Mechanical, Maritime and Materials Engineering (3mE) · Delft University of Technology

Copyright © Department of Precision and Microsystems Engineering (PME)
All rights reserved.

Table of Contents

Preface iii

Acknowledgements v

1 Introduction 1
1-1 Initial idea of project 1
1-2 Goal of literature review 2
1-3 Goal of design phase 2
1-4 Overview of report 2

2 Literature Paper 5

3 Technical Paper 23

A Supplementary material literature paper 41
A-1 Overview table of subclasses and NV-options 41

B Supplementary material technical paper 43
B-1 Details on parametric model 43
B-2 Time response plots of dynamical experiments 45
B-3 Choice of actuation 45
B-4 Optimization 46
B-5 Phase dependency 46
B-6 Primary 5DOF parametric model 47

C MATLAB scripts 49

D Kinematic designs considered for step two 53

E Experiments with monolithic printing 55

Preface

Green light with champagne

This report presents the work that I have done for my thesis project during the last 10.5 months. I feel tremendously lucky with the project that I have carried out. During my master's courses at the PME department I became fascinated by eigenfrequencies and resonance. I really find the phenomenon of resonance something magical, as only a change in frequency can make something move much more vigorously. Beside resonance, I am highly interested in optimization. That is, because with relatively simple mathematical algorithms we can optimize almost anything as long as we can mathematically describe a problem. Thirdly, ever since I was young I really enjoy building things. Luckily enough, I found a project in which all three aspects were very prominently present.

In this great project, I was supervised by two men who supported me throughout the whole year by giving me guidance, showing enthusiasm and having a critical view on my work. After every meeting with these gentlemen I was full of new ideas and had clear view on what to do next. They both extensively commented on my written work and were almost always available for discussions and intermediate questions. It was not only serious conversation with these men, there was also room for laughter and joy during the meetings. For all of this, I am sincerely grateful.

At the day of my green light meeting, Farbod was announced teacher of the year of our entire faculty. Very well deserved! Because of this, I was served champagne at the start of my green light meeting by professor Peter Steeneken. This felt like a final climax of all luck and joy I received last year.

Enjoy reading!

Delft, University of Technology J. K. Schonebaum
July 15, 2019

Acknowledgements

First of all I want to thank my supervisors Farbod and Giuseppe. Without you, I would absolutely not have enjoyed my project as much as I have.

I want to thank Farbod for his unstoppable enthusiasm and for giving me space to define my own project since our very first meeting. Also, I should thank him for borrowing his name for the robot I made, FARbot.

I'd like to thank Giuseppe for his careful and critical, yet positive view on my work and his patience during our meetings. Also, for the great support he gave me during the prototyping phase and the joy he brought me when he visited me with his children.

Also, I'd like to thank the men of PME lab support Rob, Patrick, Gideon and Bradley, whom have all helped me with prototyping at different phases of my project. I am really amazed by the skills of these guys.

Then, a word of gratitude for Peter, Hans and Miguel for taking the time to be part of my exam committee and giving me some extra time to finish my thesis.

I want to thank Hans, Davood, Hassan, Qi and Pierpaolo for the meetings I had with them.

Furthermore, I'd like to thank Boris, Gerben and my Mum for reviewing my final report.

I also want to thank my friends in the graduation office for the support and good times like 'Cookie Thursdays', my colleagues at Flying Fish for giving me all the space I needed and my house mates for the fine home they offered.

Lastly, a huge thank-you to my parents and my three big brothers for supporting me during the whole project.

Delft, University of Technology J. K. Schonebaum
July 15, 2019

Chapter 1

Introduction

The intention of this chapter is to introduce the reader to the subject of this thesis, and to explain what the relation is between the two papers in Chapters 2 and 3 that are the core of this thesis report. An overview of the project is given, which begins with the initial idea and continues with how the project evolved.

1-1 Initial idea of project

Many structures, machines and robots are designed to avoid resonance as much as possible. That is, because resonance introduces amplified motion to systems which often is undesired and can even be catastrophic. A famous example is the Tacoma Narrows Bridge which was put into resonance by the wind and collapsed due to the huge amplitude vibrations this caused. Although this was a very unfortunate event, it also showed the great power a resonant motion can contain, and that with only a simple actuation source, i.e. the wind. These properties of resonance are the basis for the idea behind this thesis, which is to design a mobile robot that is intended to use its resonance for locomotion.

The expected advantages of using resonance for a mobile robot are twofold, namely improved efficiency which corresponds to the powerful motion of the Tacoma Narrows Bridge, and simplified actuation which is in parallel with the fact that wind could bring the bridge into resonance.

The reason that a system is more efficient (or has a more powerful output) at resonance is that the inertial and the potential forces cancel each other out. Therefore, the cost of accelerating and decelerating the body parts is reduced to a minimum.

The explanation that the necessary actuation can be simplified with a resonant design is that the motion that a body exhibits at resonance is invariable. It depends on the mass distribution and stiffness of the body and is described with the eigenmodes, which are indeed constant. This means that for any energy source that supplies its power at the eigenfrequency and not perpendicular to the direction of the eigenmode, the robot will exhibit the same motion. This gives opportunities for simplification and miniaturization of actuation, and even for external untethered energy supply like sound.

The initial idea of this thesis was to design and build a mobile robot that resonates with a desired mode and at a desired eigenfrequency. With this robot we could investigate the feasibility of the expected advantages. For this, we first had to investigate (i) the current state of the art of robots that use resonance, (ii) if the expected advantages would be feasible, (iii) which type of robot would be most suitable to perform the idea on and (iv) how to implement resonance. These questions were answered during the literature study.

1-2 Goal of literature review

The purpose of the literature study is (i) to make an overview of existing mobile robots that exploit resonance, (ii) to examine the benefits that introduces, and (iii) to investigate which options exist to make use of resonance. As there exist countless mobile robots, a systematic approach to accomplish this is necessary. To this end, we introduce a novel categorization based on locomotion principles, i.e. how does the robot obtain locomotion. In this classification we only consider locomotion mechanisms that use contact with the ground for propulsion. We divide the robots such, that if a robot within a subclass exploits resonance, all other robots within the same subclass should (theoretically) be able to use it likewise.

Based on the literature study, it was chosen to design a running robot at insect scale that uses full body resonance. This is novel in the research field of meso scaled running robots. Besides, various prior papers recommend the use of resonance for improved efficiency, which proves the feasibility of the idea for this type of robot. Another reason to continue with these robots is that there is an upcoming interest in them. Therefore, an improvement can have significant impact. These statements are elaborately discuss in the technical paper in Chapter 3.

1-3 Goal of design phase

After the decision to design an insect scale running robot, further literature study was conducted on this research field. The main challenges of this type of robot were found to be efficiency, actuation and production. The first two are addressed with the use of resonance. For the third challenge we propose to make a design that can be 3D printed from one material in one piece, i.e. monolithically. This could drastically decrease the production complexity, as it avoids manual assembly which is difficult at insect scale.

With this, the goal of the design phase of the thesis project became:

Design a compliant, resonant running robot at insect scale that can be 3D printed in one piece.

1-4 Overview of report

Chapter 2 of this report contains the literature study, which is presented as a review paper that is intended to be submitted for publication in the Journal of Mechanisms and Robotics of ASME. Chapter 3 is the article that was written about the research that was done in the design phase of this thesis. It presents the design and experimental results of the robot that was built, which we called FARbot; a Frequency Actuated Resonant robot. The discussion, conclusion and recommendations are presented in each paper individually, and are therefore not presented in separate chapters of this thesis report.

The appendices of this report are documented for successors of this project. Additional material that supports the literature paper can be found in Appendix A. Supplementary material for the technical paper is presented in Appendix B. Then, Appendix C shows the most important code that was written during the project, Appendix D presents other options that were considered for the kinematic design of FARbot and Appendix E presents results of experiments that were carried out during the project.

Chapter 2

Literature Paper

This paper presents the literature study that is conducted. It is written as a review paper, which is intended to be submitted to the Journal of Mechanisms and Robotics of ASME.

Review on mobile robots that exploit resonance

J. K. Schonebaum, F. Alijani, G. Radaelli

Department of Precision and Microsystems Engineering, Faculty of Mechanical Engineering and Marine Technology, Delft University of Technology, The Netherlands

Abstract

It is expected that mobile robots can benefit from the exploitation of their resonance in terms of actuation and efficiency. Therefore, a study is conducted on the existing terrestrial mobile robots that use resonance to obtain or improve locomotion. An overview of these robots is provided, and their advantages over robots that do not use resonance are examined. A classification with fifteen subclasses is introduced based on the locomotion mechanisms that mobile robots use. In five of the fifteen subclasses, examples of mobile robots that use resonance are found. These robots prove that they can be up to 16 times more efficient and much simpler to actuate and control than their imposed counterparts. Four different methods to make use of the resonance of a mobile robot are distinguished. A systematic design approach that combines these four methods with the fifteen subclasses is proposed, which can be used to obtain unexplored concepts for mobile robots that benefit from the exploitation of their resonance.

Keywords: Mobile robots, resonance, natural vibrations, locomotion, eigenmodes, eigenfrequency, classification, robotics

1. Introduction

Mobile robots are constantly developed and explored for various purposes and application fields. With mobile robots we mean the type of robots that can move themselves through an environment. Recently, in the field of biomedicine small untethered micro robots are designed for targeted drug delivery and minimally invasive surgery [1–4]. For unmanned missions in rough terrain special robots are examined to be applied in e.g. space exploration [5]. Another use of mobile robots is to obtain further understanding of the dynamics behind human walking [6].

Prior to this work, a literature review on robots that use natural dynamics (including resonance) has been conducted by Pratt [7]. Moreover, several categorizations and overviews of mobile robots and locomotion can be found in literature. Hirose [8] divided terrestrial mobile robots in three categories, namely ‘wheels and crawler tracks’, ‘legs’ and ‘articulated bodies’. Dickinson et al. [9] made a classification for animal locomotion distinguishing three locomotor mechanisms for terrestrial animals, i.e. ‘inverted pendulum’ (walking), ‘spring-mass’ (running) and ‘ground reaction force’ (crawling like a cockroach). An overview of compliant legged robots was made by Zhou and Bi [10], who divided these type of robots in ‘compliant legs with compressed air’, ‘compliant legs with steel coil springs’, and ‘compliant legs with compliant mechanisms’. Rus and Tolley [11] made an overview of mobile soft-robotic systems inspired by biological systems. Other reviews, surveys and categorizations on more specific areas of mobile robots have been made by e.g. Armour and Vincent [12], Nelson et al.[2], Silva et al. [13] and Lee et al. [14].

A body’s resonance is the motion it exhibits at one of its eigenfrequencies, associated with one of its eigenmodes. We consider that a mobile robot *exploits* this resonance when it utilizes it to obtain or improve locomotion in some way. Resonance purely depends on the body’s properties and the corresponding motion is spontaneously carried out when the system is excited in an eigenfrequency. All other motion is called ‘imposed motion’, with corresponding ‘imposed dynamics’. Imposed motion in a body is not obtained with eigenmodes and includes therefore all non-periodic motion and all periodic motion other than eigenmodes. In contrast to the *natural* motion of resonance, imposed motion can not be obtained by merely exciting the system at a frequency, therefore this motion needs to be carefully actuated and controlled.

The purpose of this paper is (i) to make an overview of existing mobile robots that exploit resonance, (ii) to examine the benefits thereof, and (iii) to investigate which options exist to make use of these vibrations. As there exist countless mobile robots, a systematic approach to accomplish these goals is necessary. To this end, we introduce a categorization (Fig. 1) based on locomotion mechanisms, i.e. how does the robot obtain locomotion. In this classification we only consider mechanisms that use contact with the ground for propulsion. We divide the robots such, that if a robot within a subclass exploits resonance, all other robots within the same subclass should (theoretically) be able to use resonance likewise. As upper level distinction in our classification, we separate mobile robots that perform a rolling, striding and sliding motion. A notable difference between these categories is the main cause of energy loss, which is for rolling, striding and sliding respectively viscous damping due to deformation, impact at every stride and friction with the environment. Within each subclass, we discuss both robots that exploit resonance and robots that do not. The latter are dis-

---

Email address: `j.k.schonebaum@student.tudelft.nl` (J. K. Schonebaum)

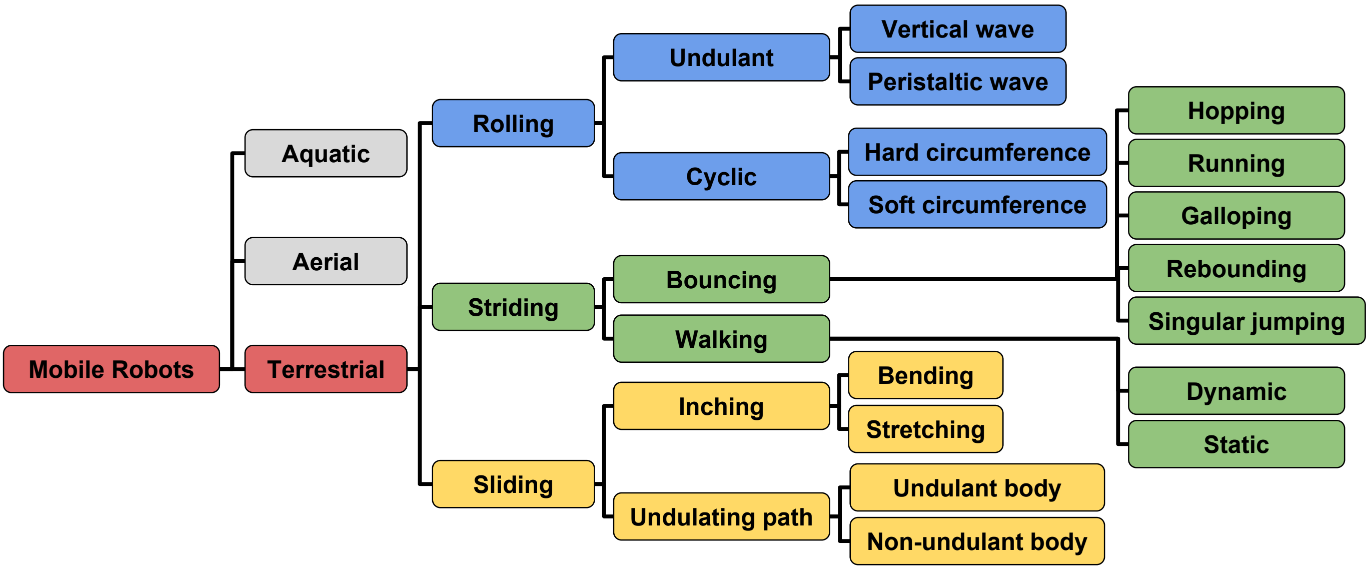

Figure 1: The tree diagram that visualizes the categorization as used in this paper.

cussed to thoroughly understand the locomotion mechanism of each subclass.

The first reason to investigate mobile robots that use resonance is that the motion of resonance is more efficient, as compared to imposed motion. Secondly, resonance is triggered easier, for which actuation and powering can be obtained with simpler and more flexible means. To put it slightly stronger, we argue that resonance can be used as a means of power transmission to convert an oscillating energy source into a desired periodic motion. The need for new mechanisms in mobile robots that improve either their efficiency or the opportunity of untethered powering is made clear in 'The grand challenges of Science Robotics' by Yang et al. [15]. In this paper, they state that actuation and energy harvesting remain major bottlenecks for robots. The expected advantages of resonance can contribute to overcoming these challenges.

The scope of this paper is terrestrial mobile robots, thus aerial and aquatic robots are excluded. Yet, in these classes there are also robots that use resonance. Examples are acoustically actuated micro swimmers [16–19], which are a good example of the opportunities for simple, untethered actuation and powering mechanisms that can be used when exploiting resonance. Moreover, for micro air vehicles the use of resonance is explored [20, 21], which is inspired by the oscillation mechanisms that are found in birds and insects [22].

When searching for relevant literature, we used several synonyms for search terms. Most notably are the synonyms we tried (i) for resonance, namely 'natural vibrations', (ii) for natural dynamics, which are 'passive dynamics' and 'eigen dynamics', (iii) for eigenfrequency, namely 'natural frequency' and 'resonance frequency' and (iv) for eigenmode, i.e. 'eigenvector', 'eigenshape', 'mode shape', 'normal mode' and 'resonance mode'.

Section 2 of this paper elaborates the properties of resonance. In Section 3 a review of existing rolling mobile robots is given, which are divided into undulant rollers (Section 3.1) and cyclic rollers (Section 3.2). Section 4 presents an overview of mobile robots in the category striding, where a distinction is made between bouncing and walking striders. These are found in Sections 4.1 and 4.2, respectively. Mobile robots in the category sliding are reviewed in Section 5, which also has been divided into two subsections: Section 5.1 discusses sliding robots that inch forward in a straight line, Section 5.2 discusses robots that slide with a undulating path. In Section 6 an overview of all findings of present research is given. Section 6.1 presents a diagram which identifies the subcategories that contain robots that use their resonance and those that do not. In Section 6.2 four distinguishable options to exploit resonance of mobile robots are discussed. Lastly, in Section 6.3 a systematic approach to develop new mobile robots is proposed.

2. Elaboration on resonance

Resonance is the periodic motion that a body exhibits at its eigenfrequency. Although periodic, the motion is not necessarily reciprocal, that is because it can consist of a combination of eigenmodes. Robots that exploit resonance do not necessarily use their *first* eigenmode, nor an eigenmode that moves the entire body.

Opposed to natural motion we consider imposed motion, which does not make use of the eigenfrequencies and eigenmodes of the body. Therefore, this motion must be enforced and controlled by local actuation within the body. This means that it counteracts the natural motion, thus for complex imposed systems often a large amount of actuators is necessary to obtain the desired motion.

At the eigenfrequency of a body, the inertial and the potential forces cancel each other out. Therefore, the only forces that act against the corresponding motion are non-conservative forces. For this reason, the output amplitude of a vibrating body is much greater when it is excited at its eigenfrequency than at another frequency for which the internal forces do not cancel out. Because of this property of resonance, natural motion is more efficient than imposed motion, and thus we expect that robots using resonance are more efficient.

Our other expectation, which concerns powering and actuation in a simpler fashion, can also be explained with the internal forces that cancel out at the eigenfrequency. A body will always adopt its minimum energy state for any combination of external forces. When the body is excited at an eigenfrequency, the minimum energy state is a motion in the corresponding eigenmode, because only for that motion the inertial and the potential forces cancel out. Hence, a body will carry out its natural motion if it is excited at the eigenfrequency, almost regardless of the point of application at the body. The only exceptions here are that the excitation force should not be applied at a node of an eigenmode or perpendicular to the direction of the mode. For this reason, mobile robots that use their resonance could be actuated with simple vibrators or untethered energy sources like acoustics and magnetics. This is an important difference with other mobile robots, where every internal movement must be controlled and actuated carefully.

3. Rolling

Rolling locomotion uses the type of contact for which consecutive points on a body make contact with the ground one after the other. Moreover, when touching, the contact points do not move with respect to the ground. There can either be a continuous or a discrete number of contact points. Different types of rolling involve caterpillar track motion, cyclic rolling of a wheel or ball and traveling waves.

This category is divided into two subcategories, namely robots that make use of undulations for locomotion (undulant rollers) and those that perform a cycle (cyclers).

3.1. Undulant rollers

There are two distinct types of undulation for rolling locomotion: (i) vertical wave undulation and (ii) peristaltic wave undulation. These classes are discussed further in the following Sections 3.1.1 and 3.1.2.

3.1.1. Vertical wave undulation

The only robot that uses resonance within this category is that of Hariri et al. [23], see Fig. 2. This robot moves as a result of a vertical traveling wave that undulates in the beam shaped body of the robot. Two piezoelectric actuators produce the traveling wave by exciting the beam at both ends in a frequency between the 16th and 17th eigenfrequency, with a phase difference of 90deg. This is a good example of a mechanism that uses resonance as a power transmission between two oscillating energy sources and a desired motion.

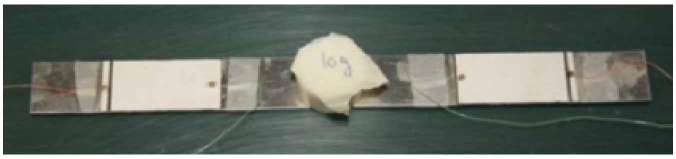

Figure 2: The traveling wave piezoelectric beam robot, courtesy of Hariri et al. [23]

All other robots within this subcategory are fully imposed. Although they are in the same subcategory, they are diverse in terms of size and actuation. The GoQBot of Lin et al. [24] for example, is a few centimetres long and actuated by an electric SMA coil. Whereas the Strandbeest of Jansen [25][1] in Fig. 3b is over 5 meters long and converts wind energy into an undulant motion by a multilinkage transmission mechanism. Another notable robot is the the Omni-directional mobile robot of Nakamura and Satoh [26], which is the only undulant robot capable of locomotion in all 2D planar directions. Other researchers that developed vertical wave undulant robots include Wright et al. [27], Hatton and Choset [28] and Hu et al. [1]. In particular, Hu et al. [1] made a 17 mm untethered robot (see Fig. 3a), that is actuated by uniform magnetic fields that change in time.

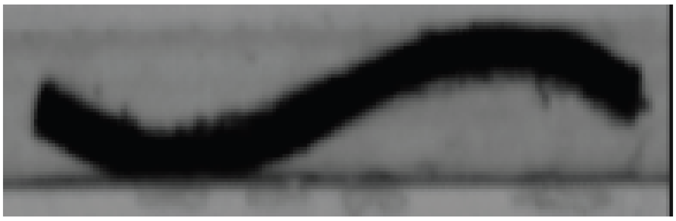

(a) Millirobot [1]

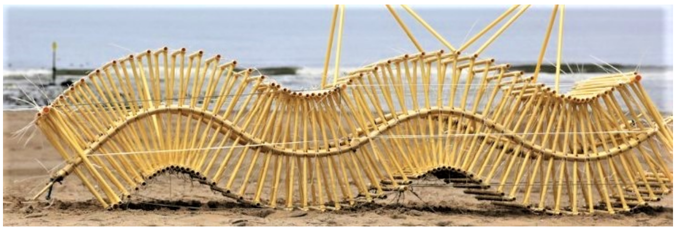

(b) Strandbeest [25]

Figure 3: The vertical wave undulation robots: the 17 mm magneto-elastic soft millirobot of Hu et al. [1] and the 5 m undulant rolling Strandbeest of Jansen [25].

3.1.2. Peristaltic wave undulation

Peristaltic waves are becoming increasingly popular as means of locomotion, because this mechanism provides opportunities to navigate in narrow tubes and through holes. Only examples of robots with imposed peristaltic motion have been found, which are actuated in diverse ways. The Meshworm in Fig. 4a by Seok et al. [29] and the origami worm robot by Onal et al. [30] are thermally actuated with nickel titanium SMA coil actuators. Others are electronically actuated, like the Softworm by Boxerbaum et al. [31] and the CMMWorm by Horchler et al. [32] (see Fig. 4b). Furthermore, Saga and Nakamura [33] developed a robot that uses magnetic fluid to obtain the peristaltic wave.

---

[1] Jansen made several of these ‘beasts’, the specific one that performs rolling with a vertical wave can be seen in the video of [25] at 1:41 minutes.

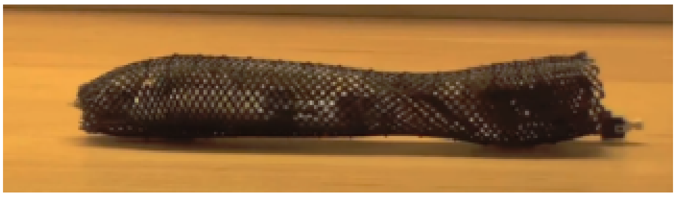

(a) Meshworm [29]

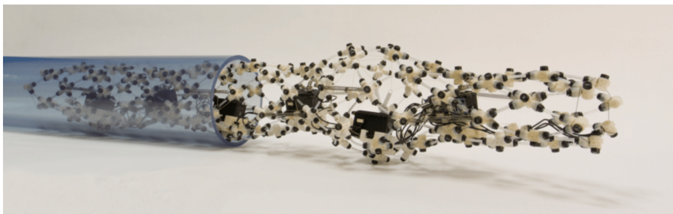

(b) CCMworm [32]

Figure 4: The peristaltic wave undulation robots: Meshworm of Seok et al. [29] and the CCMworm of Horchler et al. [32]

3.2. *Cycling rollers*

This subcategory contains all mobile robots on wheels, caterpillar tracks or balls. However, as there are near infinite examples of those, we narrow this subsection down to mobile robots that roll with their full body. With this choice we exclude the countless robotic auto mobiles and caterpillar track robots. For the latter a number of examples is given by Lee et al. [14].

Cyclic rollers are divided into robots with an undeformable (hard) circumference and those with a flexible (soft) circumference.

3.2.1. *Hard cyclic rollers*

Hard robots that perform cyclic rolling obtain their locomotion by creating a moment around the point of contact for which the ball or wheel starts rolling. The moment can only be obtained by an actuation system within the robot, that alters the centre of mass of the robot. Different techniques to move the centre of mass are developed. One of those, explored by Bicchi et al. [34], uses the principle of a hamster in a ball, in which the hamster is replaced by a little car. Another mechanism which is used by Mukherjee et al. [35] and Mojabi et al. [36] alters the center of mass by moving masses along three or four radial axles in the sphere, see Fig. 5. Armour and Vincent [12] give a broad overview of the other mechanisms used for this kind of robots.

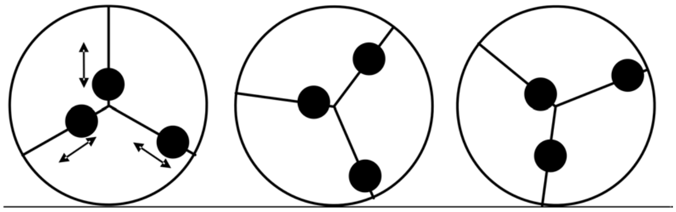

Figure 5: Visualisation of one of the working mechanism of a hard rolling robot ball that alters its centre of mass, courtesy of Armour and Vincent [12]

Some further existing hard ball robots are made by Halme et al. [37], Suomela and Ylikorpi [38], Reina et al. [39], Batten and Wentzlaff [40], Ioi et al. [41], Brown and Xu [42], Michaud and Caron [43] and Michaud et al. [44], who made the Roball, see Fig. 6.

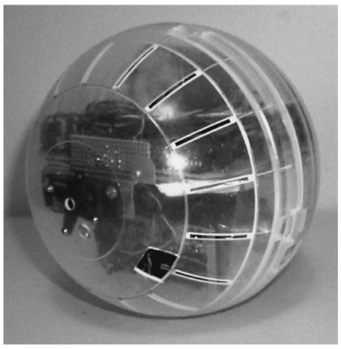

Figure 6: The Roball, courtesy of Michaud et al. [43, 44]

3.2.2. *Soft cyclic rollers*

The mobile robots in this category use different mechanisms to move. Some of them can change their outer shape such that a sort of circular traveling wave arises which causes the robot to move, e.g. the circular and spherical deformable robots by Sugiyama and Hirai [45] (see Fig. 7a) and the JSEL of Steltz et al. [46].

Other robots use projections on the circumference of the robot to push it forward, like the soft robot of Onal et al. [47] in Fig. 7b.

There is also a robot by Lin et al. [24] that launches itself into rolling like the ballistic escape movement of a mother-of-pearl moth caterpillar, as described by Brackenbury [48].

A more broadly explored area within the soft cyclic rollers is the tensegrity robots. These exist of rods that are connected via a network of cables. They have been studied extensively in the past decade by Paul et al. [49], Iscen et al. [50], Caluwaerts et al. [51] and SunSpiral et al. [5], because they provide advantages over standard mobile robots in terms of compliance, robustness and flexibility. Examples of tensegrity robots are the ones of Koizumi et al. [52], Chen et al. [53], Bruce et al. [54] and NASA's SUPER ball (Fig. 7c) by SunSpiral et al. [55] and Sabelhaus et al. [56].

A last mechanism to obtain motion in this subcategory is found in the same robot of Hu et al. [1] in Fig. 3a (section 3.1). Just like the other gaits that it can perform, it can roll due to the magnetic distribution in its body together with the changing magnetic field it is subjected to.

We did not find examples of cyclic rolling robots that make use of their resonance, neither of soft nor of hard cyclic rollers.

4. Striding

With striding we mean taking discrete steps by which contact points do not move with respect to the surrounding. The points of contact are not necessarily on consecutive locations on the body. An important mechanical difference between rolling and striding is that for the latter the body is exposed to a fairly

(a) Deformable robot [45]

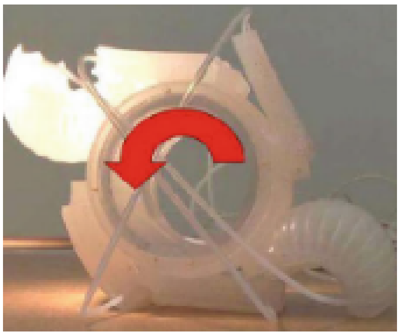

(b) Robot of Onal et al. [47]

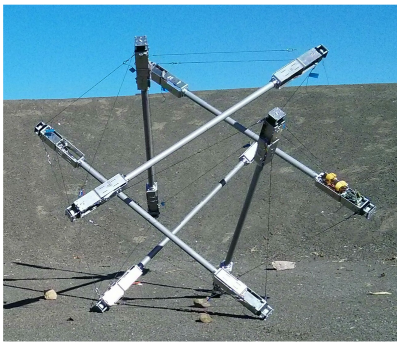

(c) SUPER ball [55, 56]

Figure 7: Three cyclic rolling robots with a soft circumference, namely the circular Deformable Robot climbing a slope of Sugiyama and Hirai [45], the robot of Onal et al. [47] with projections on the circumference, and the the spherical tensegrity robot SUPER ball of NASA [55, 56]

significant impact force with every stride. Typically, contact with the environment is made with a discrete number of legs or something alike. Striding includes walking, running, galloping, bounding, hopping and jumping.

Within this category there are many robots, therefore we focus mainly on robots that use resonance. Also we will not elaborate on different actuation types or sizes for the sake of brevity.

Striding is divided into robots that use airtime for locomotion (bouncers) and those that keep contact with the ground (walkers).

4.1. Bouncing striders

There are countless examples of bouncing striders. We separate them by the way they bounce, which is either hopping, running, singular jumping, galloping or rebounding. These terms are explained at the beginning of each paragraph.

It should be observed that for bouncers the bouncing frequency is not necessarily an eigenfrequency of the system. That is because the period of airtime of a body is only a function of gravitational acceleration, vertical speed of a body during take-off and some friction. Velocity is not an inherent property of the system, but a state and a measure of the amount of energy stored in the system. The more energy there is stored in the system, the lower the bouncing frequency becomes. This opposes the characteristics of eigenfrequencies. Nevertheless, this does not imply that there can be no bouncers that use their resonance.

4.1.1. Hopping

‘Hopping’ means a continuous jumping motion where all legs of the robot perform action simultaneously. Many hopping robots are developed to explore the energy recovery mechanisms and overall dynamics of robotic legs, e.g. by Hyon et al. [57] Fig. 8, Brown and Zeglin [58] and Ahmadi and Buehler [59]. The stabilization and control of hopping robots are the main challenges, especially for the one-legged, free hopping versions.

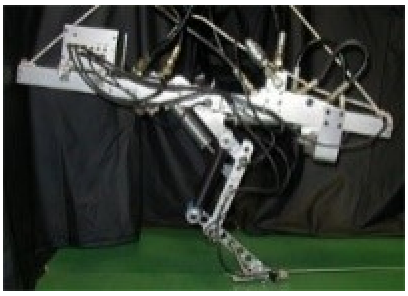

Figure 8: The one legged hopping robot Kenken, courtesy of Hyon et al. [57]

4.1.2. Running

‘Running’ is when the legs of a ‘leg pair’ move with a phase difference of about 180 degrees, where a leg pair is defined as two legs that are positioned left and right on a body on the same location. Of the many articles on running robots, there are a few that mention the use of resonance. One of these is the quadruped runner HAMR (Harvard Ambulator MicroRobot) of Baisch and Wood [60] (shown in Fig. 9) and all its other versions [61–64]. This insect scale running robot benefits from the use of its resonance. Baisch et al. [65] showed that when the HAMR-VP is actuated with increasing frequency, the speed of the robot increases up until it is actuated at the natural frequency of its legs, and decreases beyond this frequency. This is remarkable because one would expect that the speed always increases with higher stride frequency. Goldberg et al. [66] conducted a more extensive research on the actuation frequencies of HAMR. They showed that the behaviour of the robot does not improve when exciting it at lower natural frequencies for which the full body resonates, instead of only the legs.

Moreover, the hexapedal robot MinRAR of Rios et al. [67] makes use of the first two eigenfrequencies of the leg suspension to obtain the desired foot trajectory.

Birkmeyer et al. [68] suggest exploitation of resonance to increase the efficiency of the hexapedal robot DASH, however they state that further research should be done to validate this.

Other notable runners include the two legged robot Atlas of Boston Dynamics described by Feng et al. [69] and Kuindersma et al. [70], the quadruped KOLT of Estremera and Waldron [71] and the fast iSprawl by Kim et al. [72] which do not use resonance.

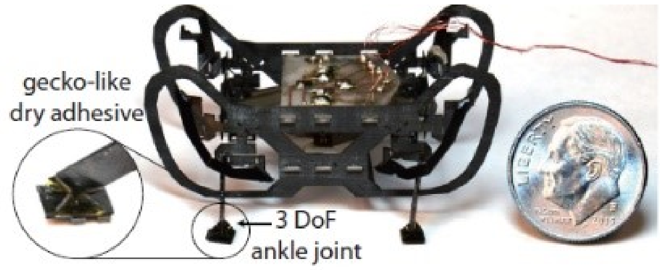

Figure 9: The insect scale running robot HAMR, courtesy of Seitz et al. [62]

4.1.3. Galloping

'Galloping' is a gait where the legs of a leg pair move simultaneously, but with a phase difference with respect to other leg pairs. Poulakakis et al. [73], Eckert et al. [74] and Seok et al. [75, 76] have developed robots that gallop. Especially Seok's MIT Cheetah performs a gait that shows much resemblance with the galloping gait of animals. Although it could be expected that resonance are used, no evidence in literature is found that this is the case. For instance, the galloping frequency is not documented as an eigenfrequency of the system. See Fig. 10 for the free running version of the MIT Cheetah, called WildCat.

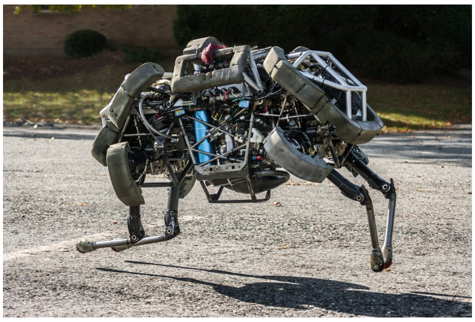

Figure 10: The galloping WildCat, courtesy of Boston Dynamics.

4.1.4. Rebounding

With 'Rebounding' robots we mean robots that have such a geometry, that a vertical impact with the ground is transferred to a horizontal motion. Some of them are actuated by a simple vertical vibrator like the ones by Rubenstein et al. [77] and Peters [78]. The latter tested with differential leg stiffness to steer his robot (Fig. 11). The idea was that the robot starts to make a turn when the stiffness of one leg is altered slightly while the vibration frequency is the same as the (initial) eigenfrequency of the legs. This is an original way of using resonance. The Kilobot of Rubenstein et al. [77] is a very simple mobile robot design that is used in SWARM experiments [79].

Miyashita et al. [80] made a robot that can wiggle vertically such that it starts bounding forward.

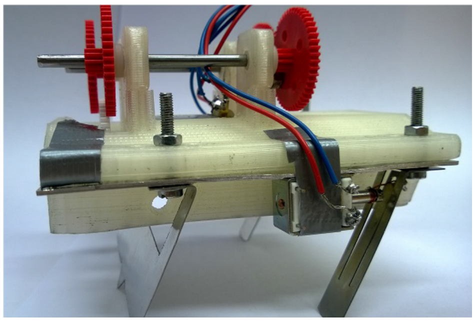

Figure 11: The rebounding robot actuated by vibration, courtesy of Peters [78].

4.1.5. Singular jumping

'Singular Jumping' means that the robot performs a single jump at a time. These robots are not considered very interesting for this paper, because they inherently do not make use of resonance as their motion is not periodic. Though, their advantage with respect to many other robots is that they can jump over obstacles. Tolley et al. [81], Bartlett et al. [82] and Haldane et al. [83] (the developers of SALTO, Fig. 12) are active in this range of robots.

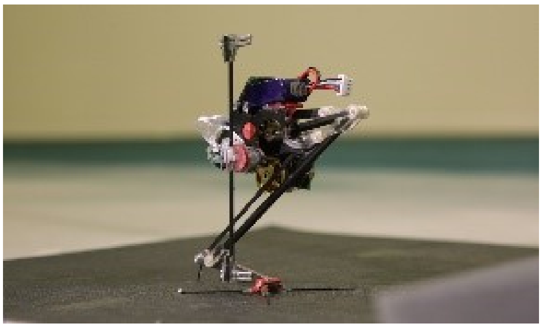

Figure 12: The singular jumping robot SALTO, courtesy of Haldane et al. [83]

4.2. Walking striders

In this subsection we distinguish dynamic and static walkers. The latter retain their centre of pressure (COP) in between the contact points with the ground throughout the entire motion. Therefore, the robot will be in balance if it freezes at any point during a stride. To accomplish that, static walkers mainly have either multiple legs or large feet. Dynamic walkers on the other hand, place their COP outside their contact points during part of a stride. Therefore, during that part of the stride it would tip over if it does not swing one of its legs forward. These walkers can have fewer legs and move more like humans. In this subclass, we find far most mobile robots that exploit resonance. Typically these robots resonate at low frequencies. For these walkers, extensive research is conducted on the use of resonance. Within that research authors often refer to 'passive' walkers, which are dynamic walkers as described before, that do not require actuation for the swinging motion of the legs.

4.2.1. Dynamic walkers

The first dynamic walkers were two-legged toys, which used natural vibrations to walk down a shallow slope without any powering, actuation or control. Just a shallow ramp and the right geometry and weight distribution makes them move. Because of the straight legs these toys have, they must rock from side to side to lift the swing leg of the ground. This results in a waddling gait that resembles that of ducks and penguins. These toys were already developed and patented around the beginning of the twentieth century [84–88][2]. More recently, Coleman and Ruina [89] and Coleman et al. [90] developed a new version of these toys and conducted research to this type of waddling bipeds.

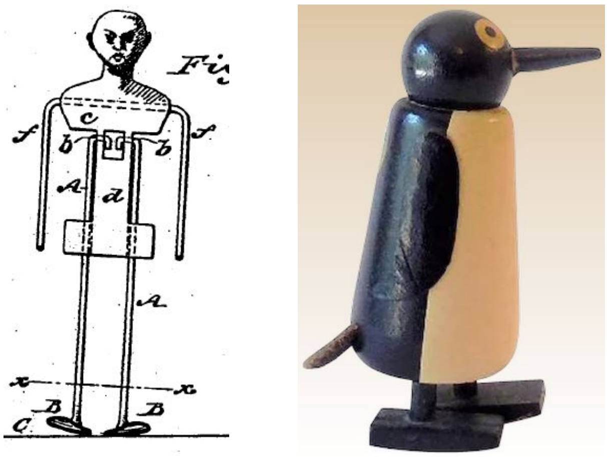

(a) Fallis's walker [84]

(b) Wilson's walker [88]

Figure 13: Two ramp-walking toys that were designed between 1888 and 1940. Both of them walk down a shallow slope using their resonance, and no powering or control.

McGeer [91, 92] invented the first modern ramp-walking robots that use resonance and conducted extensive research on them [93, 94]. The idea behind developing his passive-dynamic ramp-walkers was that he firstly wanted to master walking in a passive dynamic fashion on a ramp and eventually add actuation and control. To put it in other words, he wanted to explore the opportunities of the resonance of his robots before adding control and powering. For this method he was inspired by the Wright brothers, who developed air planes by firstly mastering gliding and subsequently adding small motors. This philosophy opposed the fully imposed robots that were developed in the previous years, like these of Mita et al. [95], Furusho and Sano [96], and Miura and Shimoyama [97].

McGeer developed two ramp-walking robots: one with straight legs [91] which performs a gait similar to a human walking with crutches, and one with knee joints [92] that exhibits a human walking gait, see Figures 15a and 15b. Both robots obtain their gait by the pendulum swinging eigenmode of their legs. Whereas the toys used the waddling gait to clear the swing leg from the ground, these robots use two different mechanisms. The straight legged version uses small actuators to fold the feet of the swing legs inward, apart from these actuators the machine is fully passive. The other robot uses its knee joints for clearance. It has joints with kneecaps with which the swing leg can swing freely once started, but the leg can not be inverted. Hence, due to conservation of angular momentum the swing foot is lifted enough to prevent contact with the ground, see Fig. 14.

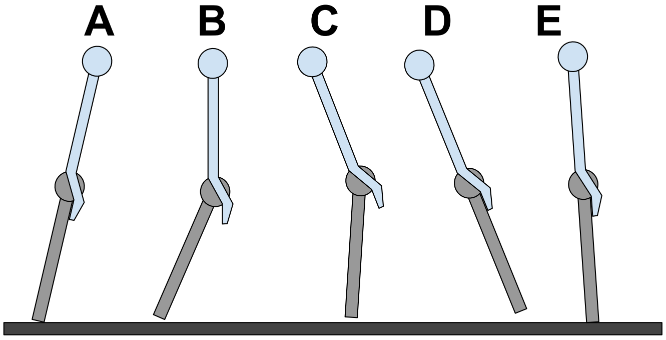

Figure 14: This diagram illustrates the passive swing of legs with knee-joints, which assures clearance of the swinging leg from the ground. The swing is initiated (A) through a forward torque on the hip, which is supplied either by gravity or by a hip actuators. The leg can swing passively (B - C) until swing is stopped (D) through a backward torque about the hip joint, again either by hip actuators or gravity. At that point the kneecap in the joint prevents the leg from inverting, because of which the food touches (E) the ground in the backward swing.

These relatively simple but revolutionary design concepts have been explored and studied elaborately in the following years by for example Goswami et al. [98] and Garcia et al. [99, 100] who made a mathematical model of McGeer's machines. Goswami [101] experimented with the geometry of the feet, and Kuo [102] investigated lateral stability. Wisse et al. [103] suggested to add free-swinging masses as arms to balance sway of the legs. This idea was slightly altered by Collins et al. [104] to a design with arms that are coupled to the legs for a simpler design. Furthermore, Dankowicz et al. [105] and Adolfsson et al. [106] investigated the existence and stability of a repetitive gait of McGeer like robots in 3D environment and in presence of discontinuities. In 2011 Chyou et al. [107] and Gomes and Ruina [108] numerically showed that passive-dynamic walkers with a spring-loaded upper body can place the swing foot smoothly on the ground by suitably adjusting the system parameters and initial state.

When the passive ramp-walking mechanism was well understood, powered versions were developed based on the same mechanism. These robots have small active power sources that substitute for gravity and can walk on level ground. They use less control and less energy than other powered robots, yet their gait shows more resemblance with humans. Three examples of these are presented by Collins et al. [6], namely the Cornell biped of Collins and Ruina [109] (see Fig. 16a), the Delft biped 'Mike' of Wisse et al. [110, 111] and the MIT biped 'Toddler' of Tedrake et al. [112].

The extensive research on these robots has revealed great advantages of natural vibrations as compared to imposed. Not only do they benefit from much simpler control and actuation,

---

[2] All available at http://ruina.tam.cornell.edu/research/history/

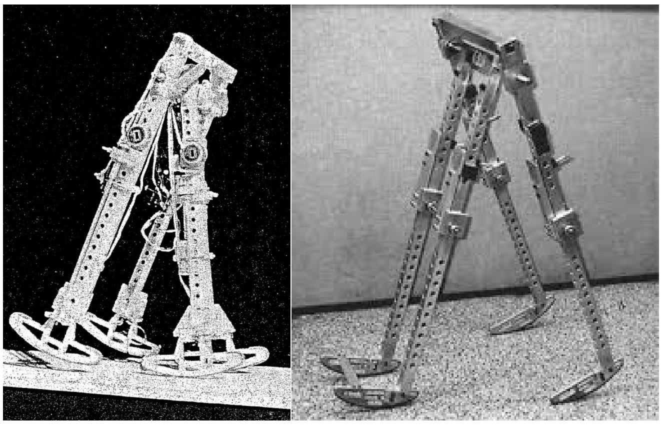

(a) McGeer's straight legged, passive walker [91]

(b) McGeer's kneed, passive walker [92]

Figure 15: The two passive ramp-walkers of McGeer. These robots were the beginning of a broad research on the resonance of dynamic walkers.

they also can be orders of magnitude more efficient. Collins and Ruina [109] present a comparison with respect to efficiency between their robot, humans and the Honda Asimo [113–115], which is a very succesfull biped walker that is fully imposed and controlled. The efficiency is measured as cost of transport c_{et} and as mechanical energy efficiency c_{mt}. Cost of transport is defined as $c_{et} = \frac{E_c}{mgu}$, where E_c is energy consumed, m is the mass of the robot, g is gravitational acceleration and u is the distance traveled. The mechanical energy efficiency c_{mt} assigns an energy cost only to the mechanical work of the actuators. For c_{mt} the natural dynamic walker of Collins and Ruina [109] out-performs Asimo with a factor 16 and for c_{mt} even with a factor 29. These efficiency performances are within 10 percent of human walking efficiency.

They conclude their paper stating that they believe that the naturally dynamic design method "will help to build walking robots that are simpler, more efficient, easier to control, and therefore more practical". However, it should be noted as well that the natural dynamic walkers can only perform one task and are typically not as robust as fully controlled versions in terms of tipping over.

There are also powered dynamic walkers that use their resonance, which are not just driven versions of ramp-walkers. These typically use a little more control, and can therefore either perform more tasks or they are slightly more robust. An example is the Spring Flamingo of Pratt and Pratt [116–118]. They managed to make a 2D walking robot that uses control, motors and force feedback, but still uses the resonance of the system for locomotion, which results in smooth motions. Just like McGeer's robots, this robot exploits resonance by using the swinging eigenmode of the legs. Pratt and Pratt state that the control of imposed bipedal robots has often been very complicated and the resultant motion often looks unnatural and is inefficient.

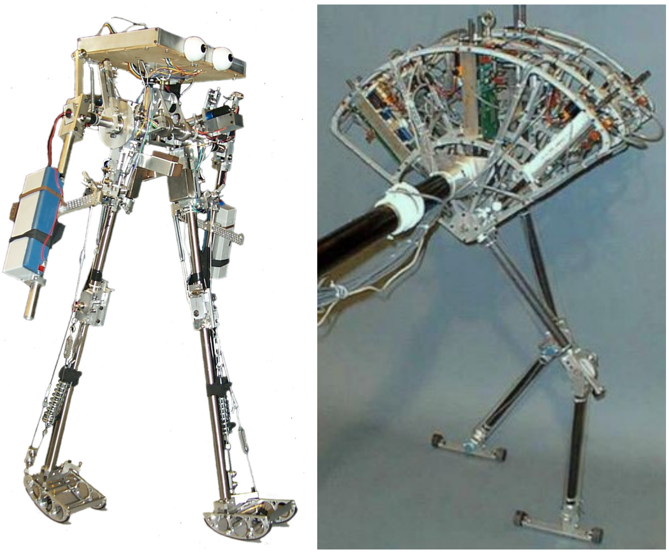

(a) Cornell walker [109]

(b) Spring Flamingo [116–118]

Figure 16: Two examples of powered, dynamic walkers that exploit resonance; The Cornell walker is courtesy of Collins and Ruina [109], the Spring Flamingo is courtesy of Pratt and Pratt [116–118]

4.2.2. *Static walkers*

Within the enormous amount of statically walking robots, two examples stand out for this paper, namely the standing wave robot of Son et al. [119] (Fig. 17a) and the myriapod of Hoffman and Wood [120–122] (Fig. 17b).

The standing wave robot is of particular interest because it fully uses its resonance to obtain locomotion. The mechanism it uses is completely different from all other walking robots. It namely exploits two of its bending modes to move little legs called projections, as seen in the graphical explanation in Fig. 18. Even bi-directional motion is achieved, which is done by placing the legs to the right of the anti nodes of one mode and to the left of anti nodes of the other mode. This motion principle is more commonly used in devices that transport small objects. An extensive explanation of this principle is given by He et al.[123].

The myriapod on the other hand stands out because it shows that undulatory gaits can increase the average speed of locomotion as compared to non-undulatory gaits for the same striding frequency. These undulations result from varying the phase difference in the stance between adjacent segments of the body, that are passively connected. The undulatory gait shows much resemblance to that of centipedes in nature.

Two other famous static walking robots that move through imposed motion are the RHEX [124, 125] and Bigdog [126] by Boston Dynamics. These robots are designed to navigate through rough terrain. More recently, an untethered multi-legged robot is developed by Lu et al. [127] to operate within a human body for medical purposes.

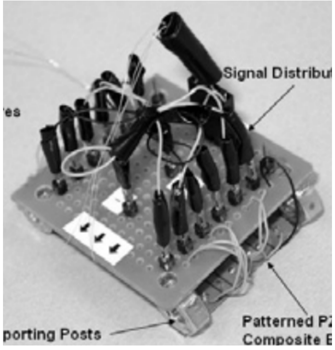

(a) Standing wave robot [119]

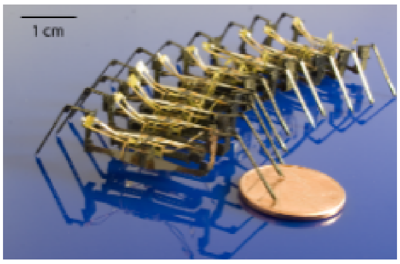

(b) Myriapod [122]

Figure 17: Two static walking robots; the standing wave robot is courtesy of Aon et al. [119] and the Myriapod is courtesy of Hoffman and Wood [122].

5. Sliding

A motion is considered sliding when part of the contact area of the body needs to move with respect to the surroundings to obtain locomotion. For this category we did not find a single mobile robot that uses its resonance. Still, we defined two subcategories: (i) the 'inching sliders' discussed in Section 5.1 and (ii) the 'undulating path sliders' presented in Section 5.2. Inching sliding robots propel themselves by pushing in the longitudinal direction of their heading. Therefore, they typically show a straight lined trajectory. On the other hand, undulating path sliding robots partly push in the transversal direction, which results in a slightly undulant locomotion path.

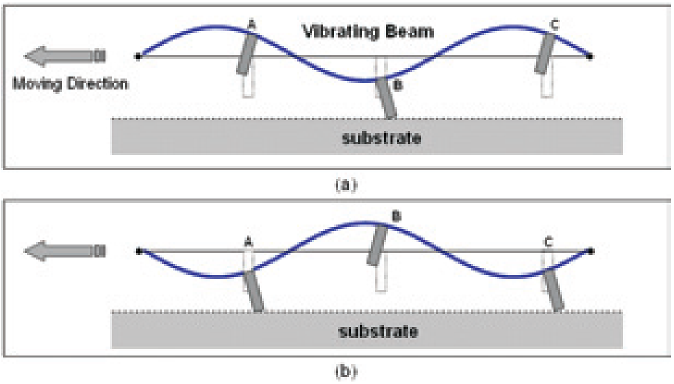

Figure 18: This diagram explains the working principle of the standing wave actuated walking robot. Due to the placement of the legs on the bending beam, the legs rotate clockwise when lifted and counter clockwise when lowered. The legs are located just next to the apex of the standing wave. This diagram is courtesy of Son et al. [119]

5.1. *Inching sliders*

To obtain locomotion, this kind of robot makes reciprocal internal movements whereby one part of the body always anchors to the ground, while the rest of the body slides along. Two types of internal motion for this gait were found, namely bending and stretching. Bending inchers have an Ω-shaped body, which they bend and relax to inch forward. Stretching inchers elongate and shorten their bodies.

5.1.1. *Bending*

Most of the robots in this category are inspired by the gait of the inchworm *ascotis selenaria*. Examples of robots that inch while bending their body are the Omegabot by Koh and Cho [128, 129] (Fig. 19) and the robots of Wang et al. [130], Felton et al. [131] and Moreira et al. [132]. Sizes of these robots differ between 66cm for the latter, and a few centimetres for most others. These robots all use different anchoring mechanisms for their locomotion.

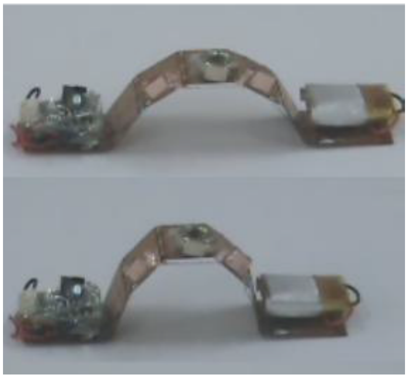

Figure 19: The Omegabot, which performs a inching gait by bending its body, courtesy of Koh and Cho [128, 129]

5.1.2. *Stretching*

We discuss two examples of longitudinally stretching inchers that use different anchoring mechanisms. The first uses its two ends to anchor one after the other. This robot is made by Lim et al. [133] for pipe inspection (Fig. 20a). The other robot [134] uses the directional friction of its snake-like kirigami skin, see Fig. 20b. The difference between the two robots is that the latter uses its full body for anchoring, whereas the first uses only its two ends.

5.2. *Undulating path sliders*

Even though all robots in this subclass make use of an undulating path while moving, they do not all exhibit undulant motion within their bodies. Hence, we define two distinct types of sliding robots that move with an undulating path: (i) those that exhibit undulant motion within their body and (ii) those that do not perform internal undulant motion to slide with an undulating trajectory. These subgroups are discussed in the following Sections 5.2.1 and 5.2.2, respectively.

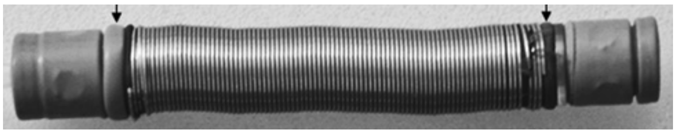

(a) The pneumatic pipe robot, courtesy of Lim et al. [133]

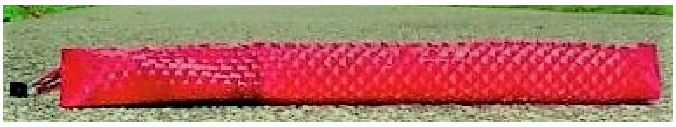

(b) The inching robot with kirigami skin, courtesy of Rafsanjani et al. [134]

Figure 20: These two sliding robots both stretch their bodies to inch forward, their anchoring mechanism is rather different however. The difference between them is that the robot with kirigami skin uses its full body for anchoring, whereas the pipe robot only uses its two ends.

5.2.1. *Undulant bodies*

A number of robots are inspired by the crawling gait of a snake. These robots make use of a directional friction coefficient to obtain locomotion. The first qualitative research on biologically inspired serpentine robots was done by Hirose [135]. Other examples are the ones by Saito et al. [136], by Bayraktaroglu [137] (see Fig. 21a) and by Maity et al. [138].

Some snake-like robots are suspended by wheels (e.g. the GMD-SNAKE2 by Klaassen and Paap [139] and the Amphibot I and II by Crespi et al. [140, 141]), these however do not classify as sliders, hence they do not belong to this category.

A slightly different type of robot are the salamander robots developed by IJspeert et al. [142–144], see Fig. 21b. These robots slide with their bodies over the ground in a serpentine fashion, while also pushing with their legs.

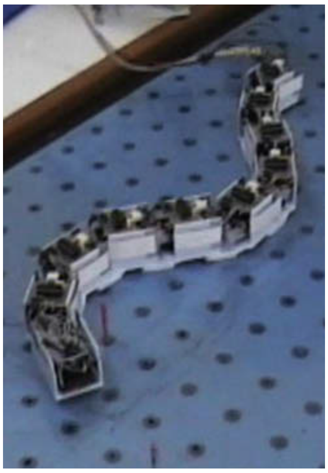

(a) Snake-like robot [137]

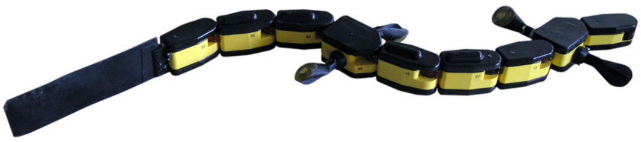

(b) Salamandra Robotica II [144]

Figure 21: The undulating path sliders with undulant bodies of Bayraktaroglu [137] and Crespi et al. [144]

5.2.2. *Non-undulant bodies*

An example of a system that slides with an undulating path, while it does not undulate its body is an ice skating human. Therefore, human ice skating is a gait that would perfectly fit in this subcategory. Although some attempts have been made by e.g. Iverach-Brereton et al [145] to mimic this gait with a robot, they do not yet move as smooth and efficient as humans do. Still, the sideways pushing mechanism that the Ice Skating Humanoid Robot (Fig. 22) uses, is similar to that of humans.

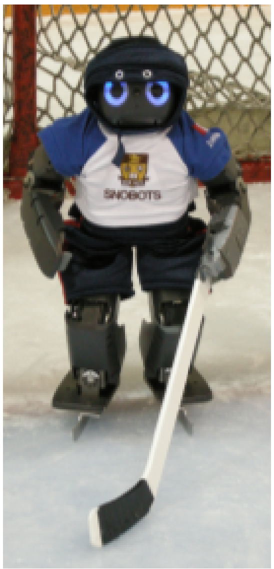

Figure 22: The Ice Skating Humanoid Robot, courtesy of Iverach-Brereton [145]

6. Discussion

In this section we give an overview of the most relevant findings of present research and we discuss the opportunities of using them.

6.1. *Overview of subclasses and robots exploiting resonance*

In Fig. 23 we give an overview of the subclasses that contain robots that use resonance. This diagram clearly shows that the striding category contains most robots that exploit resonance within a variety of subclasses. It should be noted that the three dynamic walking robots in this figure are not the only examples found. The diagram also shows that for the rolling class only one robot was found to exploit its resonance and for the sliding class none.

6.2. *Methods to exploit resonance in robot dynamics*

The mobile robots that are investigated show three distinct fundamental methods to exploit resonance. These methods are enumerated below, together with a fourth option that we propose as a result of examining imposed robots. We will refer to these methods with 'NV-methods' from here on.

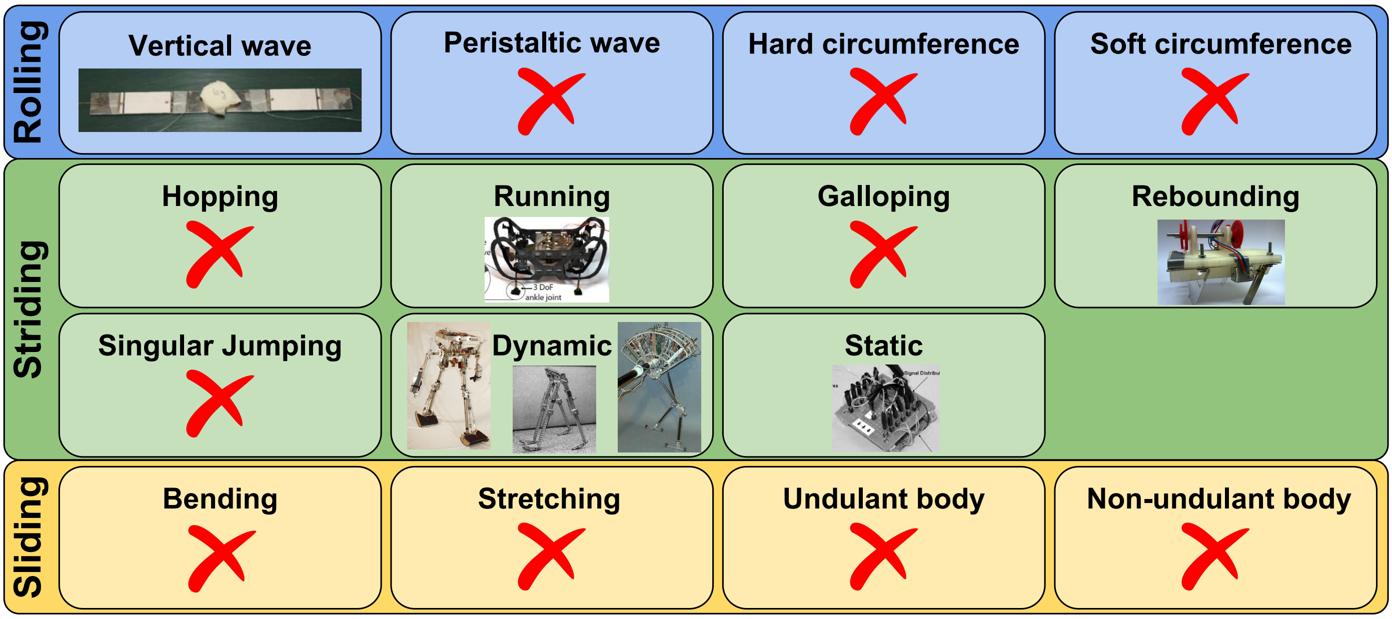

Figure 23: This overview diagram identifies which subclasses contain robots that use resonance and those that do not. The mobile robots shown in the dynamic walking subclass are just three of the many examples we found. All the pictures within this figure have been used previously in this paper in separate figures, they are courtesy of respectively: Hariri et al. [23], Seitz et al. [62], Peters [78], Collins and Ruina [109], McGeer [92], Pratt and Pratt [116] and Son et al. [119].

1. The resonance of the body is the only motion of the system that can cause locomotion. Therefore, the robot will only move when it is actuated in the right eigenfrequency, triggering the right eigenmode.
2. Resonance of the body support locomotion in some way, e.g. in terms of efficiency, speed, steering or stability. Hence, the robot does also move without actuation in eigenfrequencies, but its locomotion performance improves when actuated at the right natural frequency.
3. A relatively large part of the body resonates, which moves smaller parts that are directly attached to it. These smaller parts propel the robot.
4. A relatively large part of the body resonates, which is connected to a transmission mechanism that has an eigenfrequency much higher than that of the resonating body. This mechanism can transform the motion of the natural vibration into a desired propelling motion.

In Fig. 24 an overview is presented that shows which of the four options are used by the mobile robots examined in the present paper.

6.3. Systematic approach of combining subclasses and NV-methods

In the overviews given in this section, it was made clear that there are many gaps that can be filled. In principle, it should be possible to develop a robot for every combination of subclass and NV-method. If one would systematically combine the four NV-methods and 15 subclasses, no less than 60 different types of robots can be designed. Only five of these combinations already exist; i.e.

- Vertical wave rolling with NV-method 1, in the robot of Hariri et al. [23] presented in Section 3.1.1, Fig. 2.
- Running with NV-method 2, in HAMR-VP of Baisch et al. [65] presented in Section 4.1.2, Fig. 9.
- Rebounding with NV-method 2, in the robot of Peters [78] presented in Section 4.1.4, Fig. 11.
- Dynamic walking with NV-method 1, in many of the dynamic walking robots presented in Section 4.2.1, e.g. the robots of McGeer [91, 92] in Fig. 15a and 15b.
- Static walking with NV-method 3, in the standing wave robot of Son et al. [119], presented in Section 4.2.2, Fig. 17a.

Hence, there are still fifty-five different non-existing types of robots to be explored. A systematic approach of combining subclasses and NV-methods gives inspiration for new concepts of robots that can benefit from resonance in all subclasses. In Sections 3 and 4 we showed that exploiting resonance indeed can have great advantages for the robots we presented. Hence, the proposed systematic design approach will give rise to new mobile robots with properties that will potentially overcome the grand challenges in robotics as presented by Yang et al. [15]. We expect that for most of the combinations a design could be developed, serving a wide variety of opportunities and application fields. However, not all combinations will give a fruitful concept. For example, the subclass on singular jumping has a fundamental reason that resonance can not be used, i.e. it does by definition not move continuously, and thus also not periodically.

7. Conclusions

The purpose of this paper is (i) to provide an overview of mobile robots that exploit their resonance for locomotion, (ii)

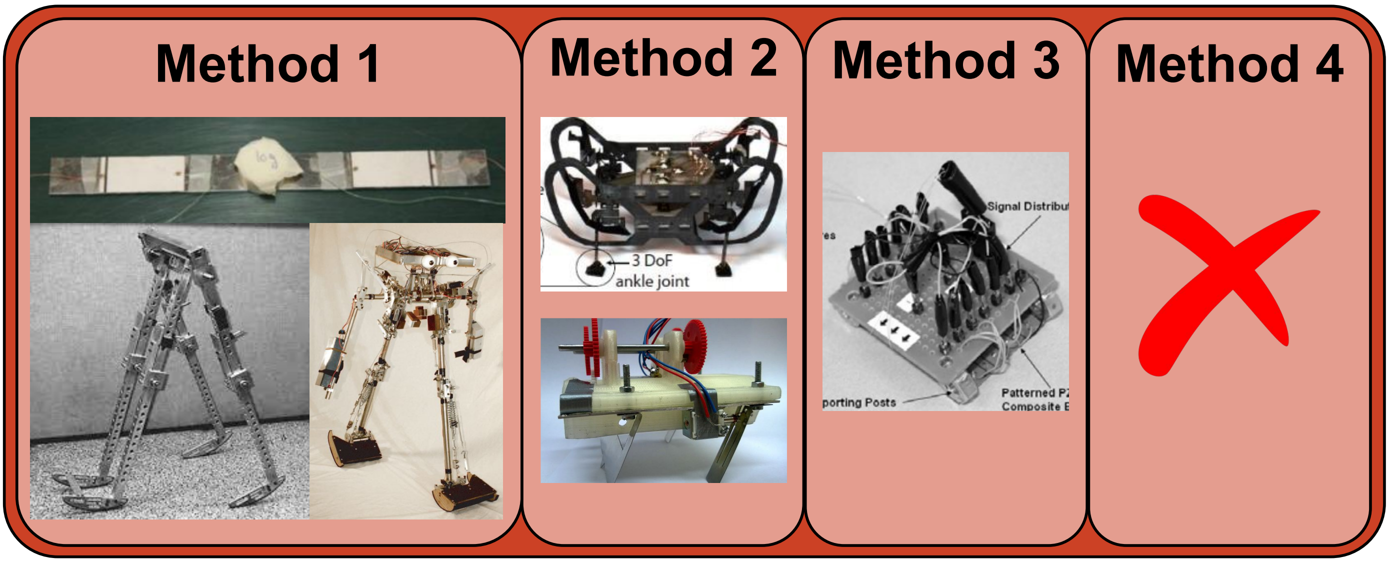

Figure 24: This diagram shows the four options that a mobile robot can use to exploit resonance. For most robots that are examined in the present paper it is shown here which NV-method is used. However, not all dynamic walking robots that use resonance are presented in this diagram, because there are so many. All of the examples mentioned in Section 4.2.1, which are not in this diagram also use NV-method 1. The pictures within this figure have been used previously in this paper in separate figures,, they are courtesy of respectively: Hariri et al. [23], McGeer [92], Collins and Ruina [109], Seitz et al. [62], Peters [78] and Son et al. [119].

to examine their properties with respect to robots that do not use resonance (iii) and to investigate which methods there are to use these vibrations. In order to provide a good overview, a classification for mobile robots is introduced based on their locomotion mechanisms, with as main classes rolling, striding and sliding. The locomotion mechanism of the 15 subclasses is explained with the use of examples of mobile robots that both do, and do not use resonance. The subclasses are chosen such that all robots within the same subclass should be able to use resonance in the same way.

Only in five of the 15 subclasses we found robots that use resonance. The subclass of dynamic walkers contains by far the most examples. For this type of robot very elaborate research has been conducted on the use of resonance. It has been shown that dynamic walkers which exploit resonance can be up to 16 times more efficient than their imposed counterparts. These walkers also prove that with the use of resonance, robots can be actuated in a simpler fashion and their control is easier. Besides that, the traveling wave robot in the undulant rolling class, demonstrates that resonance can be used to convert an oscillating energy source into a desired complex motion. It only needs two vibrating elements to exhibit a traveling wave, for which other robots need either extensive actuation or complex transmission mechanisms. In conclusion, we expect that robots can in general benefit from using resonance. However, we must be careful with expecting that advantages within one subclass, also apply to others.

Moreover, it was found that there are four methods to exploit resonance in mobile robots. A systematic approach is proposed for combining these four NV-methods with the fifteen subclasses that were presented in the present paper. We expect that with this approach novel and unexplored robot concepts can arise, which will potentially overcome the grand challenges of robotics as presented by Yang et al. [15], due to the advantages of resonance.

In future work, it is recommended to extend the presented research to non-terrestrial robots. Especially in the research field of micro air vehicles and micro swimmers the use of resonance is explored elaborately. It would be valuable to investigate the techniques and benefits that are described for robots in these field, and to add it to the present review to obtain a broader overview of the opportunities of resonance.

References

[1] W. Hu, G. Z. Lum, M. Mastrangeli, M. Sitti, Small-scale soft-bodied robot with multimodal locomotion, Nature 554 (2018) 81–85. URL: http://dx.doi.org/10.1038/nature25443. doi:10.1038/nature25443. arXiv:NIHMS150003.

[2] B. J. Nelson, I. K. Kaliakatsos, J. J. Abbott, Microrobots for minimally invasive medicine, Annual review of biomedical engineering 12 (2010) 55–85.

[3] M. Sitti, H. Ceylan, W. Hu, J. Giltinan, M. Turan, S. Yim, E. Diller, Biomedical applications of untethered mobile milli/microrobots, Proceedings of the IEEE 103 (2015) 205–224.

[4] M. Sitti, Miniature devices: Voyage of the microrobots, Nature 458 (2009) 1121.

[5] V. SunSpiral, G. Gorospe, J. Bruce, A. Iscen, G. Korbel, S. Milam, A. Agogino, D. Atkinson, Tensegrity based probes for planetary exploration: Entry, descent and landing (edl) and surface mobility analysis, International Journal of Planetary Probes 7 (2013).

[6] S. H. Collins, A. Ruina, R. Tedrake, M. Wisse, Efficient bipedal robots based on passive-dynamic walkers, Science 307 (2005) 1082–1085.

[7] J. E. Pratt, Exploiting Inherent Robustness and Natural Dynamics in the Control of Bipedal Walking Robots, Ph.D. thesis, Massachusetts Institute of Technology, 2000.

[8] S. Hirose, Three basic types of locomotion in mobile robots, 1991. URL: http://ieeexplore.ieee.org/document/240483/. doi:10.1109/ICAR.1991.240483.

[9] M. H. Dickinson, C. T. Farley, R. J. Full, M. Koehl, R. Kram, S. Lehman, How animals move: an integrative view, science 288 (2000) 100–106.

[10] X. Zhou, S. Bi, A survey of bio-inspired compliant legged robot designs, Bioinspiration & biomimetics 7 (2012) 041001.

[11] D. Rus, M. T. Tolley, Design, fabrication and control of soft robots, Nature 521 (2015) 467.

[12] R. H. Armour, J. F. Vincent, Rolling in nature and robotics: a review, Journal of Bionic Engineering 3 (2006) 195–208.

[13] M. F. Silva, J. T. Machado, J. K. Tar, A survey of technologies for climbing robots adhesion to surfaces, in: 2008 IEEE International Conference on Computational Cybernetics, IEEE, 2008, pp. 127–132.

[14] G. Lee, H. Kim, K. Seo, J. Kim, M. Sitti, T. Seo, Series of multi-linked caterpillar track-type climbing robots, Journal of Field Robotics 33 (2016) 737–750.

[15] G.-Z. Yang, J. Bellingham, P. E. Dupont, P. Fischer, L. Floridi, R. Full, N. Jacobstein, V. Kumar, M. McNutt, R. Merrifield, et al., The grand challenges of science robotics, Science Robotics 3 (2018) eaar7650.

[16] K. E. Peyer, L. Zhang, B. J. Nelson, Bio-inspired magnetic swimming microrobots for biomedical applications, Nanoscale 5 (2013) 1259–1272. doi:10.1039/c2nr32554c.

[17] N. Bertin, T. A. Spelman, O. Stephan, L. Gredy, M. Bouriau, E. Lauga, P. Marmottant, Propulsion of bubble-based acoustic microswimmers, Physical Review Applied 4 (2015) 1–5. doi:10.1103/PhysRevApplied.4.064012.

[18] D. Ahmed, T. Baasch, B. Jang, S. Pane, J. Dual, B. J. Nelson, Artificial Swimmers Propelled by Acoustically Activated Flagella, Nano Letters 16 (2016) 4968–4974. doi:10.1021/acs.nanolett.6b01601.

[19] M. Kaynak, A. Ozcelik, A. Nourhani, P. E. Lammert, V. H. Crespi, T. J. Huang, Acoustic actuation of bioinspired microswimmers, Lab on a Chip 17 (2017) 395–400. doi:10.1039/c6lc01272h.

[20] C. Bolsman, J. Goosen, F. van Keulen, Design Overview of a Resonant Wing Actuation Mechanism for Application in Flapping Wing MAVs, International Journal of Micro Air Vehicles 1 (2009) 263–272.

[21] J. Yan, R. J. Wood, S. Avadhanula, M. Sitti, R. S. Fearing, Towards flapping wing control for a micromechanical flying insect, in: Robotics and Automation, 2001. Proceedings 2001 ICRA. IEEE International Conference on, volume 4, IEEE, 2001, pp. 3901–3908.

[22] C. H. Greenewalt, The Wings of Insects and Birds as Mechanical Oscillators Author (s): Crawford H . Greenewalt, Proceedings of the American Philosophical Society 104 (1960) 605–611.

[23] H. Hariri, Y. Bernard, A. Razek, A traveling wave piezoelectric beam robot, Smart Materials and Structures 23 (2014). doi:10.1088/0964-1726/23/2/025013.

[24] H.-T. Lin, G. G. Leisk, B. Trimmer, Goqbot: a caterpillar-inspired soft-bodied rolling robot, Bioinspiration & biomimetics 6 (2011) 026007.

[25] T. Jansen, Strandbeest evolution, 2017. URL: https://youtu.be/LewVEF2B_pM?t=101.

[26] T. Nakamura, K. Satoh, Development of an omni-directional mobile robot using traveling waves based on snail locomotion, Industrial Robot: An International Journal 35 (2008) 206–210.

[27] C. Wright, A. Johnson, A. Peck, Z. McCord, A. Naaktgeboren, P. Gianfortoni, M. Gonzalez-Rivero, R. Hatton, H. Choset, Design of a modular snake robot, in: Intelligent Robots and Systems, 2007. IROS 2007. IEEE/RSJ International Conference on, IEEE, 2007, pp. 2609–2614.

[28] R. L. Hatton, H. Choset, Generating gaits for snake robots: annealed chain fitting and keyframe wave extraction, Autonomous Robots 28 (2010) 271–281.

[29] S. Seok, C. D. Onal, K.-J. Cho, R. J. Wood, D. Rus, S. Kim, Meshworm: a peristaltic soft robot with antagonistic nickel titanium coil actuators, IEEE/ASME Transactions on mechatronics 18 (2013) 1485–1497.

[30] C. D. Onal, R. J. Wood, D. Rus, An origami-inspired approach to worm robots, IEEE/ASME Transactions on Mechatronics 18 (2013) 430–438.

[31] A. Boxerbaum, H. Chiel, R. Quinn, Softworm: A soft, biologically inspired worm-like robot, in: Neuroscience Abstracts, volume 315, 2009, p. 44106.

[32] A. D. Horchler, A. Kandhari, K. A. Daltorio, K. C. Moses, J. C. Ryan, K. A. Stultz, E. N. Kanu, K. B. Andersen, J. A. Kershaw, R. J. Bachmann, et al., Peristaltic locomotion of a modular mesh-based worm robot: precision, compliance, and friction, Soft Robotics 2 (2015) 135–145.

[33] N. Saga, T. Nakamura, Development of a peristaltic crawling robot using magnetic fluid on the basis of the locomotion mechanism of the earthworm, Smart materials and structures 13 (2004) 566.

[34] A. Bicchi, A. Balluchi, D. Prattichizzo, A. Gorelli, Introducing the" sphericle": an experimental testbed for research and teaching in nonholonomy, in: Robotics and Automation, 1997. Proceedings., 1997 IEEE International Conference on, volume 3, IEEE, 1997, pp. 2620–2625.

[35] R. Mukherjee, M. A. Minor, J. T. Pukrushpan, Simple motion planning strategies for spherobot: a spherical mobile robot, in: Decision and Control, 1999. Proceedings of the 38th IEEE Conference on, volume 3, IEEE, 1999, pp. 2132–2137.

[36] P. Mojabi, et al., Introducing august: a novel strategy for an omnidirectional spherical rolling robot, in: Robotics and Automation, 2002. Proceedings. ICRA'02. IEEE International Conference on, volume 4, IEEE, 2002, pp. 3527–3533.

[37] A. Halme, T. Schonberg, Y. Wang, Motion control of a spherical mobile robot, in: Advanced Motion Control, 1996. AMC'96-MIE. Proceedings., 1996 4th International Workshop on, volume 1, IEEE, 1996, pp. 259–264.

[38] J. Suomela, T. Ylikorpi, Ball-shaped robots: an historical overview and recent developments at tkk, in: Field and service robotics, Springer, 2006, pp. 343–354.

[39] G. Reina, M. Foglia, A. Milella, A. Gentile, Rough-terrain traversability for a cylindrical shaped mobile robot, in: Mechatronics, 2004. ICM'04. Proceedings of the IEEE International Conference on, IEEE, 2004, pp. 148–153.

[40] C. Batten, D. Wentzlaff, Kickbot: a spherical autonomous robot, Massachusetts Institute of Technology (2006).

[41] K. Ioi, H. Igarashi, A. Murakami, Design of a gravitational wheeled robot, Advanced Robotics 16 (2002) 785–793.

[42] H. B. Brown, Y. Xu, A single-wheel, gyroscopically stabilized robot, in: Robotics and Automation, 1996. Proceedings., 1996 IEEE International Conference on, volume 4, IEEE, 1996, pp. 3658–3663.

[43] F. Michaud, S. Caron, Roball, the rolling robot, Autonomous robots 12 (2002) 211–222.

[44] F. Michaud, J.-F. Laplante, H. Larouche, A. Duquette, S. Caron, D. Létourneau, P. Masson, Autonomous spherical mobile robot for child-development studies, IEEE Transactions on Systems, Man, and Cybernetics-Part A: Systems and Humans 35 (2005) 471–480.

[45] Y. Sugiyama, S. Hirai, Crawling and jumping by a deformable robot, The International journal of robotics research 25 (2006) 603–620.

[46] E. Steltz, A. Mozeika, N. Rodenberg, E. Brown, H. M. Jaeger, Jsel: Jamming skin enabled locomotion, in: Intelligent Robots and Systems, 2009. IROS 2009. IEEE/RSJ International Conference on, IEEE, 2009, pp. 5672–5677.

[47] C. D. Onal, X. Chen, G. M. Whitesides, D. Rus, Soft mobile robots with on-board chemical pressure generation, in: Robotics Research, Springer, 2017, pp. 525–540.

[48] J. Brackenbury, Caterpillar kinematics, Nature 390 (1997) 453.

[49] C. Paul, F. J. Valero-Cuevas, H. Lipson, Design and control of tensegrity robots for locomotion, IEEE Transactions on Robotics 22 (2006) 944–957.

[50] A. Iscen, A. Agogino, V. SunSpiral, K. Tumer, Flop and roll: Learning robust goal-directed locomotion for a tensegrity robot, in: Intelligent Robots and Systems (IROS 2014), 2014 IEEE/RSJ International Conference on, IEEE, 2014, pp. 2236–2243.

[51] K. Caluwaerts, J. Despraz, A. Işçen, A. P. Sabelhaus, J. Bruce, B. Schrauwen, V. SunSpiral, Design and control of compliant tensegrity robots through simulation and hardware validation, Journal of the royal society interface 11 (2014) 20140520.

[52] Y. Koizumi, M. Shibata, S. Hirai, Rolling tensegrity driven by pneumatic soft actuators, in: Robotics and Automation (ICRA), 2012 IEEE International Conference on, IEEE, 2012, pp. 1988–1993.

[53] L.-H. Chen, K. Kim, E. Tang, K. Li, R. House, E. L. Zhu, K. Fountain, A. M. Agogino, A. Agogino, V. Sunspiral, et al., Soft spherical tensegrity robot design using rod-centered actuation and control, Journal of Mechanisms and Robotics 9 (2017) 025001.

[54] J. Bruce, K. Caluwaerts, A. Iscen, A. P. Sabelhaus, V. SunSpiral, Design and evolution of a modular tensegrity robot platform, in: Robotics and Automation (ICRA), 2014 IEEE International Conference on, IEEE, 2014, pp. 3483–3489.

[55] V. SunSpiral, A. Agogino, D. Atkinson, Super ball bot-structures for planetary landing and exploration, niac phase 2 final report, NASA In-

novative Advanced Concepts (NIAC) Program, Phase 2, Final Report (2015).

[56] A. P. Sabelhaus, J. Bruce, K. Caluwaerts, P. Manovi, R. F. Firoozi, S. Dobi, A. M. Agogino, V. SunSpiral, System design and locomotion of superball, an untethered tensegrity robot, in: Robotics and Automation (ICRA), 2015 IEEE International Conference on, IEEE, 2015, pp. 2867–2873.

[57] S. Hyon, T. Emura, T. Mita, Dynamics-based control of a one-legged hopping robot, Proceedings of the Institution of Mechanical Engineers, Part I: Journal of Systems and Control Engineering 217 (2003) 83–98.

[58] B. Brown, G. Zeglin, The bow leg hopping robot, in: Proceedings. 1998 IEEE International Conference on Robotics and Automation (Cat. No. 98CH36146), volume 1, IEEE, 1998, pp. 781–786.

[59] M. Ahmadi, M. Buehler, The arl monopod ii running robot: Control and energetics, in: Robotics and Automation, 1999. Proceedings. 1999 IEEE International Conference on, volume 3, IEEE, 1999, pp. 1689–1694.

[60] A. T. Baisch, R. J. Wood, Design and fabrication of the harvard ambulatory micro-robot, in: Robotics Research, Springer, 2011, pp. 715–730.

[61] A. T. Baisch, C. Heimlich, M. Karpelson, R. J. Wood, Hamr3: An autonomous 1.7 g ambulatory robot, in: Intelligent Robots and Systems (IROS), 2011 IEEE/RSJ International Conference on, IEEE, 2011, pp. 5073–5079.

[62] B. F. Seitz, B. Goldberg, N. Doshi, O. Ozcan, D. L. Christensen, E. W. Hawkes, M. R. Cutkosky, R. J. Wood, Bio-inspired mechanisms for inclined locomotion in a legged insect-scale robot, 2014 IEEE International Conference on Robotics and Biomimetics, IEEE ROBIO 2014 (2014) 791–796. doi:10.1109/ROBIO.2014.7090428.

[63] Y. Chen, N. Doshi, B. Goldberg, H. Wang, R. J. Wood, Controllable water surface to underwater transition through electrowetting in a hybrid terrestrial-aquatic microrobot, Nature Communications 9 (2018) 1–11. URL: http://dx.doi.org/10.1038/s41467-018-04855-9. doi:10.1038/s41467-018-04855-9.

[64] S. D. de Rivaz, B. Goldberg, N. Doshi, K. Jayaram, J. Zhou, R. J. Wood, Inverted and vertical climbing of a quadrupedal microrobot using electroadhesion, Science Robotics 3 (2018) eaau3038.

[65] A. T. Baisch, O. Ozcan, B. Goldberg, D. Ithier, R. J. Wood, High speed locomotion for a quadrupedal microrobot, International Journal of Robotics Research 33 (2014) 1063–1082. doi:10.1177/0278364914521473.

[66] B. Goldberg, N. Doshi, K. Jayaram, R. J. Wood, Gait studies for a quadrupedal microrobot reveal contrasting running templates in two frequency regimes, Bioinspiration & biomimetics 12 (2017) 046005.

[67] S. A. Rios, A. J. Fleming, Y. K. Yong, Miniature resonant ambulatory robot, IEEE Robotics and Automation Letters 2 (2017) 337–343.

[68] P. Birkmeyer, K. Peterson, R. S. Fearing, Dash: A dynamic 16g hexapedal robot, in: Intelligent Robots and Systems, 2009. IROS 2009. IEEE/RSJ International Conference on, IEEE, 2009, pp. 2683–2689.

[69] S. Feng, E. Whitman, X. Xinjilefu, C. G. Atkeson, Optimization based full body control for the atlas robot, in: Humanoid Robots (Humanoids), 2014 14th IEEE-RAS International Conference on, IEEE, 2014, pp. 120–127.

[70] S. Kuindersma, R. Deits, M. Fallon, A. Valenzuela, H. Dai, F. Permenter, T. Koolen, P. Marion, R. Tedrake, Optimization-based locomotion planning, estimation, and control design for the atlas humanoid robot, Autonomous Robots 40 (2016) 429–455.

[71] J. Estremera, K. J. Waldron, Thrust control, stabilization and energetics of a quadruped running robot, The International Journal of Robotics Research 27 (2008) 1135–1151.

[72] S. Kim, J. E. Clark, M. R. Cutkosky, isprawl: Design and tuning for high-speed autonomous open-loop running, The International Journal of Robotics Research 25 (2006) 903–912.

[73] I. Poulakakis, J. A. Smith, M. Buehler, Modeling and experiments of untethered quadrupedal running with a bounding gait: The scout ii robot, The International Journal of Robotics Research 24 (2005) 239–256.

[74] P. Eckert, A. Spröwitz, H. Witte, A. J. Ijspeert, Comparing the effect of different spine and leg designs for a small bounding quadruped robot, in: Robotics and Automation (ICRA), 2015 IEEE International Conference on, IEEE, 2015, pp. 3128–3133.

[75] S. Seok, A. Wang, M. Y. Chuah, D. Otten, J. Lang, S. Kim, Design principles for highly efficient quadrupeds and implementation on the mit cheetah robot, in: Robotics and Automation (ICRA), 2013 IEEE International Conference on, IEEE, 2013, pp. 3307–3312.

[76] S. Seok, A. Wang, M. Y. M. Chuah, D. J. Hyun, J. Lee, D. M. Otten, J. H. Lang, S. Kim, Design principles for energy-efficient legged locomotion and implementation on the mit cheetah robot, IEEE/ASME Transactions on Mechatronics 20 (2015) 1117–1129.

[77] M. Rubenstein, C. Ahler, R. Nagpal, Kilobot: A low cost scalable robot system for collective behaviors, in: Robotics and Automation (ICRA), 2012 IEEE International Conference on, IEEE, 2012, pp. 3293–3298.

[78] H. J. Peters, A controllability approach for resonant compliant systems: applied to a flapping wing micro air vehicle, Ph.D. thesis, Delft University of Technology, 2016.

[79] I. Slavkov, D. Carrillo-Zapata, N. Carranza, X. Diego, F. Jansson, J. Kaandorp, S. Hauert, J. Sharpe, Morphogenesis in robot swarms, Science Robotics 3 (2018) eaau9178.

[80] S. Miyashita, S. Guitron, M. Ludersdorfer, C. R. Sung, D. Rus, An untethered miniature origami robot that self-folds, walks, swims, and degrades, Robotics and Automation (ICRA), 2015 IEEE International Conference on (2015) 1490–1496.

[81] M. T. Tolley, R. F. Shepherd, M. Karpelson, N. W. Bartlett, K. C. Galloway, M. Wehner, R. Nunes, G. M. Whitesides, R. J. Wood, An untethered jumping soft robot, IEEE International Conference on Intelligent Robots and Systems (2014) 561–566. doi:10.1109/IROS.2014.6942615.

[82] N. W. Bartlett, M. T. Tolley, J. T. Overvelde, J. C. Weaver, B. Mosadegh, K. Bertoldi, G. M. Whitesides, R. J. Wood, A 3d-printed, functionally graded soft robot powered by combustion, Science 349 (2015) 161–165.

[83] D. W. Haldane, M. M. Plecnik, J. K. Yim, R. S. Fearing, Robotic vertical jumping agility via series-elastic power modulation, Science Robotics 1 (2016) eaag2048. URL: http://robotics.sciencemag.org/lookup/doi/10.1126/scirobotics.aag2048. doi:10.1126/scirobotics.aag2048.

[84] G. T. Fallis, Walking toy, U.S. Patent 376588 (1888).

[85] B. B. Bechstein, P. O. Uhlig, Improvements in and relating to toys, U.K. Patent No. 7453 (1912).

[86] J. J. Mahan, Walking toy, U.S. Patent No. 1007316, Serial Nos. 541801 and 796095 (1914).

[87] H. Allison, Toy, U.S. Patent No. 1207464, Serial No. 825444 (1916).

[88] J. E. Wilson, Walking toy, U.S. Patent No. 2140275, Serial No. 105763 (1938).

[89] M. J. Coleman, A. Ruina, An uncontrolled walking toy that cannot stand still, Physical Review Letters 80 (1998) 3658.

[90] M. J. Coleman, M. Garcia, K. Mombaur, A. Ruina, Prediction of stable walking for a toy that cannot stand, Physical Review E 64 (2001) 022901.

[91] T. McGeer, et al., Passive dynamic walking, I. J. Robotic Res. 9 (1990) 62–82.

[92] T. McGeer, Passive walking with knees, in: Proceedings., IEEE International Conference on Robotics and Automation, IEEE, 1990, pp. 1640–1645.

[93] T. McGeer, Stability and control of two-dimensional biped walking, Center for Systems Science, Simon Fraser University, Burnaby, BC, Canada, Technical Report 1 (1988).

[94] T. McGeer, Dynamics and control of bipedal locomotion, Journal of Theoretical Biology 163 (1993) 277–314.

[95] T. Mita, T. Yamaguchi, T. Kashiwase, T. Kawase, Realization of a high speed biped using modern control theory, International Journal of Control 40 (1984) 107–119.

[96] J. Furusho, A. Sano, Sensor-based control of a nine-link biped, The International Journal of Robotics Research 9 (1990) 83–98.

[97] H. Miura, I. Shimoyama, Dynamic walk of a biped, The International Journal of Robotics Research 3 (1984) 60–74.

[98] A. Goswami, B. Espiau, A. Keramane, Limit cycles in a passive compass gait biped and passivity-mimicking control laws, Autonomous Robots 4 (1997) 273–286.

[99] M. Garcia, A. Chatterjee, A. Ruina, Speed, efficiency, and stability of small-slope 2d passive dynamic bipedal walking, in: Robotics and Automation, 1998. Proceedings. 1998 IEEE International Conference on, volume 3, IEEE, 1998, pp. 2351–2356.

[100] M. Garcia, A. Chatterjee, A. Ruina, M. Coleman, The simplest walking model: stability, complexity, and scaling, Journal of biomechanical engineering 120 (1998) 281–288.

[101] A. Goswami, Postural stability of biped robots and the foot-rotation indicator (fri) point, The International Journal of Robotics Research 18 (1999) 523–533.

[102] A. D. Kuo, Stabilization of lateral motion in passive dynamic walking, The International journal of robotics research 18 (1999) 917–930.

[103] M. Wisse, A. L. Schwab, et al., A 3d passive dynamic biped with yaw and roll compensation, Robotica 19 (2001) 275–284.

[104] S. H. Collins, M. Wisse, A. Ruina, A three-dimensional passive-dynamic walking robot with two legs and knees, The International Journal of Robotics Research 20 (2001) 607–615.

[105] H. Dankowicz, J. Adolfsson, A. B. Nordmark, Repetitive gait of passive bipedal mechanisms in a three-dimensional environment, Journal of biomechanical engineering 123 (2001) 40–46.

[106] J. Adolfsson, H. Dankowicz, A. Nordmark, 3d passive walkers: Finding periodic gaits in the presence of discontinuities, Nonlinear Dynamics 24 (2001) 205–229.

[107] T. Chyou, G. Liddell, M. Paulin, An upper-body can improve the stability and efficiency of passive dynamic walking, Journal of theoretical biology 285 (2011) 126–135.

[108] M. Gomes, A. Ruina, Walking model with no energy cost, Physical Review E 83 (2011) 032901.

[109] S. H. Collins, A. Ruina, A bipedal walking robot with efficient and human-like gait, in: Robotics and Automation, 2005. ICRA 2005. Proceedings of the 2005 IEEE International Conference on, IEEE, 2005, pp. 1983–1988.

[110] M. Wisse, J. Van Frankenhuyzen, Design and construction of mike; a 2-d autonomous biped based on passive dynamic walking, in: Adaptive motion of animals and machines, Springer, 2006, pp. 143–154.

[111] M. Wisse, A. L. Schwab, R. Q. van der Linde, F. C. van der Helm, How to keep from falling forward: elementary swing leg action for passive dynamic walkers, IEEE Transactions on robotics 21 (2005) 393–401.

[112] R. Tedrake, T. W. Zhang, M.-f. Fong, H. S. Seung, Actuating a simple 3d passive dynamic walker, in: Robotics and Automation, 2004. Proceedings. ICRA'04. 2004 IEEE International Conference on, volume 5, IEEE, 2004, pp. 4656–4661.

[113] K. Hirai, M. Hirose, Y. Haikawa, T. Takenaka, The development of honda humanoid robot, in: Robotics and Automation, 1998. Proceedings. 1998 IEEE International Conference on, volume 2, IEEE, 1998, pp. 1321–1326.

[114] Y. Sakagami, R. Watanabe, C. Aoyama, S. Matsunaga, N. Higaki, K. Fujimura, The intelligent asimo: System overview and integration, in: Intelligent Robots and Systems, 2002. IEEE/RSJ International Conference on, volume 3, IEEE, 2002, pp. 2478–2483.

[115] J. Chestnutt, M. Lau, G. Cheung, J. Kuffner, J. Hodgins, T. Kanade, Footstep planning for the honda asimo humanoid, in: Robotics and Automation, 2005. ICRA 2005. Proceedings of the 2005 IEEE International Conference on, IEEE, 2005, pp. 629–634.

[116] J. E. Pratt, G. A. Pratt, Exploiting natural dynamics in the control of a planar bipedal walking robot, in: Proceedings of the Annual Allerton Conference on Communication Control and Computing, volume 36, Citeseer, 1998, pp. 739–748.

[117] J. Pratt, G. Pratt, Intuitive control of a planar bipedal walking robot, in: ICRA, 1998, pp. 2014–2021.

[118] J. Pratt, G. Pratt, Exploiting natural dynamics in the control of a 3d bipedal walking simulation, in: Proceedings of the International Conference on Climbing and Walking Robots (CLAWAR99), 1999, pp. 1–11.

[119] K. J. Son, V. Kartik, J. A. Wickert, M. Sitti, An ultrasonic standing-wave-actuated nano-positioning walking robot: piezoelectric-metal composite beam modeling, Journal of vibration and control 12 (2006) 1293–1309.

[120] K. L. Hoffman, R. J. Wood, Myriapod-like ambulation of a segmented microrobot, Autonomous Robots 31 (2011) 103–114. doi:`10.1007/s10514-011-9233-4`.

[121] K. L. Hoffman, R. J. Wood, Passive undulatory gaits enhance walking in a myriapod millirobot, IEEE International Conference on Intelligent Robots and Systems 2 (2011) 1479–1486. doi:`10.1109/IROS.2011.6048268`.

[122] K. L. Hoffman, R. J. Wood, Turning gaits and optimal undulatory gaits for a modular centipede-inspired millirobot, Proceedings of the IEEE RAS and EMBS International Conference on Biomedical Robotics and Biomechatronics (2012) 1052–1059. doi:`10.1109/BioRob.2012.6290288`.

[123] S. He, W. Chen, X. Tao, Z. Chen, Standing wave bi-directional linearly moving ultrasonic motor, IEEE transactions on ultrasonics, ferroelectrics, and frequency control 45 (1998) 1133–1139.

[124] U. Saranli, M. Buehler, D. E. Koditschek, Rhex: A simple and highly mobile hexapod robot, The International Journal of Robotics Research 20 (2001) 616–631.

[125] R. Altendorfer, N. Moore, H. Komsuoglu, M. Buehler, H. Brown, D. McMordie, U. Saranli, R. Full, D. E. Koditschek, Rhex: A biologically inspired hexapod runner, Autonomous Robots 11 (2001) 207–213.

[126] M. Raibert, K. Blankespoor, G. Nelson, R. Playter, Bigdog, the rough-terrain quadruped robot, IFAC Proceedings Volumes 41 (2008) 10822–10825.

[127] H. Lu, M. Zhang, Y. Yang, Q. Huang, T. Fukuda, Z. Wang, Y. Shen, A bioinspired multilegged soft millirobot that functions in both dry and wet conditions, Nature communications 9 (2018) 3944.

[128] J.-S. Koh, K.-J. Cho, Omegabot: Biomimetic inchworm robot using sma coil actuator and smart composite microstructures (scm), in: Robotics and Biomimetics (ROBIO), 2009 IEEE International Conference on, IEEE, 2009, pp. 1154–1159.

[129] J.-S. Koh, K.-J. Cho, Omegabot: Crawling robot inspired by ascotis selenaria, in: Robotics and Automation (ICRA), 2010 IEEE International Conference on, IEEE, 2010, pp. 109–114.

[130] W. Wang, J.-Y. Lee, H. Rodrigue, S.-H. Song, W.-S. Chu, S.-H. Ahn, Locomotion of inchworm-inspired robot made of smart soft composite (ssc), Bioinspiration & biomimetics 9 (2014) 046006.

[131] S. M. Felton, M. T. Tolley, C. D. Onal, D. Rus, R. J. Wood, Robot self-assembly by folding: A printed inchworm robot, in: Robotics and Automation (ICRA), 2013 IEEE International Conference on, IEEE, 2013, pp. 277–282.

[132] F. Moreira, A. Abundis, M. Aguirre, J. Castillo, P. A. Bhounsule, An inchworm-inspired robot based on modular body, electronics and passive friction pads performing the two-anchor crawl gait, Journal of Bionic Engineering 15 (2018) 820–826.

[133] J. Lim, H. Park, J. An, Y.-S. Hong, B. Kim, B.-J. Yi, One pneumatic line based inchworm-like micro robot for half-inch pipe inspection, Mechatronics 18 (2008) 315–322.

[134] A. Rafsanjani, Y. Zhang, B. Liu, S. M. Rubinstein, K. Bertoldi, Kirigami skins make a simple soft actuator crawl, Science Robotics 3 (2018) eaar7555.

[135] S. Hirose, Biologically inspired robots: snake-like locomotors and manipulators, volume 1093, Oxford University Press Oxford, 1993.

[136] M. Saito, M. Fukaya, T. Iwasaki, Modeling, analysis, and synthesis of serpentine locomotion with a multilink robotic snake, IEEE control systems magazine 22 (2002) 64–81.

[137] Z. Y. Bayraktaroglu, Snake-like locomotion: Experimentations with a biologically inspired wheel-less snake robot, Mechanism and Machine Theory 44 (2009) 591–602.

[138] A. Maity, S. Majumder, S. Ghosh, Serpentine robot locomotion: Implementation through simulation, International Journal of Innovative Technology and Creative Engineering 1 (2011) 58–63.

[139] B. Klaassen, K. L. Paap, Gmd-snake2: a snake-like robot driven by wheels and a method for motion control, in: Robotics and Automation, 1999. Proceedings. 1999 IEEE International Conference on, volume 4, IEEE, 1999, pp. 3014–3019.

[140] A. Crespi, A. Badertscher, A. Guignard, A. J. Ijspeert, Amphibot i: an amphibious snake-like robot, Robotics and Autonomous Systems 50 (2005) 163–175.

[141] A. Crespi, A. J. Ijspeert, Amphibot ii: An amphibious snake robot that crawls and swims using a central pattern generator, in: Proceedings of the 9th international conference on climbing and walking robots (CLAWAR 2006), BIOROB-CONF-2006-001, 2006, pp. 19–27.

[142] A. J. Ijspeert, A. Crespi, D. Ryczko, J.-M. Cabelguen, From swimming to walking with a salamander robot driven by a spinal cord model, science 315 (2007) 1416–1420.

[143] A. Crespi, A. J. Ijspeert, Salamandra robotica: a biologically inspired amphibious robot that swims and walks, in: Artificial Life Models in Hardware, Springer, 2009, pp. 35–64.

[144] A. Crespi, K. Karakasiliotis, A. Guignard, A. J. Ijspeert, Salamandra robotica ii: an amphibious robot to study salamander-like swimming and walking gaits, IEEE Transactions on Robotics 29 (2013) 308–320.

[145] C. Iverach-Brereton, A. Winton, J. Baltes, Ice skating humanoid robot, in: Conference Towards Autonomous Robotic Systems, Springer, 2012, pp. 209–219.

Chapter 3

Technical Paper

The article presented in this chapter describes the research that was done in the design phase of this thesis. It presents the design and experimental results of the robot that was built, which is called FARbot; a Frequency Actuated Resonant robot.

The design of a monolithic, compliant, resonant running robot at insect scale

J. K. Schonebaum, F. Alijani, G. Radaelli

Department of Precision and Microsystems Engineering, Faculty of Mechanical Engineering and Marine Technology, Delft University of Technology, The Netherlands

---

Abstract

Running robots at insect scale are an upcoming research field, because of their numerous potential applications like exploration of hazardous environments such as collapsed buildings, natural disaster sites and debris. To date no report exists on such a robot that either exploits its resonance, or that is monolithic. These properties, however, could improve the performance of these robotic insects in terms of efficiency, actuation complexity, manufacturing tolerance, suitability for rapid prototyping, large number reproduction and miniaturization. This article presents the monolithic design of FARbot; a Frequency Actuated Resonant robot that uses resonance to increase its stride length and consists of one single piece. To achieve the design of FARbot a novel design methodology is presented and utilized to systematically obtain the necessary compliant mechanism that resonates in a desired motion and at a desired frequency. The final design has been manufactured monolithically from the material HTM140-V2 using digital light processing 3D-printing technology. In terms of production time FARbot outperforms all other robots in this research field. An earlier produced, non-monolithic prototype shows resonance at the desired eigenfrequency at which its stride length is amplified by a maximum factor of 22.74 for constant energy demand. This proves the benefit of using resonance and also validates the proposed design methodology.

Keywords: Resonance, Robotics, Eigenfrequency, Monolithic, Compliant

---

1. Introduction

Over the past decade, there has been an increasing interest in insect-like, autonomous running robots. Their small size and low mass give them numerous advantages over larger robots, such as navigation into confined spaces, high agility, the ability to climb obstacles and survive falls. These properties give opportunities for many applications. For example, they can be used to explore hazardous environments like collapsed or damaged buildings, natural disaster sites, debris and war zones, where wheeled or bigger robots can not operate. When equipped with the right sensors, they can also detect hazards as chemical toxicity and extreme temperatures, assist in rescue escorts by locating survivors, and carry out measurements for research of environments in general. Most of these applications could be carried out even more effectively if these robots operate in a group using SWARM technology [1].

The current state of the art of these robotic insects shows already many of the potential benefits. The 10cm robot of Birkmeyer et al. [2] for example, is able to mount obstacles higher than its own body, demonstrating the ability of traversing rough terrain. It is capable of surviving collisions with the ground after a fall of 28m, at which it reaches its terminal velocity, which shows the favorable strength to weight ratio at this scale. Moreover, the 10cm robot of Haldane et al. [3], obtains speeds 27 body lengths per second (BL/s), demonstrating the high potential in terms of velocity as this reaches to the velocity cockroaches (50 BL/s) [4]. Furthermore, Baisch et al. [5] show that their 4.4cm robot can perform multiple gaits, which proves the capability to navigate in different environments and on different surfaces. Lastly, Slavkov et al. [6] present experiments with SWARM technology with the robot of Rubenstein et al. [7].

Main challenges associated with designing robots at insect scale are the efficiency [2, 3, 8], actuation [9] and manufacturing [10, 11]. The small scale of the robots increases complexity of energy supply, mechanical design and, control and actuation of the robot. Also, these so-called meso scale devices remain difficult to produce, and manufacturing difficulty increases even more with miniaturization. This is a drawback for prototyping and makes production in big quantities nearly impossible. To be suitable for application in large quantities and thus in SWARM technology, the robots should be easy and cheap to reproduce.

We propose two novel solutions to overcome these challenges. First, with a resonant design we expect to increase efficiency and improve actuation simplicity. Second, we suggest a monolithic design that requires no manual assembly steps, simplifying production and improving tolerances and therefore, making the robots more suitable for miniaturization. These solutions are further explained in the remainder of this section, together with additional advantages they introduce. The solutions are implemented in the design of our test platform 'FARbot', a Frequency Actuated Resonant robot.

To improve efficiency, this article proposes the use of full body resonance for amplification of the stride length. When a

---

Email address: `j.k.schonebaum@student.tudelft.nl` (J. K. Schonebaum)

system moves in its eigenfrequency, it is most power efficient, because the inertial and the potential forces cancel each other out. Therefore, the costs of accelerating and decelerating the legs is reduced to a minimum. FARbot is designed such that its first eigenmode exhibits the horizontal motion of all four legs, which means that its stride length increases when it is actuated at its first eigenfrequency. This results either in an increase of velocity for constant energy demand or a reduction of energy demand for the same velocity. Also, it implies that FARbot only needs one actuator for the generation of the horizontal motion of its four legs.

The idea of using resonance can already be found in literature on prior robots in various fields. Baisch et al. [5] found that their quadrupedal robot HAMR-VP runs fastest when it is actuated at the natural frequency of the suspension of its legs. It was however not intentionally designed for that purpose, therefore they recommend to include resonance in the design. Moreover, the hexapedal robot MinRAR of Rios et al. [11] makes use of the first two eigenfrequencies of the leg suspension to obtain the desired foot trajectory. In other research fields, like micro air vehicles [12, 13] and bipedal walking robots [14], the idea of intentional design for the use of resonance is investigated and used to be more efficient and simpler in terms of actuation. A review of these and other terrestrial robots that exploit resonance and the benefits thereof is presented in [15].

Increasing the stride length is found to be an effective approach to improve the running performance in research on insects and in particular the American cockroach *Periplaneta americana*. This animal attains its highest speed by increasing its stride length, whereas an increased stride frequency showed little effect on speed [4].

To make the robot easy and cheap to manufacture, we propose a monolithic mechanical design, with which we mean that the mechanical body of the robot consists of one single piece and one material. The mechanical body includes all mechanisms and all moving parts, it only excludes the actuators and electronics. Such a monolithic design can improve the robot in terms of manufacturing complexity, production tolerances, rapid prototyping, large number reproduction and miniaturization opportunities.

In the field of terrestrial robots at this scale, no literature was found about robots that are fully monolithic. Sreetharan et al. [10] however, introduce a manufacturing technique for an insect scale air vehicle called PC-MEMS, which is loosely based on printed circuit board manufacturing techniques. They define this technique as monolithic, however they make use of several materials and it includes steps as folding and locking of miniature parts. As mentioned before, our definition of monolithic implies usage of one material only.

FARbot is designed such that it's mechanical body consists of one material and one piece, and that zero manual assembly steps are required after production in a 3D printer. Only electrical parts have to be assembled after production of the monolithic body. Production of the prototypes is carried out on lithography based 3D-printers of EnvisionTEC, that use digital light processing (DLP) with an enhanced resolution module (ERM) and anti aliasing technology to obtain resolution of 25-30 μm. With the reported production method and material, you do need some post processing to remove the support material.

To design a system that is both resonant and monolithic, we propose to use theory of compliant mechanisms [16–18]. A compliant mechanism obtains its functionality through elastic deformation, i.e. conventional hinges and joints are replaced by flexible counterparts. These flexible parts can be integrated in a monolithic design, while their stiffness can be tuned to meet a desired eigenfrequency. A compliant design also adds other general advantages to the robot, because compliant mechanisms don't wear, have no backlash, are suitable for miniaturization and they don't require lubricants.

The focus of this research is twofold: it is on the design and testing of the resonant mechanism of FARbot, and on designing and producing it monolithically. The first eigenmode of the robot increases the stride length at a desired eigenfrequency. The monolithic design enables the body of the robot to be printed in one piece on a 3D printer. The design of FARbot that is presented in this article is an iteration of a primary design. The results of both FARbot and the primary design are presented.

The method section begins with an overview of the entire mechanical design and explains top level design choices. After, we describe the five-step methodology that is used to obtain the resonant design of the mechanism that generates horizontal motion of the feet. These five steps are carried out in Sections 2.3 - 2.7. Part of which is explanation on the monolithic design, described in Section 2.5. Next, the other mechanisms of the robot are discussed. Section 3 presents the results on (i) modeling and simulation, (ii) the primary design and prototype of FARbot, (iii) monolithic experiments and (iv) the design and kinematics of FARbot. All results and choices are discussed in Section 4. In that section we also make recommendations for future work. Finally, the main conclusions of this work are presented in Section 5.

2. Method: Design

This section presents the method to design FARbot, which has as main requirements that it must have increased stride length when resonating and that it is monolithic and compliant.

This section is structured as follows, first an overview of the mechanical design is given. Second, we explain the five step method that we use to develop the resonant design of the mechanism that generates the horizontal motion of the feet. This part includes the actuation choice, the description of the monolithic design and the method to optimize it for a desired system eigenfrequency. Afterwards, we present the mechanism that generates the vertical motion of the feet, and eventually, the compliant mechanism that couples the vertical and horizontal motion is discussed.

2.1. Overview of mechanical design

The mechanical design of FARbot can be divided into seven main parts or mechanisms, i.e. the horizontal motion mechanism, the vertical motion mechanism, the center body, the two coupling mechanisms and the two leg pairs. Figure 1 shows an overview of the entire mechanical design.

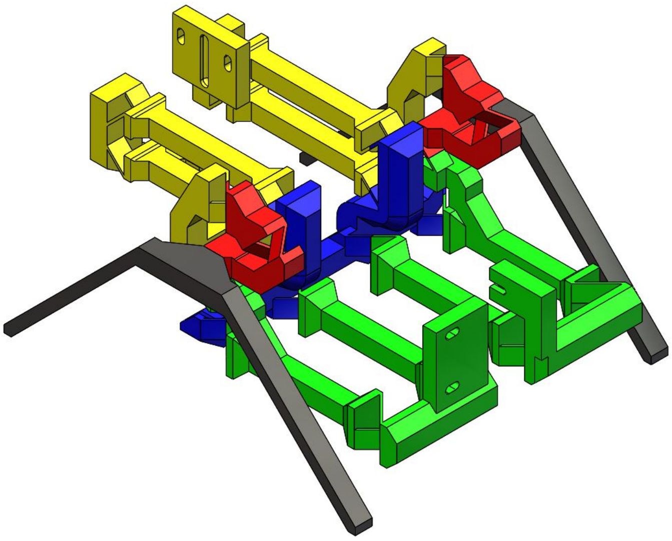

Figure 1: An overview of the entire monolithic mechanical design of FARbot. The horizontal motion mechanism is colored green, the vertical motion mechanism yellow, the center body is blue, the two coupling mechanisms are red and the two leg pairs are colored black.

2.1.1. *Four legs*

A quadrupedal design was chosen for FARbot, because it provides passive stability with a minimal number of legs. From a stability perspective the robot must have more than two legs to ensure passive stability. In terms of complexity, the lowest number of leg pairs is preferable, which is two for passive stability. Several insects and other running robots use six legs, because that provides a tripod[1] gait, which is sometimes presented to be necessary for stable locomotion. Nevertheless, the cockroach Periplaneta americana demonstrates that this is not always optimal for fast locomotion. Even though it has six legs, it switches to quadrupedal or bipedal running when reaching highest velocities up to 50 body lengths per second (BL/s) [4]. This indicates that four legs suffice for running.

2.1.2. *Stride mechanism*

The feet of FARbot simultaneously make an elliptical motion in the sagittal plane, and are diagonally synchronized. This means that the left foreleg and right hind leg move in sync and in anti-phase with the other two legs, see Figure 2. The elliptical motion can be divided into a horizontal and a vertical component for which two separate mechanisms are designed. The mechanisms both generate their motion direction of all four feet with just one actuator. They are actuated with 90° phase difference to obtain the elliptical motion and mixed with a coupling mechanism.

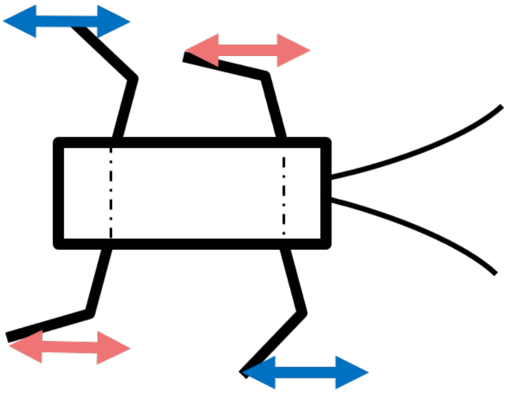

Figure 2: The motion that the horizontal mechanism must exhibit when it resonates. The left foreleg and the right hind leg move synchronously, and in anti-phase with respect to the other two legs.

This separation permits that resonance increases the stride length, without increasing the height. That is because the mechanism that generates the horizontal motion is designed to resonate at the stride frequency of FARbot, while the vertical is not. This way, the elliptical trajectory of the feet widens. The coupling mechanism is designed in such a way that minimal dynamic interaction between the two motion mechanisms occurs.

2.2. *Method to obtain resonant motion*

In order to design a compliant mechanism that resonates with a desired motion in a desired frequency, we propose a systematic design methodology. It consists of five consecutive steps:

1. Define a desired output motion and eigenfrequency
2. Choose an actuation type and design a kinematic model that carries out the desired output upon actuation
3. Convert the kinematic model to a compliant design
4. Derive the eigenmodes and eigenfrequencies of the system
5. Optimize the stiffness of the compliant parts to match the desired eigenfrequency

Throughout the next five subsections this methodology is more extensively explained and used as a guidance to obtain the resonant mechanism that generates the horizontal motion of FARbot.

2.3. *Step 1: Desired output motion and eigenfrequency*

The horizontal motion mechanism of FARbot is desired to move periodically as described in Section 2.1.2. Hence, it should simultaneously provide the horizontal motion of all four legs, see Figure 2.

The eigenfrequency for the suspension mechanism determines the stride frequency of FARbot, and is chosen to be 15Hz. This frequency is partially inspired by the stride frequency of cockroaches of around 10Hz [19]. Our first prototype though, had a 12Hz eigenfrequency, and demonstrated that a design with higher frequency benefits in terms of robustness and dimension. These results are presented in the results section.

---

[1] A tripod gait means that there are always three points of contact with the ground while moving.

2.4. Step 2: Kinematic design and actuation

The second step in the design method is to make a kinematic design that can achieve the desired output motion, and to choose the type of actuation. As the actuation and kinematic mechanism depend on each other, these are chosen within the same step. The kinematic design should have the desired motion output as its only degree of freedom (DOF) that can be actuated. This makes the motion a full body eigenmode.

For a few reasons it is beneficial to design a mechanism that uses a full body eigenmode rather than higher eigenmodes of individual parts (e.g. legs). First, a full body eigenmode that performs the desired motion of all four legs, implies that only one actuator is needed for all legs. As long as the energy source supplies its power at eigenfrequency and not perpendicular to the direction of the eigenmode, the robot will exhibit the motion. This gives opportunities for simplification and miniaturization of actuation, and eventually even for external untethered energy supply. Second, a full body resonance is beneficial over individually resonating parts from a manufacturing point of view, and in particular because of production tolerances. Eigenfrequencies are very sensitive to production errors, therefore it is likely that the individual components do not end up having the exact same resonance frequency, e.g. [5, 11], which can result in undesired running behavior. Conversely, when full body resonance is used, all four legs automatically move in the same frequency, even if this frequency is slightly different than the intended frequency due to manufacturing imperfections. Another reason is that an eigenmode with greater generalized mass can store more energy in a resonant motion at a certain desired eigenfrequency and motion amplitude. The generalized mass of the eigenmode is higher for full body resonance than for individually resonating parts. When the desired eigenfrequency of the system is to be constant, the generalized stiffness increases proportionally to the generalized mass. Therefore, both the kinetic energy and the potential energy are greater for full body resonance. Finally, the increase in the two energies relates to greater inertial and elastic forces, for which the system becomes relatively less sensitive to damping forces.

The motion of the four legs is obtained with one linear straight line solenoid. These are force actuators, as they generally have no internal stiffness. They are suitable for 5V actuation and are available off-the-shelf.

The kinematic design comprises of two rectangular four-bar-linkages (i.e. 2-4-3-9 and 5-7-6-9, respectively), that are connected to a center body (part 9), see Figure 3. The motor components (10 and 11) are mounted on parts 4 and 7 and the legs are attached to links 2 and 6. In the final 3D design in Figure 1 the coupling mechanisms are located between the links and the legs. However, they are left out of this kinematic model, because in horizontal plane they function as a stiff connection, and do therefore not effectively change the kinematic design of the horizontal mechanism.

This 2D kinematic design has two internal degrees of freedom, see Figure 4 which become the first and second (non-rigid body) eigenmode of the system when the mechanism is converted into a compliant design. Only the desired eigenmode can be actuated by the actuator, because the other is perpendicular to the action of the solenoids. The motor parts are prevented from rotation, because the four-bar-linkages are rectangular. As long as the legs move approximately in symmetry about the frontal plane, the motor components stay aligned. Little misalignment is permitted for the solenoids that are used in this system.

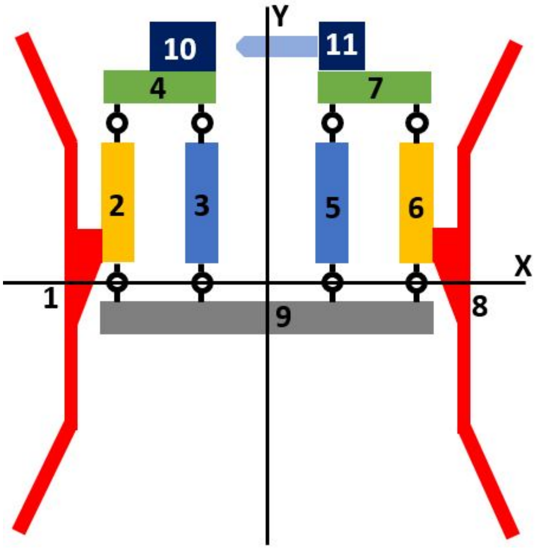

Figure 3: The kinematic design of the mechanism that generates the horizontal motion of FARbot. It consists of two rectangular four-bar-linkages, i.e. 2-4-3-9 and 5-7-6-9, respectively. The legs (1 and 8) are attached to parts 2 and 6, which rotate around the revolute joints that connect them to the center bar 9. The motor parts 10 and 11 are mounted to bar 4 and 7 respectively. They are prevented from rotation, because the four-bar-linkages are rectangular. The system has two internal degrees of freedom, which are the motions of the two four-bar-linkages.

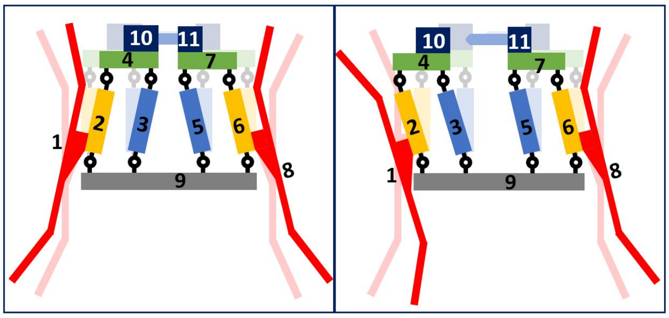

Figure 4: The two internal degrees of freedom of the kinematic model. The left motion is the desired eigenmode of the system and is the only motion that can be actuated with the solenoid.

2.5. Step 3: Conversion to compliant design

The next step is to convert the kinematic model into a compliant design. To this end, kinematic hinges and joints are replaced by compliant components. These components must have low stiffness in the functional direction and high stiffness in all other directions. There are several standard compliant joints for many different types of constraints, varying between simple and very complex. In this step, we took into account the demand for monolithic production to make choices for FARbot.

For FARbot we make use of distributed cross flexures. The choice for distributed flexures instead of lumped flexures is made, because these are subjected to lower maximal deformation upon rotation, see Figure 5 for the difference. Cross flexures, see Figure 6, have been used because instead of straight flexures, because of their high resistance to torsion and their relatively small axis drift. Moreover, with respect to other compliant hinges that are suitable for the necessary rotational degree of freedom, the cross flexure is mainly beneficial in terms of simplicity and the amount of space it uses.

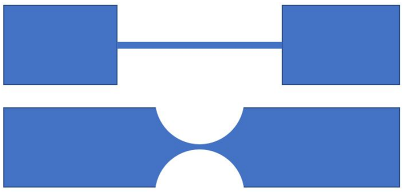

Figure 5: A schematic drawing of a distributed flexure (top) and a lumped flexure (bottom). In FARbot the distributed flexure is used.

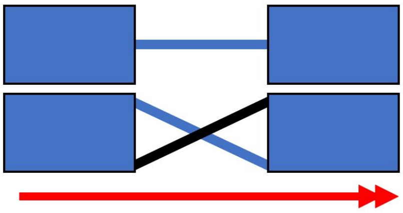

Figure 6: A schematic drawing of a straight flexure (top) and a cross flexure (bottom). The solid red arrow indicates which axis of rotation is better constraint in cross flexures than in straight flexures.

2.6. *Step 4: Calculation of eigenfrequencies*

The fourth step of our methodology is to obtain a model which can calculate the eigenfrequencies. We choose to do this with a 2D parametric model of the compliant design, which will be used in an optimization scheme to obtain the desired eigenfrequency.

The 2D parametric model of the mechanism comprises of four moving masses and five torsional springs, see Figure 7, and obtains only the desired eigenfrequency. The parts that are rigidly attached to each other are merged and described as a single mass. The cross flexures are described by five torsional springs with zero mass. For this model it is assumed that the desired first eigenfrequency of FARbot equals the eigenfrequency of this simplified model. Also it is assumed that the full mechanism is perfectly symmetric in the Y-axis and that the center body (part 9 in Figure 3) does not move at resonance. In this configuration, one would expect just four springs, as the four-bar-linkages contain four joints. However, a fifth cross flexure is part of the coupling mechanism and is located exactly above one of the other cross flexures. All flexures are identical and move synchronously. They are identified in Figure 8.

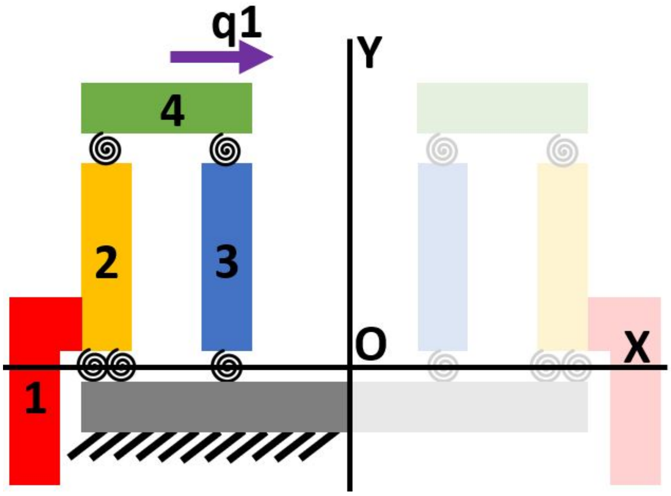

Figure 7: A schematic drawing of the parametric model that is used for the calculation of the eigenfrequency. The model comprises of four moving masses and five torsional springs. Mass 1 is a lumped representation of the legs and all other parts that move with the legs. Masses 2 and 3 are identical links and mass 4 resembles the solenoid and the part to which it is attached. This model assumes that the mechanism is perfectly symmetric about the Y-axis, that the center body is fixed and that the eigenfrequency of this simplified system equals the first eigenfrequency of FARbot. The displacement of mass 4 in X-direction is chosen to be the the generalized coordinate $q1$ of this model.

2.6.1. *Kinetic energy*

The kinetic energy T of the system is obtained using the following equation

$$T = \frac{1}{2}\dot{\boldsymbol{x}}^{\mathrm{T}}\mathbf{M}\dot{\boldsymbol{x}} \qquad \text{with} \quad \dot{\boldsymbol{x}} = \dot{\boldsymbol{x}}(\boldsymbol{q}, \dot{\boldsymbol{q}}). \tag{1}$$

Here $\dot{\boldsymbol{x}}$ is the time derivative of the position of the four parts and $\mathbf{M}$ is the diagonal mass matrix with the mass and inertia of the parts. Vector $\boldsymbol{q}$ contains the generalized coordinate q_1 as visualized in Figure 7. In the supplementary material the details on these vectors and matrices are given.

2.6.2. *Potential energy*

It is assumed that gravitational force and energy do not influence the horizontal mechanism. Therefore, we only consider elastic potential energy. To calculate this, an expression to describe the compliant joints as rotational stiffnesses is found. We present both the stiffness of a straight flexure and that of a cross flexure. For the straight flexure this can be derived using the Euler-Bernoulli equation for beam theory;

$$\frac{\mathrm{d}^2}{\mathrm{d}x^2}\left(EI\frac{\mathrm{d}^2 w}{\mathrm{d}x^2}\right) = z. \tag{2}$$

Here E is Young's modulus, I is the moment of inertia, w is displacement and z is load in N/m. This yields an equivalent torsional stiffness for straight beams of

$$k_{r,s} = \frac{EI}{l}, \tag{3}$$

with l the lenght of the flexure. The stiffness of a cross flexure can be approximated using the pseudo-rigid-body model (PRBM) for a cross-axis flexural pivot, as described by Jensen

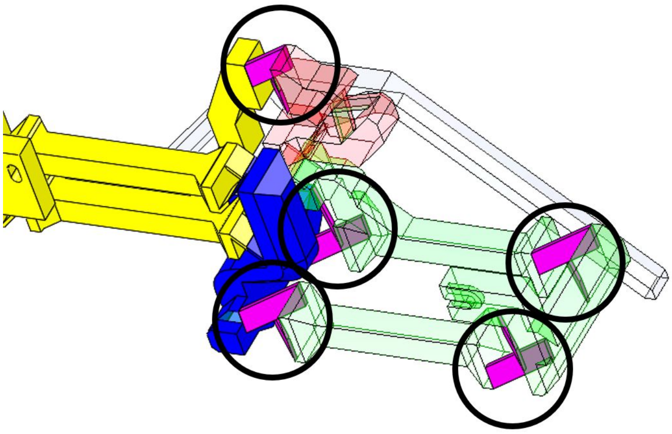

Figure 8: An overview of the five flexures that deform upon motion of the horizontal mechanism. Only half of FARbot is shown in this figure. In the parametric model, the cross flexures are described as torsional springs. The fifth and extra spring in the parametric model resembles the upper cross flexures in this figure. The function of the upper flexure is explained in Subsection 2.9.

and Howell [20]. PRBM allows flexible bodies to be modeled as rigid bodies. Although it does not give an exact result, it simplifies the derivation of the stiffness properties significantly as:

$$k_{r,c} = \frac{K_\theta EI}{2l}, \tag{4}$$

where E is Young's modulus, I is the moment of inertia of the flexible sections, l is the length of the flexible segments, and K_θ is known as the stiffness coefficient. This coefficient depends on the angle between the two flexures of the cross flexure. For the present application the cross flexures are perpendicular to each other, which yields a value of 4.3079. More information on these parameters can be found in Table 1.

Subsequently, the potential energy of the system is obtained as

$$V = \frac{1}{2}\boldsymbol{u}^{\mathrm{T}}\mathbf{K}\boldsymbol{u} \qquad \text{with} \quad \boldsymbol{u} = \boldsymbol{u}(\boldsymbol{q}). \tag{5}$$

Here, $\boldsymbol{u}$ is the deformation of the springs and $\mathbf{K}$ is the diagonal stiffness matrix with the torsional stiffnesses of either equation (3) or (4). In the supplementary material the details on these vectors and matrices are given.

2.6.3. *Equation of motion*

The equation of motion for the system is derived Lagrange equations:

$$\boldsymbol{f} = \frac{\mathrm{d}}{\mathrm{d}t}\left(\frac{\partial T}{\partial \dot{\boldsymbol{q}}}\right) - \frac{\partial T}{\partial \boldsymbol{q}} + \frac{\partial V}{\partial \boldsymbol{q}} = 0. \tag{6}$$

Here, we assume that there are no damping forces in the system. This formula yields one equation of motion as our parametric model has one generalized coordinate.

2.6.4. *Eigenmode and eigenfrequency*

Using equation (6) one can obtain the generalized mass and stiffness matrices $\mathbf{M}_g$ and $\mathbf{K}_g$ at the equilibrium points. These are points of zero velocity and acceleration. In our case, the generalized coordinate is chosen such that when it equals zero, the system is in stable equilibrium. Hence, we find the generalized mass and stiffness matrices as

$$\mathbf{M}_g = \left.\frac{\partial \boldsymbol{f}}{\partial \ddot{\boldsymbol{q}}}\right|_{\substack{\ddot{\boldsymbol{q}}=\mathbf{0}\\ \dot{\boldsymbol{q}}=\mathbf{0}\\ \boldsymbol{q}=\mathbf{0}}}, \tag{7}$$

$$\mathbf{K}_g = \left.\frac{\partial \boldsymbol{f}}{\partial \boldsymbol{q}}\right|_{\substack{\ddot{\boldsymbol{q}}=\mathbf{0}\\ \dot{\boldsymbol{q}}=\mathbf{0}\\ \boldsymbol{q}=\mathbf{0}}}. \tag{8}$$

For multi-degree of freedom systems, this yields two symmetric and positive definite matrices. With these, the eigenfrequencies and eigenmodes of the system can be derived using

$$\mathbf{K}_g \boldsymbol{x}_s = \omega^2 \mathbf{M}_g \boldsymbol{x}_s, \tag{9}$$

which is an eigenvalue problem and gives the system's eigenmodes $\boldsymbol{x}_s$ and the corresponding eigenfrequencies squared ω^2 in rad/s. However, for a 1 DOF system like the parametric model of FARbot, the generalized mass and stiffness are scalars ($\mathbf{M}_g = M_g$ and $\mathbf{K}_g = K_g$). Therefore, the eigenfrequency can be obtained simply as

$$\omega = \sqrt{\frac{K_g}{M_g}}. \tag{10}$$

The eigenmode in this case is simply the motion in the direction of the only degree of freedom.

Using this, the eigenfrequency of the horizontal motion of FARbot is a function of the 24 physical parameters that are listed in Table 1 on page 30.

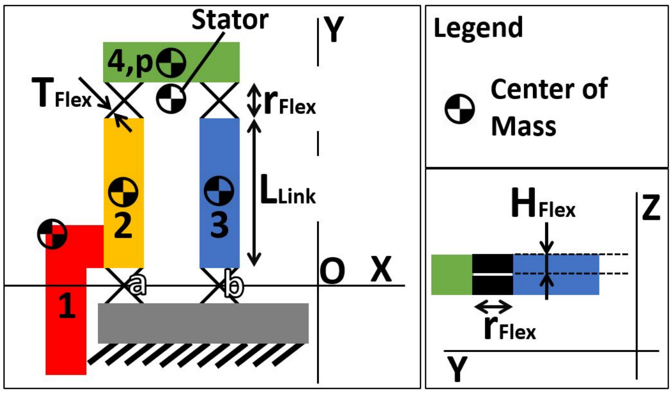

Figure 9: The dimensional parameters that are presented in Table 1. The drawings represent the horizontal motion mechanism. The left drawing is a top view, the right is a side view. The position of the centers of masses is indicated as stated in the legend. It should be noted that the parameters of the stator and the mass of part 4,p are merged to become one lumped part 4.

2.7. *Step 5: Optimization*

The last step in the design method is to optimize the physical parameters to match the specified desired eigenfrequency.

Name	Value	Unit	Description
T_{Flex}	0.18	mm	Flexure thickness
r_{Flex}	3.80	mm	Span cross flexure, **optimization parameter**
H_{Flex}	2.50	mm	Height of individual flexures, **optimization parameter**
L_{Link}	19.01	mm	Length of links, **optimization parameter**
CoM_1	$(-18.6,\ 1.5)$	mm	$(x,\ y)$-position of center of mass with respect to origin part 1
CoM_2	$(-15,6,\ 11.4)$	mm	$(x,\ y)$-position of center of mass with respect to origin part 2
CoM_3	$(-5.2,\ 11.4)$	mm	$(x,\ y)$-position of center of mass with respect to origin part 3
$CoM_{4,p}$	$(-7.8,\ 27.7)$	mm	$(x,\ y)$-position of center of mass with respect to origin part 4
CoM_{stator}	$(-7.8,\ 24.7)$	mm	$(x,\ y)$-position of center of mass with respect to origin stator
CoR_a	$(-15.6,\ 0)$	mm	$(x,\ y)$-position of center of rotation cross flexure a with respect to origin
CoR_b	$(-5.2,\ 0)$	mm	$(x,\ y)$-position of center of rotation cross flexure b with respect to origin
V_1	$555.5e{-9}$	m^3	Volume lumped part 1
V_2	$139.9e{-9}$	m^3	Volume part 2
V_3	$136.5e{-9}$	m^3	Volume part 3
$V_{4,p}$	$222.6e{-9}$	m^3	Volume part 4, without motor
m_{stator}	$1.32e{-3}$	kg	Mass of stator component of the motor
I_1	$50.8e{-9}$	$kg\,m^2$	Mass moment of inertia lumped part 1
I_2	$3.1e{-9}$	$kg\,m^2$	Mass moment of inertia part 2
I_3	$3.0e{-9}$	$kg\,m^2$	Mass moment of inertia part 3
$I_{4,p}$	$5.2e{-9}$	$kg\,m^2$	Mass moment of inertia part 4, without motor
I_{stator}	$15.8e{-9}$	$kg\,m^2$	Mass moment of inertia stator component
ρ	1100	kg/m^3	Density of HTM140V2, experimentally determined
E	3.35e9	Pa	Young's modulus HTM140V2, from [21]
K_θ	4.3079	–	Stiffness coefficient of cross flexure with −45°/45° orientation [20]

Table 1: An overview the 24 physical parameters in the 1 DOF parametric model. A visualization of the dimensional parameters in this table is given in Figure 9.

We derived an optimization scheme that uses all physical parameters of the prototype to obtain the desired eigenfrequencies and also to find parameter sensitivities.

2.7.1. *Mathematical description of problem*

We formulate a normalized mathematical description of the difference between the desired eigenfrequency and the eigenfrequency for a certain set of parameters. This equation is used as objective function for the sensitivity analysis and as non-linear equality constraint for the optimization algorithm. It is derived such that it can be used for an optimization scheme in negative null form as

$$\mathrm{f}_{\mathrm{dif}}(\boldsymbol{x}) = \frac{\sqrt{(\mathrm{f}(\boldsymbol{x}) - \mathrm{f}_{\mathrm{des}})^2}}{\sqrt{(\mathrm{f}(\boldsymbol{x}_0) - \mathrm{f}_{\mathrm{des}})^2}}. \tag{11}$$

Here, $\boldsymbol{x}$ is the entire set of physical parameters, $\boldsymbol{x}_0$ is the initial set of parameters that is fed to the algorithm, f is the eigenfrequency in Hz, $\mathrm{f}_{\mathrm{des}}$ is the desired eigenfrequency and $\mathrm{f}_{\mathrm{dif}}$ is the normalized difference.

2.7.2. *Sensitivity analysis*

To reduce the optimization problem, we determine to which parameters the eigenfrequency is most sensitive. Only the most important parameters that are variable are selected for the optimization, which increases the algorithm's efficiency. Another benefit of deducing the parameters' sensitivities is that it provides insight into the effect of imperfections during manufacturing. It provides reasoning for producing certain components with higher precision than others.

For the sensitivity analysis we use the mathematical description of (11) as objective function. The sensitivities of the objective function in a certain design point $\boldsymbol{x}_d$ are obtained by taking the partial derivative of the objective function with respect to all parameters at the design point:

$$S_i(\boldsymbol{x}_d) = \left.\frac{\partial f_{\mathrm{obj}}}{\partial x_i}\right|_{\boldsymbol{x}_d} \qquad i = 1, 2, \ldots, n. \tag{12}$$

Here, S_i is the sensitivity value of the i-th physical parameter x_i, and n the total number of parameters.

To allow for comparison between the parameters, the normalized sensitivity values are required. To this end the logarithmic sensitivity is calculated, by taking the partial derivative of the log of the objective function with respect to the log of the parameters:

$$S_{i,log}(\boldsymbol{x}_d) = \left.\frac{\partial \log f_{\mathrm{obj}}}{\partial \log x_i}\right|_{\boldsymbol{x}_d} = \frac{x_i}{f_{\mathrm{obj}}} \left.\frac{\partial f_{\mathrm{obj}}}{\partial x_i}\right|_{\boldsymbol{x}_d} \qquad i = 1, 2, \ldots, n \tag{13}$$

These derivatives can not be derived analytically though, therefore they are approximated with the central finite difference method, which is based on the Taylor series

$$\frac{\partial f}{\partial x_i} \approx \frac{f(x_i + h) - f(x_i - h)}{2h}. \tag{14}$$

Parameter	Min (mm)	Max (mm)
r_{Flex}	1.5	5
L_{Link}	2.5	5
H_{Flex}	5	25

Table 2: This table presents the ranges used for the three optimization parameters.

Here, h is the perturbation step size. For the central difference method, the sensitivity values rely on this perturbation step size. Therefore, it is necessary to obtain the sensitivity value for several different step sizes and validate if they converge to equal values, which sometimes is not the case due e.g. to truncation errors. To this end, the sensitivity value is calculated for perturbation step sizes that range between $10^{-13}\%$ and 10% of the parameter in the design point $x_{d,i}$. The algorithm determines convergence of the sensitivity value by checking the difference between the obtained sensitivity values. It selects a value if the tolerance criterion of 10^{-6} difference between the values is achieved.

The sensitivity value of the following 12 physical parameters was determined: the length, height and thickness of the flexures (r_{Flex}, H_{Flex} and T_{Flex}), the length of links 2 and 3 (L_{Link}) and the masses and inertias of the four bodies of the model ($m_{1,2,3,4,p}$ and $I_{1,2,3,4,p}$). For part four the motor mass is not taken into account, because it can not be changed. Notable is that some of these parameters depend on each other, e.g. the inertia and mass (I_2 and m_2) of link 2 are depended on its length L_{Link}. With this set of parameters we are able to investigated if small changes in the masses and inertias of the parts are important.

The results of the sensitivity analysis are presented in Section 3.1. Based on the results three parameters are chosen as optimization parameters, namely L_{Link}, r_{Flex} and H_{Flex} (the physical meaning of these parameters is explained in Table 1 and Figure 9). Even though the flexure stiffness T_{Flex} has a much higher sensitivity value, it was left out of the optimization. That is, because it was found in an early stage that the desired eigenfrequency would only be obtained if the flexures have the minimal thickness possible. Although it is not used as an optimization parameter, it is very clear that the thickness of the flexures is very important to be measured after manufacturing, in order to interpret results.

2.7.3. Optimizing using Sequential Quadratic Programming

For the optimization problem, the mathematical description of the desired eigenfrequency (11) is used as a non-linear equality constraint. The optimization objective is to minimize the width of the robot, which depends on the length of the flexures and links. These lengths are subject to the constraint that the link length should be significantly greater than that of the flexures, because otherwise the assumptions of the PRBM method do not hold. We use a minimal difference of a factor five. To finish the optimization problem description, we define a feasible range $\mathcal{R}(x)$ for the three parameters, see Table 2. The entire reduced optimization problem yields

$$\min_{\boldsymbol{x}_{opt}} \quad r_{Flex} + L_{Link} \tag{15}$$

$$\text{s.t.} \quad \frac{\sqrt{(\mathrm{f}(\boldsymbol{x}) - \mathrm{f}_{\mathrm{des}})^2}}{\sqrt{(\mathrm{f}(\boldsymbol{x_0}) - \mathrm{f}_{\mathrm{des}})^2}} = 0 \tag{16}$$

$$r_{Flex} - 0.2 L_{Link} \leq 0 \tag{17}$$

$$\boldsymbol{x}_{opt} \in \mathcal{R}(\boldsymbol{x}) \tag{18}$$

$$\text{with} \quad \boldsymbol{x}_{opt} = (r_{Flex}\ L_{Link}\ H_{Flex})^{\mathrm{T}} \tag{19}$$

For the optimization we use the sequential quadratic programming algorithm (SQP) [22], which is known as a good general-purpose method for constrained problems. Properties of SQP are that it does not need a feasible starting point and that it accepts non-linear constraints as well as equality constraints. To find the optimum, this method uses the Newton-Raphson method to solve the Karush-Kuhn-Tucker (KKT) optimality conditions [2].

A disadvantage of SQP is that it stops when it finds a local minimum, as such a point satisfies the KKT condition. Therefore, this method does not necessarily give the global optimum if the objective function has several local minima. Nevertheless, we expect only one minimum, because the optimization objective (15) is linear for all the three optimization parameters. Therefore, SQP can be safely used for our problem. To implement the SQP algorithm we used the MATLAB™function `fmincon`. There, we set the maximum number of iterations to 400 and both the optimality and constraint tolerance to 10^{-6}.

The resulting parameters of the reduced optimization for FARbot's eigenfrequency are included in Table 1. Other optimization results are presented in Section 3.1. Figure 10 shows the resulting 3D design that was obtained for the horziontal motion mechanism.

2.8. Vertical motion mechanism

The mechanism that generates the vertical motion of FARbot's legs is shown in Figure 11. It is functionally and kinematically the same as the horizontal motion mechanism, but it moves in the frontal plane and is designed to have an eigenfrequency of 25Hz, which is well away from the eigenfrequency of the horizontal mechanism. This difference is necessary to avoid eigenmode interactions between the horizontal and vertical motion mechanism. With this orientation of the two motion mechanisms FARbot is well balanced, because the masses of the two motors are equally far away from the center line of the robot.

2.9. Coupling mechanism

The coupling device (Figure 12) is a compliant mechanism that combines the straight line vertical and horizontal motions,

---

[2] The standard form of the KKT optimality conditions is presented in the supplementary material.

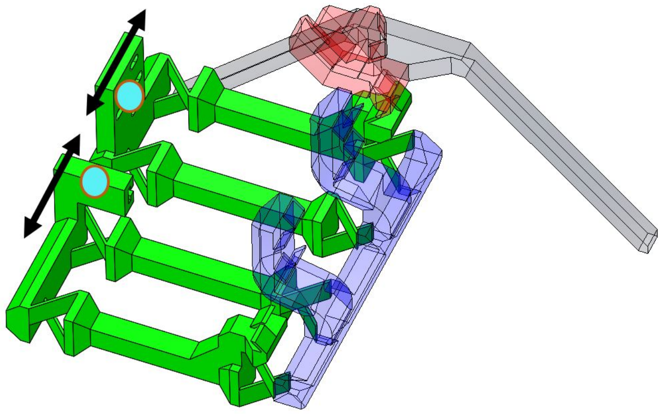

Figure 10: The 3D design of the horizontal motion mechanism of FARbot in green, which was developed using the five step method that is presented in this paper. This sub-mechanism of the robot is designed to resonate at 15 Hz and moves as indicated by the black arrows. It is attached to the center body (blue transparent) and the coupling mechanisms (red transparent). The second coupling mechanism and leg pair, as well as the vertical motion mechanism, are left out of the figure for clarity. The blue dots indicate where the solenoid parts are mounted.

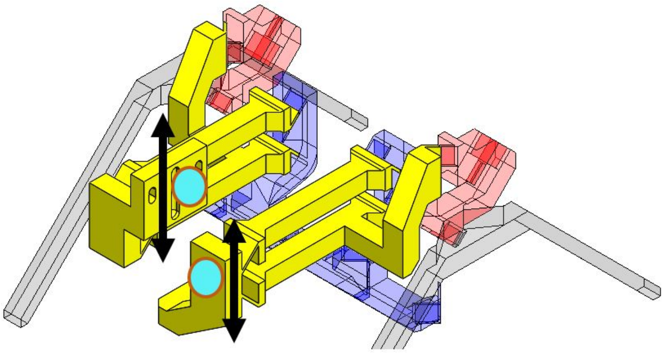

Figure 11: In yellow the 3D design of the vertical motion mechanism of FARbot, which is kinematically and functionally the same as the horizontal motion mechanism. This sub-mechanism of the robot is designed to resonate at 25 Hz and moves as indicated by the black arrows. It is attached to the center body (blue transparent) and the coupling mechanisms (red transparent). The second coupling mechanism and leg pair, as well as the horizontal motion mechanism, are left out of the figure for clarity. The blue dots indicate where the solenoid parts are mounted.

which must both be controllable and should not interfere one another. In prior work we found a few mechanisms that could fulfill the required function. Baisch et al. use a five linkage mechanism for circular output in their prototypes called HAMR-3 [8], HARM-V [23] and HAMR-VP [5]. Hoffman and Wood use two four-bar-linkages in the Myriapod [24] and Birkmeyer et al. designed a four bar mechanism for this purpose for DASH [2], which was also used by Hoover et al. in RoACH [25].

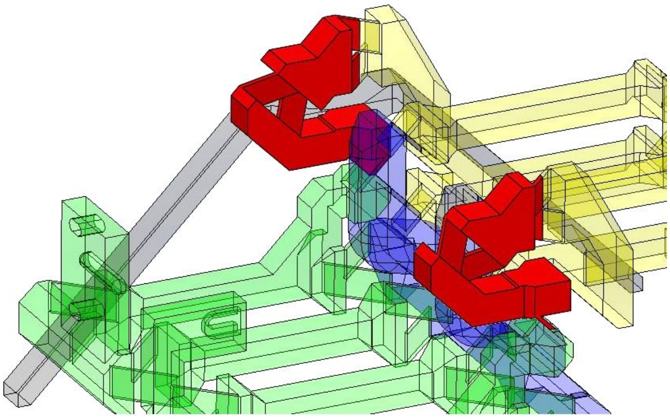

Figure 12: In red the 3D design of the coupling mechanisms of FARbot. The mechanisms consists of two rigid parts and one flexure. They are rigidly connected to the leg pairs and attached to the horizontal and vertical motion mechanism with cross flexures. The working principle of this mechanism is explained in Figure 13.

The mechanism we designed is based on the five linkage mechanism of Baisch et al.[8]. The working principle is based on a few essential requirements in terms of constraints and motion freedom, which are easiest to understand using the Freedom and Constraint Topology (FACT) theory of Hopkins and Culpepper [17]. The mechanism has 3 axes of rotation which do not lay in the same plane, but intersect in one common point to form a 'Sphere'. With this, the end effector, i.e. a leg pair, has two rotational degrees of freedom about the center of the sphere. In the design of FARbot, these requirements are applied such that hinge A and B are in line, as well as hinge C and D, their axes of rotation cross at the point where also the axis of rotation of hinge E intersects, see Figure 13.

3. Results

The results section is divided into three subsections, which describe the results on modeling and simulation (Section 3.1), the primary non-monolithic prototype (Section 3.2), and the final prototype of FARbot (Section 3.3).

3.1. Modeling and simulation results

The results of the sensitivity analysis are presented in Figure 14 and clearly show that the eigenfrequency is most sensitive to changes in the flexure stiffness. Also, the length and height of the flexures and the length of links 2 and 3 are important. All other values are more than ten times smaller than the aforementioned ones. This sensitivity analysis was carried out for

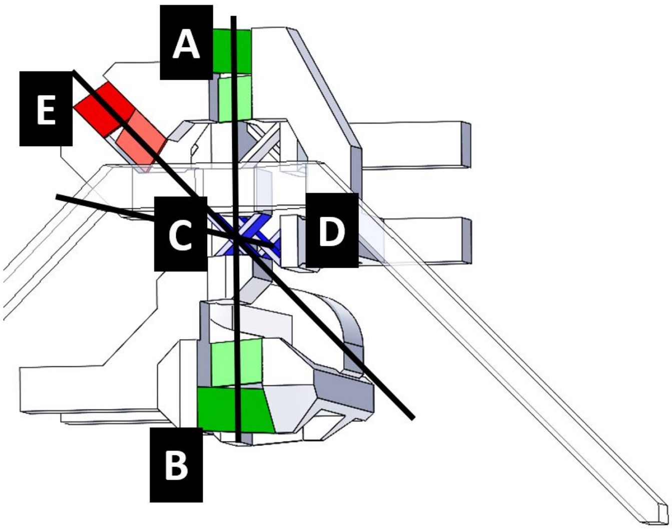

Figure 13: An overview of the five flexures that are essential for the coupling mechanism. Cross flexures A and B are in line, as well as flexures C and D. Their axes of rotation cross at the point where also the axis of rotation of cross flexure E intersects. The orientation of the axes of rotation is crucial for the functionality of the coupling mechanism.

the presented design of FARbot. A sensitivity analysis for the primary prototype that uses straight flexures instead of cross flexures gives similar results.

Because of the low sensitivity of the masses $m_{1,2,3,4,p}$ and inertias $I_{1,2,3,4,p}$, it was decided to keep these values constant during optimization, even though they in fact slightly change with the variation of optimization parameters. The reason not to take these changes into account is to simplify obtaining of new models for new designs.

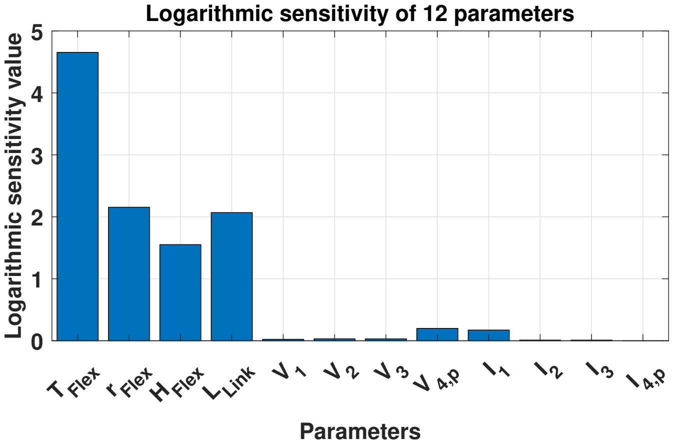

Figure 14: The logarithmic sensitivity values of twelve physical parameters of the 1DOF parametric model of FARbot. It clearly shows that the system is most sensitive to change in the left four parameters. The parameters used for this analysis are the length, height and thickness of the flexures (L_{Link}, r_{Flex} and H_{Flex}), the length of links 2 and 3 (L_{Link}) and the masses and inertias of all four bodies of the model ($m_{1,2,3,4,p}$ and $I_{1,2,3,4,p}$). The physical meaning of these parameters is more extensively explained in Table 1 and Figure 9).

The script that performs the optimization finds a feasible solution within the value of the optimality tolerances in 8.4 seconds. The obtained parameters are included in Table 1 and they are used for the final design of FARbot.

3.2. *Primary non-monolithic prototype*

In an earlier stage of this project, a first prototype of the robot was built to test the subsystems. It is different from FARbot in a few aspects, namely its design is not monolithic, straight flexures are used instead of cross flexures, a different design was used for the vertical motion mechanism and it was optimized for 12Hz instead of 15Hz. The new monolithic design that will be discussed in Section 3.3 is obtained based on the results of this primary prototype. The horizontal motion mechanism though, is kinematically and functionally equal to that of FARbot and is obtained with the same five step method that is mentioned in Section 2.2. This prototype was used to test the performance of the horizontal motion mechanism at resonance, to validate the design methodology and the parametric model and to test the actuation.

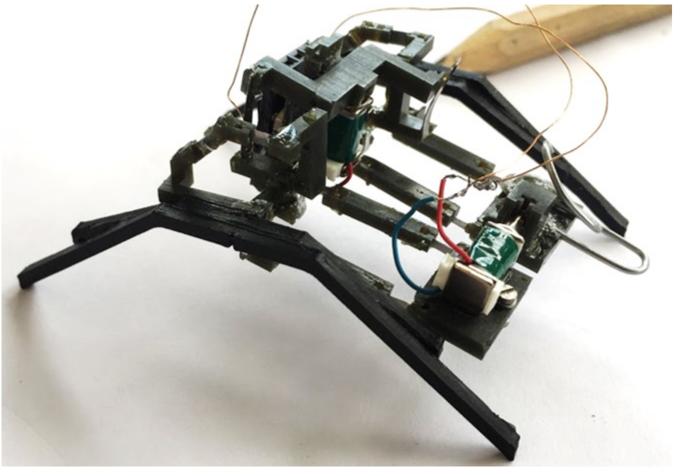

Figure 15: A picture of the primary prototype that was built. The prototype exists of 36 mechanical parts, i.e. 18 printed parts and 18 flexures.

This prototype is actuated with 1.3gram solenoids that operate between 0V and 12V. The same has also been used for FARbot. The electrical input to the solenoid is a block wave with a frequency that can be controlled by the user via an Arduino Mega2560 in a simple electrical circuit. The power is provided by an external energy source, on which the input voltage can be tuned.

3.2.1. *Manufacturing*

The primary prototype exists of 36 parts, namely 18 printed parts and 18 flexures. The printed parts are manufactured from HTM140V2 on an EnvisionTEC 3D Perfactory printer. The parts were simultaneously printed in a 3D support structure that keeps them in position with respect to each other. That is to simplify the alignment and assembly process. The flexures are cut from a 0.05mm thick sheet of stainless spring steel.

The manual assembly of the parts lasted three days and consisted mainly of gluing the flexures between the parts, and cutting loose the support material piece by piece. As the material HTM140V2 is known to be rather brittle, often a piece would break and had to be attached again, with probable misalignment

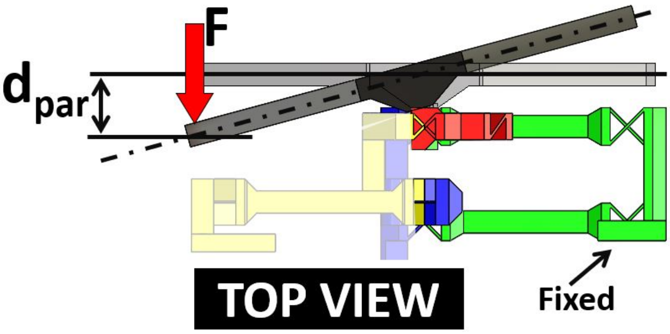

Figure 16: A visualization of the parasitic motion in horizontal direction that is observed in the prototypes. When the horizontal motion mechanism (green) is fixed, the legs (black) can still move horizontally due to undesired flexibility in the coupling mechanism (red). This low stiffness is experimentally quantified by applying a force F on the leg tips and measuring their displacement. The results are presented in Table 3.

	Primary design	**FARbot**
Leg length (mm)	35	26
Parasitic motion d_{par} (mm)	8.1	0.5
Torsional stiffness (Nm/rad)	3.6e−3	32.4e−3

Table 3: The results of the experiments to quantify the parasitic motion of both prototypes. Only the torsional stiffness that corresponds to the absolute parasitic motion d_{par} can be used for comparison between the two prototypes. The torsional stiffness of FARbot is nine time greater than that of the primary prototype. The parasitic motion is visualized in Figure 16.

as a result. After the assembly process, an additional two days were necessary for alignment and adjustments to make the prototype operative. Hence, the total amount of time necessary to produce the prototype is approximately 40 hours.

3.2.2. *Parasitic motion*

The legs show a parasitic motion in the horizontal direction, which is visualized in Figure 16. This is a result of undesired low stiffness in the flexure that connects the horizontal mechanism to the coupling mechanism. An experiment is carried out to quantify the parasitic motion and to compare it with the new design of FARbot. For this a force of 23.9mN is applied on the leg tips, while fixing the horizontal motion mechanism. The displacement of the leg tips that results from the applied force is measured. This displacement however, can not be used for comparison, because the legs of the two prototypes do not have the same length. Therefore, the torsional stiffness of the coupling mechanism in the parasitic motion direction is calculated. The torsional stiffness of the new design of FARbot is nine times greater than for the primary design, which implies a significant decrease of parasitic motion.

The horizontal motion of this prototype can successfully be actuated with the solenoids, the vertical motion can not however. Therefore, this prototype is not able to run.

3.2.3. *Experimental results of the dynamical behavior*

The dynamic response of the system is the most important for this research, as it can validate the design method and the parametric model. For the dynamical experiments, the prototype was suspended on a socket to perform an in-air test, see Figure 17. This way, no frictional forces from the ground apply to the feet, which would cause an increased damping in the system. During the tests, the motion of the robot has been recorded by a high speed camera at 240fps. A rectangular crop of the video image is used to extract data on the X-position of one of the legs at every frame. The chosen leg is driven by the stator of the solenoid, because the parametric model uses the mass of the stator to calculate the eigenfrequency.

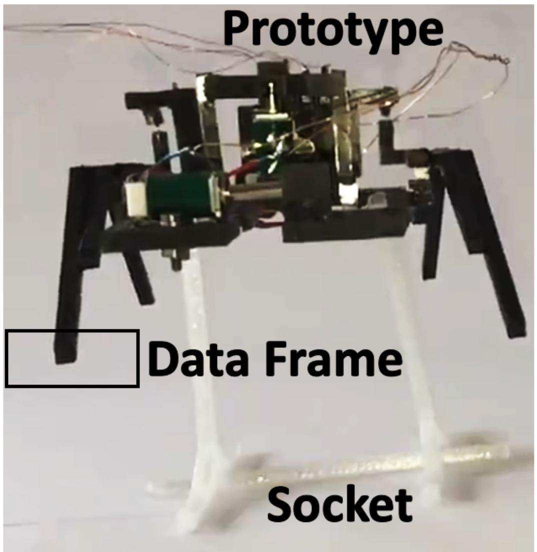

Figure 17: The experimental set up to test the dynamical behavior of the primary prototype. The prototype is suspended on a socket to test in-air behavior. The data frame that is drawn in this figure shows which part of the video is used for data extraction.

To determine the resonance frequency of the prototype it is actuated with an increasing frequency from 1Hz up to 16Hz and back to 1Hz again. This up and down sweeping is carried out at a continuous sweeping pace of maximum 1Hz per second. The experiment is carried out twice, i.e. once with an input voltage of 5V and once at 6V. The time data that is obtained with these experiments is transformed into frequency response data, see Figure 18. Each dot in the plots is obtained with a Fourier transform over a block of 1.5seconds of the time data.

The frequency response curve of a mass-spring-damper system is fitted on the data of the 5V experiment. The transfer function of such system is

$$H(s) = \frac{1}{ms^2 + cs + k}. \tag{20}$$

Mass m, damping c and stiffness k are used as fitting parameters. The curve fits the experimental data best with the following values $m = 0.006$, $c = 0.020$ and $k = 34.11$. With these values we can extract the quality factor of the system as

$$Q = \frac{\sqrt{mk}}{c}. \tag{21}$$

The quality factor equals 22.74 for the prototype. Physically this means that the motion of the legs is amplified at resonance by a factor 22.74 as compared to off resonance conditions. Curve fitting is not performed for the 6V experiment, because it shows non-linear resonance.

In Figure 18 we find that resonance occurs at 12Hz for the 5V experiment, which is exactly the desired eigenfrequency. The 6V experiment though, shows an unexpected hysteresis for the up and down sweep. At the up sweep the system resonates at 12Hz, at the down sweep the system resonates between 12Hz and 6.5Hz. The system consumes equally much power at all frequencies, including at resonance frequency. This means that the motion amplification by the quality factor of 22.74 does not require energy.

3.2.4. Stand on its own feet

In a last experiment the prototype was put on different surfaces, standing on its legs and actuated it several frequencies. On a smooth surface, the feet would not move at most frequencies, except for eigenfrequency at which the feet started moving with amplitudes approximately comparable with these in the previous experiment. However, the robot would not move forward or backwards, because the feet just skidded over the smooth surface.

On a rougher surface, the feet did not move even at eigenfrequency. Still, the resonance was observed, though as an internal motion of the system which is equivalent to the parasitic motion that is visualized in Figure 16.

3.3. FARbot

The manufacturing process of FARbot (Figure 19) is tremendously simplified as compared to the primary prototype, because of its monolithic design. After printing, it takes only about 16 minutes to finish the robot, which is less than any other robot in this research field. It takes 15 minutes to remove support material and 1 additional minute to mount the solenoids. For the mechanical body it takes just 15 minutes of manual labor to obtain a prototype of FARbot that consists of 17 stiff parts and 28 compliant elements (i.e. 14 cross flexures), with dimensions ranging between 0.18mm and 40mm. Moreover, the solenoid parts are instantly aligned, which saves much tuning time. The printing process takes approximately four hours, in which simultaneously four robots can be produced. We made eight in total, which all show constant printing results.

We tested the motion mechanisms of FARbot by manually actuating it. For this, the vertical and horizontal actuators were displaced to certain positions and the resulting displacement of one leg tip was measured. The results are presented in Figure 20 and show that the legs can be well actuated with the mechanism. Also, it can be observed that input of the *horizontal* actuator does not influence the *vertical* displacement of the leg, and that vice versa the influence is small. This indicates that the coupling mechanism functions as desired. Furthermore, the range of motion of the legs is in all directions greater than the 3mm where they are designed for.

The parasitic motion that was a problem in the primary version is significantly reduced in this redesign. The experiment that proves this and the results are presented in Figure 16 and Table 3. These results validate the benefit of using cross flexures instead of straight flexures.

4. Discussion

In this section we first discuss the modeling and optimization done in this project, then the results of the older prototype and next we discuss the results and potential of FARbot. Afterward, we present some thoughts on methods to reduce the generalized stiffness, the usage of leg compliance for improved running behavior and alternative actuation.

4.1. Modeling and optimization

The model that is used to optimize the eigenfrequency of the prototype has been simplified at several stages and on several levels. Firstly, a parametric model was used instead of a full FEM simulation, which would give a more detailed result. Secondly, the 5 DOF parametric model was simplified to a 1 DOF model. Lastly, some physical properties (like masses and inertias) were assumed to be constant, because the system's eigenfrequency is not sensitive to change in these values. Beside these model simplifications, the optimization problem was also reduced to a problem with only three optimization parameters. The result of all these simplifications is an optimization script that finds the optimum in only 8.4 seconds. The experiments carried out with the prototype have shown that the eigenfrequency of the system is almost exactly the desired frequency. This justifies all model simplifications that have been made to make the optimization script more efficient.

The high sensitivity of length L_{Link} is a result of the dependency of the deformation angle θ on this parameter. The greater this length, the smaller the deformation of the cross flexures is upon input motion. This results in lower potential energy and therefore a smaller generalized stiffness of the system. The high sensitivity value is clearly not a result of the change in mass m_2 and m_3 and inertia I_2 and I_3 that comes with change in L_{Link}, because the sensitivity value of those parameters is very low. Another sensitivity value worth to discuss is that of the inertia of part four, which equals zero. This value was expected though, because part four does not rotate upon resonance.

The optimization problem presented in equations (15) - (19) is relatively limited in the sense that it could cover many more sub problems. This was deliberately not done in present research, as we fully focused on the eigenfrequency optimization and the validation thereof. However, now that the optimization and underlying models are validated, it can be used to serve a much broader problem. We could for example include constraints for minimal stiffness of the flexures in all directions to reduce parasitic motion and ensure sufficient strength in structure. Also, we could add demands for minimal or maximal dimensions of the robot for manufacturing purposes.

4.2. Primary prototype

It has been shown that the kinematic design that was chosen for the horizontal motion mechanism functions just as desired. This design was the simplest of all options that were considered

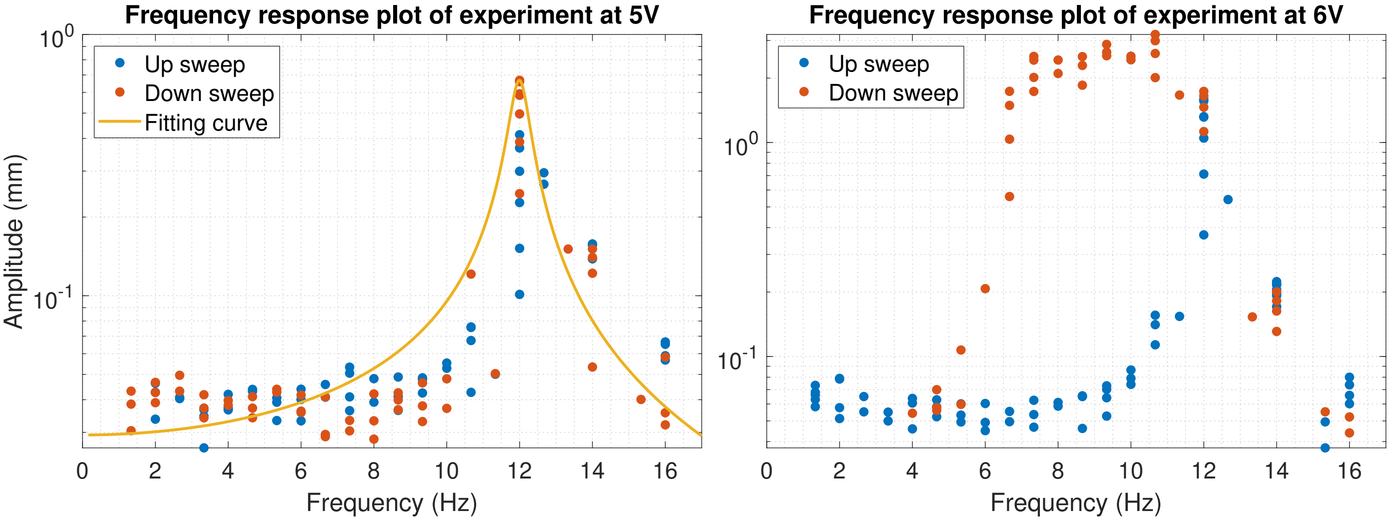

Figure 18: The frequency response plots that are obtained with the frequency sweeping experiments. The 5V experiment in the left graph shows linear resonance behavior with an eigenfrequency at 12Hz. A frequency response curve of a mass-spring-damper system is fitted on the data, for which a quality factor of 22.74 is found. The 6V experiment on the right show non linear resonance, as there is a clear difference between the up sweep and the down sweep. This hysteresis phenomenon is a typical property of dynamic softening. It is observed that during the down sweep the two solenoid parts collide while resonating, which could be the explanation for the non linear behavior at 6V. This theory is strengthened by the observation that at a 5V input voltage, neither collision nor hysteresis occurs.

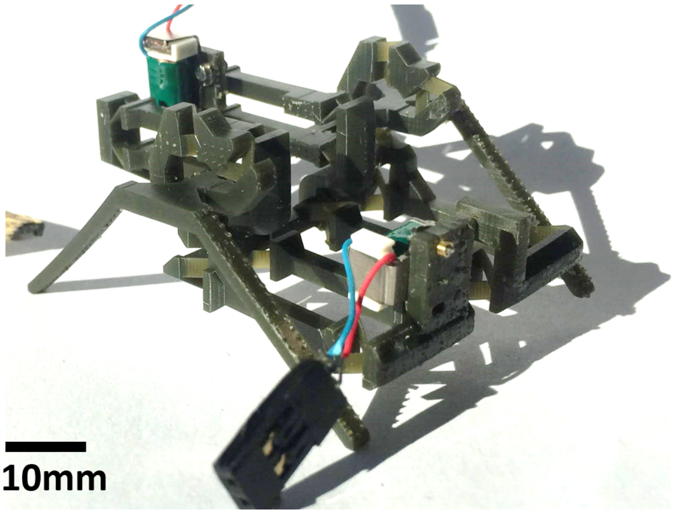

Figure 19: A picture of one of eight prototypes of FARbot that we built. The prototypes exist of one mechanical body and two solenoids and has a total mass of 9.5g. The 5.7g mechanical body contains 17 stiff parts and 28 flexure elements, that are all printed in one piece and do not require assembly afterward. After printing, it takes approximately 16 minutes to finish the robot, which requires removing the print support material and mounting the solenoids.

to perform the task. Even the alignment of the motor parts, which was a potential struggle for this design, worked fine after some tuning.

Also, the system exhibits the expected dynamic behavior, i.e. the eigenfrequency of the system is as desired and it performs the required motion. Hence, we conclude that we derived a successful design with our novel and rather straightforward design methodology. The quality factor of 22.74 that we derived from experiments shows the potential of using resonance in the design. Even though the experiments give reasonably clear results, they were subject to relatively high noise due to the sweeping which could cause errors. Therefore, other and more suitable experiments should be carried out if a more accurate result on the quality factor is desired.

The vertical mechanism of the primary design is not able to perform its function and was therefore completely redesigned for the final design of FARbot. The new design is kinematically equal to the horizontal motion mechanism. Furthermore, the primary prototype showed parasitic motion in horizontal direction, which causes undesired flexibility in the transmission between the motor and legs. Because of this, FARbot is designed with cross flexures instead of straight flexures which are stiffer in the undesired motion direction. This was experimentally shown to be a successful modification.

The softening behavior that is observed in the system is a result of non-linear dynamics in the system, which is probably caused by the collision of the motor parts. It would be interesting to further investigate this behavior, as it could be used for new designs. Potentially, a design could be obtained that resonates over a larger range of frequencies due to softening, which means that the robot could run with various stride frequencies. This opposes the current design of FARbot which is designed for only one frequency. For future work it is therefore recommended to obtain a non-linear dynamic model to predict

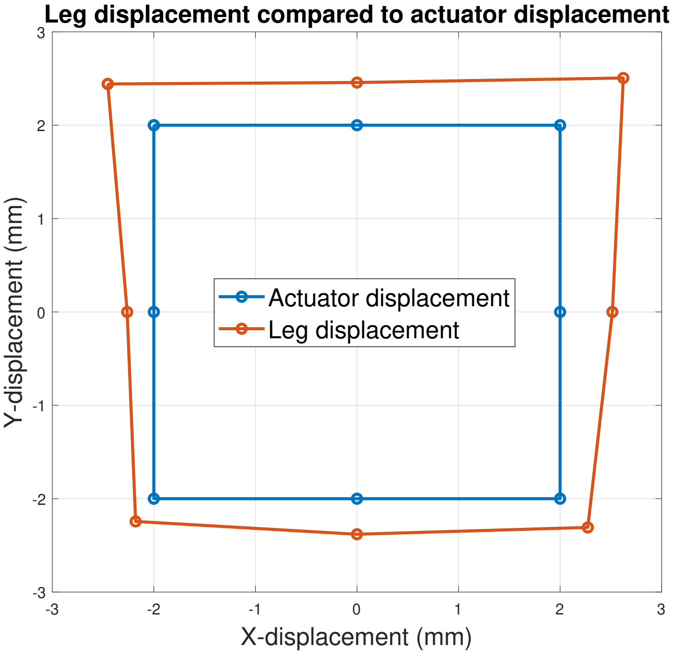

Figure 20: The results of the manual experiment that is carried out to test FARbot's mechanisms. The blue markers represent the displacement of the horizontal and vertical actuator. The red markers represent the corresponding measured displacement of the leg tip. We moved the mechanism to eight positions in a square around the neutral position. From this graph we can deduce if there is interference between the two motion mechanisms. In the case that there were no interference, the red and blue line would be perfectly parallel. In the horizontal direction they approximately are, which therefore implies that the *vertical* leg motion is successfully decoupled from *horizontal* actuation. However, for the vertical direction, we observe a slight dependency. The graph shows in actuation point (-2,-2) a smaller X-displacement of the leg than at (-2,2). The same difference is observed between (2,-2) and (2,2). Even though the difference is small, it could indicate an undesired coupling between the *vertical* actuation and the *horizontal* leg displacement. We conclude that the coupling mechanism of FARbot operates approximately as desired, as the dependency in vertical direction is only small and there is none in the other direction.

this behavior and to conduct new experiments to obtain more data on this behavior in the older prototype.

In other experiments, we found that the input phase between the horizontal and vertical motor influences the horizontal amplitude of the legs at resonance. This is unexpected, as such dependency can only occur when there is interaction between the vertical and horizontal motion mechanism. This would mean that the coupling mechanism does not fulfill its function perfectly. The interaction should be investigated more broadly in future work to understand its effect on the dynamic behavior of the system.

The manufacturing process of the older model showed that manual assembly is not ideal in the sense of tolerances, time consumption and opportunity for miniaturization. Although the prototype showed the desired behavior, we must note that it is not fully certain that all dimensions in the prototype are equal to those in the design. Because of these manufacturing struggles, it was decided to make FARbot fully monolithic, i.e. existent of one piece and one material.

4.3. FARbot

Due to the monolithic design of FARbot, the time needed for manual labor is reduced to 16 minutes per prototype, which is - to the authors' knowledge - less than any other reported robot in this and similar research fields. With respect to the primary prototype, it resulted in a reduction of manual production time by a factor 150. The printing process of FARbot is fully automatic and takes approximately three hours in which four robots are produced simultaneously. Part of the printing process is rinsing in alcohol and curing in a UV oven. Printing FARbot from the material HTM140V2 is successful. A property of HTM140V2 however is that it hardens further over time, even after curing. This could influence the properties of FARbot, which must be observed over time. Also, miniaturization is an opportunity, because there is no assembly necessary in the production process of FARbot's design. Furthermore, the design is suitable for other production methods like laser sintering. Also injection molding would be an option, which is suitable for industrial production in large quantities.

The coupling mechanism is found to function well for all eight prints that were made, this shows both the possibility of monolithically printing rather complex compliant mechanisms, and the repeatability of this way of manufacturing. Unfortunately though, FARbot was not tested extensively due to time constraints. It is however expected that FARbot is able to run due to the improvements with respect to the primary prototype. We anticipate that FARbot will show that running at resonance indeed increases speed and efficiency.

4.4. Decreasing generalized stiffness

During the design of FARbot and the primary prototype, it was found that it is challenging to decrease the stiffness of the system after reaching the minimum thickness of the flexures, which was necessary to obtain the desired eigenfrequency. An effective way to decrease stiffness in the current design is to increase the lengths of the flexures and links, hence to increase the size of the robot. This means that if the mass of the robot would decrease, due to, e.g. miniaturization of the actuation, this would result in an undesired increase of the size of the robot. This proves that something should fundamentally change about the stiffness design to make it suitable for miniaturization.

An option could be to find a material for the flexures that can be produced with less thickness and which has a lower Young's modulus. Another option is to make use of a different type of compliant mechanism. There are compliant flexure types that have an increased *effective* flexure length, without a significant increase of the size of the mechanism. Yet another option is to add negative stiffness to the mechanism. Negative stiffness can be obtained by implementing elements that are bistable when standalone. Figure 21 shows schematically how this solution could be added to the current design with a compression spring. New research should be conducted on these possibilities to decrease the stiffness of the system.

4.5. SLIP

The eigenfrequency of FARbot was chosen to be 15Hz, which also corresponds to its stride frequency. In principal, any fre-

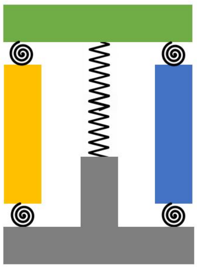

Figure 21: A schematic drawing of how negative stiffness could be added to the current design with a compression spring. In order to decrease the generalized stiffness of the system, the spring should be put into pretension.

quency could be chosen as stride frequency. However, it was found that the running performance of robots can be optimized with stride frequency, if they use SLIP (Spring Loaded Inverted Pendulum) behavior [26]. The SLIP model, which depends amongst other aspects on the stride frequency, describes how much of the energy of a bounding gait (e.g. running) is elastically stored and reused by a leg during the stance phase. Many animals are found to use SLIP in their gaits [27]. Also, the robot R-HEX [28] was optimized to use it. In order to improve FARbot's running behavior it would be interesting to investigate how the frequency and other parameters can be designed such that it uses SLIP upon running.

4.6. Actuation

Even though the solenoids work fine for current the design, they are not optimal. The reason is that they only provide a pulling force, so just half of the motion of a period is actuated. This works fine because it does fulfill the requirement to actuate an eigenmode, i.e. the force should be excited in the eigenfrequency of the mode and not perpendicular to the direction of the mode. Still, it would be beneficial to actuate a full motion cycle, because it requires less actuation power for the same energy supply. The reason is that for a solenoid, all energy that is supplied to the system must be delivered in only half of the cycle. Hence, twice the power is needed to supply the same amount of energy. Less power translates to lower voltage or current, which is beneficial for the demand of the electronics of the system. Another benefit of full cycle actuation is that it provides control over the entire cycle.

An actuator type that would be suitable for full cycle actuation are voice coils, which are small Lorenz actuators. They use electromagnetism just like solenoids, but provide both pushing and pulling force. It was found that these motors can also be produced at sub-millimeter scale [3]. This is a benefit as well, because the dimensions of FARbot are mainly restricted by the size of the currently used solenoid actuators. Hence, the advantages of these voice coils are twofold, i.e. full cycle actuation and optional miniaturization. Therefore, the use of voice coils is recommended to consider for a redesign of FARbot.

5. Conclusion

5.1. FARbot

We have presented the design of FARbot, a 9.5g quadrupedal small scale robot that is compliant, monolithic and uses its resonance to increase its stride length. The main novelties of this work are the intentional design for the use of resonance, and the monolithic, compliant design that causes drastic reduction in production complexity.

This work shows that without an increase of power demand the stride length of the robot can go up by a factor of 12 at a desired resonance frequency. This would result in either more efficient or faster locomotion once the robot is in motion. Thus, the presented work demonstrates the benefits that are achievable when mechanisms are designed for the exploitation of resonance. It is also proposed that a resonating motion can be mixed with a non-resonant motion using a coupling mechanism to obtain a desired, partially periodic output motion.

The design and manufacturing technique of FARbot outperforms all other robots in this research field with respect to production time and simplicity. Indeed, FARbot shows that a monolithic design of mechanisms at meso scale comes with tremendous decrease of manufacturing complexity. Not only manufacturing time is decreased, but also repeatability is improved and precision with respect to the alignment of parts is obtained automatically. All of these advantages are necessary when insect scale running robots are to be miniaturized or to be produced in large numbers.

To obtain a resonant and monolithic design, a five step method is proposed with which compliant mechanisms in general can be designed to make use of full body resonance. These step are used to design the resonant mechanism that synchronously generates the horizontal motion of all four feet. The methodology is proven to be successful for our project and was also found to be suitable for obtaining the fully monolithic design.

References

[1] E. Şahin, Swarm robotics: From sources of inspiration to domains of application, in: International workshop on swarm robotics, Springer, 2004, pp. 10–20.

[2] P. Birkmeyer, K. Peterson, R. S. Fearing, Dash: A dynamic 16g hexapedal robot, in: Intelligent Robots and Systems, 2009. IROS 2009. IEEE/RSJ International Conference on, IEEE, 2009, pp. 2683–2689.

[3] D. W. Haldane, K. C. Peterson, F. L. G. Bermudez, R. S. Fearing, Animal-inspired design and aerodynamic stabilization of a hexapedal millirobot, in: Robotics and Automation (ICRA), 2013 IEEE International Conference on, IEEE, 2013, pp. 3279–3286.

[4] R. J. Full, M. S. Tu, Mechanics of a rapid running insect: two-, four- and six-legged locomotion, Journal of Experimental Biology 156 (1991) 215–231.

[5] A. T. Baisch, O. Ozcan, B. Goldberg, D. Ithier, R. J. Wood, High speed locomotion for a quadrupedal microrobot, International Journal of Robotics Research 33 (2014) 1063–1082. doi:`10.1177/0278364914521473`.

[6] I. Slavkov, D. Carrillo-Zapata, N. Carranza, X. Diego, F. Jansson, J. Kaandorp, S. Hauert, J. Sharpe, Morphogenesis in robot swarms, Science Robotics 3 (2018) eaau9178.

[7] M. Rubenstein, C. Ahler, R. Nagpal, Kilobot: A low cost scalable robot system for collective behaviors, in: Robotics and Automation (ICRA), 2012 IEEE International Conference on, IEEE, 2012, pp. 3293–3298.

---

[3] See www.audemars.com for a company that produces micro components for these motors

[8] A. T. Baisch, C. Heimlich, M. Karpelson, R. J. Wood, Hamr3: An autonomous 1.7 g ambulatory robot, in: Intelligent Robots and Systems (IROS), 2011 IEEE/RSJ International Conference on, IEEE, 2011, pp. 5073–5079.

[9] R. Wood, E. Steltz, R. Fearing, Optimal energy density piezoelectric bending actuators, Sensors and Actuators A: Physical 119 (2005) 476–488.

[10] P. S. Sreetharan, J. P. Whitney, M. D. Strauss, R. J. Wood, Monolithic fabrication of millimeter-scale machines, Journal of Micromechanics and Microengineering 22 (2012) 055027.

[11] S. A. Rios, A. J. Fleming, Y. K. Yong, Miniature resonant ambulatory robot, IEEE Robotics and Automation Letters 2 (2017) 337–343.

[12] S. S. Baek, K. Y. Ma, R. S. Fearing, Efficient resonant drive of flapping-wing robots, in: 2009 IEEE/RSJ International Conference on Intelligent Robots and Systems, IEEE, 2009, pp. 2854–2860.

[13] C. Bolsman, J. Goosen, F. van Keulen, Design Overview of a Resonant Wing Actuation Mechanism for Application in Flapping Wing MAVs, International Journal of Micro Air Vehicles 1 (2009) 263–272.

[14] S. H. Collins, A. Ruina, R. Tedrake, M. Wisse, Efficient bipedal robots based on passive-dynamic walkers, Science 307 (2005) 1082–1085.

[15] J. K. Schonebaum, F. Alijani, G. Radaelli, Review on mobile robots that exploit natural vibrations, Journal of Mechanisms and Robotics (2019). To be submitted.

[16] L. L. Howell, S. P. Magleby, B. M. Olsen, Handbook of compliant mechanisms, John Wiley & Sons, 2013, pp. 55–76.

[17] J. B. Hopkins, M. L. Culpepper, Synthesis of multi-degree of freedom, parallel flexure system concepts via freedom and constraint topology (fact)–part i: Principles, Precision Engineering 34 (2010) 259–270.

[18] J. B. Hopkins, M. L. Culpepper, Synthesis of multi-degree of freedom, parallel flexure system concepts via freedom and constraint topology (fact). part ii: Practice, Precision Engineering 34 (2010) 271–278.

[19] D. M. Dudek, R. J. Full, Passive mechanical properties of legs from running insects, Journal of Experimental Biology 209 (2006) 1502–1515.

[20] B. D. Jensen, L. L. Howell, The modeling of cross-axis flexural pivots, Mechanism and machine theory 37 (2002) 461–476.

[21] EnvisionTEC, "Data sheet HTM 140 V2, EnvisionTEC, 2018.

[22] K. Schittkowski, Nlpql: A fortran subroutine solving constrained nonlinear programming problems, Annals of operations research 5 (1986) 485–500. Section 2.

[23] O. Ozcan, A. T. Baisch, D. Ithier, R. J. Wood, Powertrain selection for a biologically-inspired miniature quadruped robot, in: Robotics and Automation (ICRA), 2014 IEEE International Conference on, IEEE, 2014, pp. 2398–2405.

[24] K. L. Hoffman, R. J. Wood, Myriapod-like ambulation of a segmented microrobot, Autonomous Robots 31 (2011) 103–114. doi:10.1007/s10514-011-9233-4.

[25] A. M. Hoover, E. Steltz, R. S. Fearing, Roach: An autonomous 2.4 g crawling hexapod robot, in: Intelligent Robots and Systems, 2008. IROS 2008. IEEE/RSJ International Conference on, IEEE, 2008, pp. 26–33.

[26] P. Holmes, R. J. Full, D. Koditschek, J. Guckenheimer, The dynamics of legged locomotion: Models, analyses, and challenges, SIAM review 48 (2006) 207–304.

[27] R. Blickhan, R. Full, Similarity in multilegged locomotion: bouncing like a monopode, Journal of Comparative Physiology A 173 (1993) 509–517.

[28] R. Altendorfer, N. Moore, H. Komsuoglu, M. Buehler, H. Brown, D. McMordie, U. Saranli, R. Full, D. E. Koditschek, Rhex: A biologically inspired hexapod runner, Autonomous Robots 11 (2001) 207–213.

Appendix A

Supplementary material literature paper

A-1 Overview table of subclasses and NV-options

In Section 6.3 of the literature paper we present a systematic approach of combining subclasses and NV-methods. We mention that there are 60 different combinations that can all yield a robot design, 55 of them have not been explored yet. Figure A-1 gives an overview of all combinations.

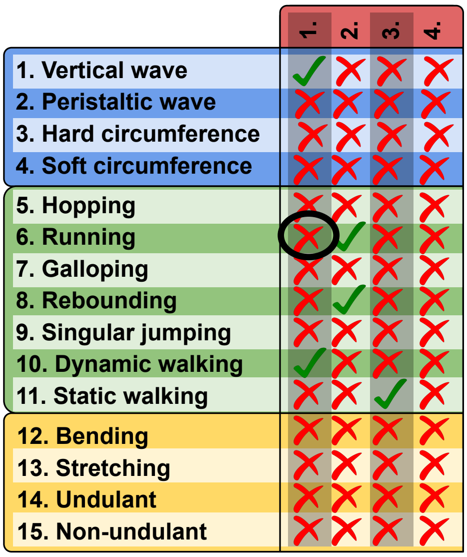

	1.	2.	3.	4.
1. Vertical wave	✓	✗	✗	✗
2. Peristaltic wave	✗	✗	✗	✗
3. Hard circumference	✗	✗	✗	✗
4. Soft circumference	✗	✗	✗	✗
5. Hopping	✗	✗	✗	✗
6. Running	✗	✓	✗	✗
7. Galloping	✗	✗	✗	✗
8. Rebounding	✗	✓	✗	✗
9. Singular jumping	✗	✗	✗	✗
10. Dynamic walking	✓	✗	✗	✗
11. Static walking	✗	✗	✓	✗
12. Bending	✗	✗	✗	✗
13. Stretching	✗	✗	✗	✗
14. Undulant	✗	✗	✗	✗
15. Non-undulant	✗	✗	✗	✗

Figure A-1: An overview table of all 60 combinations of locomotion mechanisms and NV-methods. It identifies which combinations have already been used by robots of prior work. The black circle represents the combination that is used for FARbot.

Appendix B

Supplementary material technical paper

B-1 Details on parametric model

This appendix elaborates on the vectors and matrices used to obtain the eigenfrequency of FARbot, which are used in Section 2.6 of the technical paper.

The displacement rotation angle of the cross flexures is defined as

$$\theta = -\sin^{-1}\left(\frac{q}{(r_{horFlex} + L_{horLink}}\right), \tag{B-1}$$

where q is the generalized coordinate.

The position vector $\boldsymbol{x}$ is

$$\boldsymbol{x}(\boldsymbol{q}) = \begin{pmatrix} x_1 & y_1 & \theta & x_2 & y_2 & \theta & x_3 & y_3 & \theta & x_4 & y_4 \end{pmatrix}^{\mathrm{T}}. \tag{B-2}$$

Here $(x_i\, y_i)^{\mathrm{T}}$ depends on the rotation of the center of mass CoM_i about its center of rotation CoR_i. These CoRs are presented in Table 1 of the technical paper. The position $(x_i\, y_i)^{\mathrm{T}}$ is obtained using a rotation matrix

$$\begin{pmatrix} x_i \\ y_i \end{pmatrix} = \begin{pmatrix} \cos(\theta) & -\sin(\theta) \\ \sin(\theta) & \cos(\theta) \end{pmatrix} \begin{pmatrix} CoMx_i - CoRx_i \\ CoMy_i - CoRy_i \end{pmatrix} + \begin{pmatrix} CoRx_i \\ CoRy_i \end{pmatrix}. \tag{B-3}$$

The time derivative of $\boldsymbol{x}$ is obtained as

$$\dot{\boldsymbol{x}}(\boldsymbol{q}, \dot{\boldsymbol{q}}) = \frac{\partial \boldsymbol{x}}{\partial \boldsymbol{q}} \dot{\boldsymbol{q}}. \tag{B-4}$$

The mass matrix is defined as

$$\mathbf{M} = \begin{pmatrix} m_1 & 0 & 0 & 0 & 0 & 0 & 0 & 0 & 0 & 0 & 0 \\ 0 & m_1 & 0 & 0 & 0 & 0 & 0 & 0 & 0 & 0 & 0 \\ 0 & 0 & I_1 & 0 & 0 & 0 & 0 & 0 & 0 & 0 & 0 \\ 0 & 0 & 0 & m_2 & 0 & 0 & 0 & 0 & 0 & 0 & 0 \\ 0 & 0 & 0 & 0 & m_2 & 0 & 0 & 0 & 0 & 0 & 0 \\ 0 & 0 & 0 & 0 & 0 & I_2 & 0 & 0 & 0 & 0 & 0 \\ 0 & 0 & 0 & 0 & 0 & 0 & m_3 & 0 & 0 & 0 & 0 \\ 0 & 0 & 0 & 0 & 0 & 0 & 0 & m_3 & 0 & 0 & 0 \\ 0 & 0 & 0 & 0 & 0 & 0 & 0 & 0 & I_3 & 0 & 0 \\ 0 & 0 & 0 & 0 & 0 & 0 & 0 & 0 & 0 & m_4 & 0 \\ 0 & 0 & 0 & 0 & 0 & 0 & 0 & 0 & 0 & 0 & m_4 \end{pmatrix} \tag{B-5}$$

The stiffness matrix is defined as

$$\mathbf{K} = \begin{pmatrix} k_1 & 0 & 0 & 0 & 0 \\ 0 & k_1 & 0 & 0 & 0 \\ 0 & 0 & k_1 & 0 & 0 \\ 0 & 0 & 0 & k_1 & 0 \\ 0 & 0 & 0 & 0 & k_2 \end{pmatrix} \tag{B-6}$$

Here, k_1 is the stiffness of the cross flexures in the four-bar-linkages, k_2 is the stiffness of the flexure in the coupling mechanism. The displacement vector $\boldsymbol{u}$ is

$$\boldsymbol{u} = \begin{pmatrix} \theta \\ \theta \\ \theta \\ \theta \\ \theta \end{pmatrix} \tag{B-7}$$

One note on the physical meaning of the parameters is that we use $r_{horFlex}$ as a length measure for the flexures. The actual length of the cross flexures is

$$L_{horFlex} = \sqrt{(2r_{horFlex}^2)}. \tag{B-8}$$

B-2 Time response plots of dynamical experiments

Here we present the time data that was obtained in dynamical experiments, in Figure B-1. A Fourier transform is applied on blocks of 1.5 seconds of this data to extract frequency response data.

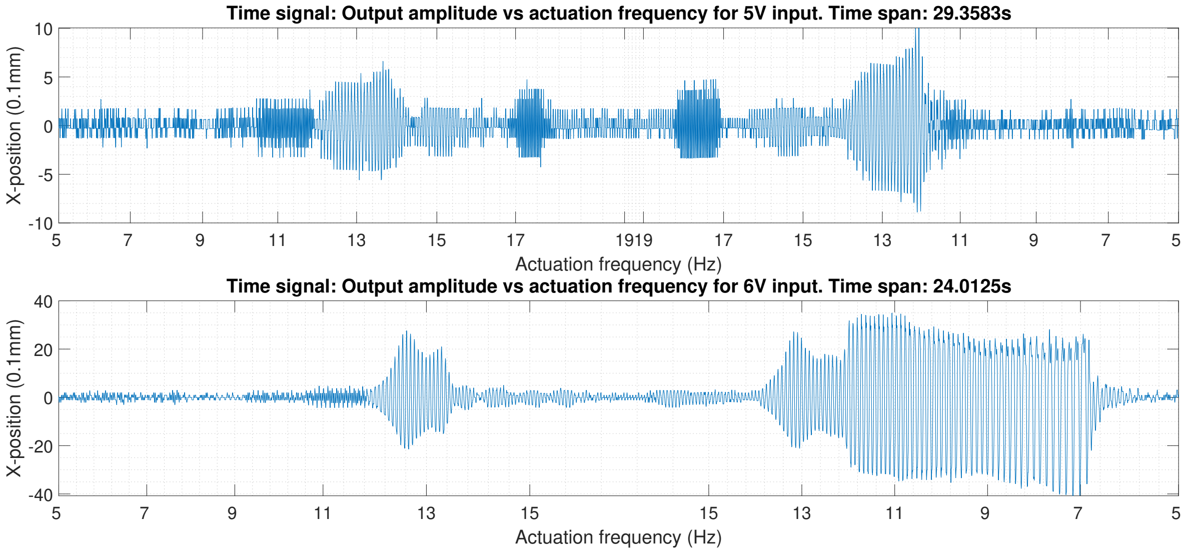

Figure B-1: This figure shows the time response data in a certain time range that was obtained with the experiment where the actuation frequency was swept up and down again. The X-position in time of one leg is plotted against the actuation frequency, in order to identify at which actuation frequencies the system resonates. During the up sweep we observed resonance between 12Hz and 13.5-14Hz for all experiments, that is also at the four other experiments which are not presented in this figure. For the down sweep at 5V input, resonance behavior is seen in the same frequency range. Conversely, during the down sweep for higher actuation voltages the system keeps resonating up until much lower actuation frequencies, i.e. 6.5Hz for the 6V graph shown in this figure. This hysteresis phenomenon is a typical property of dynamic softening and is probably a caused by the two motor parts that collide at resonance at input voltages of 6V or higher. This theory is strengthened by the observation that at a 5V input voltage, neither collision nor hysteresis occurs. Based on the data shown in this figure an amplification factor of respectively 6.5 and 12 can be determined for 5V and 6V actuation.

B-3 Choice of actuation

The motion of the four legs is obtained with one linear straight line solenoid. Additional motors, such as piezoelectric and shape memory alloy (SMA) actuators were considered for the FARbot. SMA actuators have a lower actuation bandwidth than solenoids, which would limit experiments at higher frequencies. DC motors at small scales tend to have very low power densities due to their use of rotating components which suffer from the effects of friction at this scale. The dual piezoelectric bimorph cantilever actuators described by R.J. Wood et al. [1] and used in [2, 3, 4], are the best alternative for solenoids as they are very small, light weight and they have great mass to power ratio. However, these actuators are not available to buy and hard to make, they are not robust and they need very high voltages. The latter property implies the need for either an external voltages amplifier or an internal self-made amplifier as in [5]. Moreover, a piezo bending actuator has a high internal stiffness and is therefore a displacement actuator, which has consequences on the resonance behavior.

B-4 Optimization

This appendix elaborates on the optimization algorithm we used: the Sequential Quadratic Programming method. As mentioned, the SQP method uses the Newton Rhapson method to solve the KKT conditions. The KKT conditions are defined as follows:

$$\begin{array}{lll} \min\limits_{\mathbf{x}} & f(\mathbf{x}) & \text{Lagrangian:} \\ \text{s.t.} & \mathbf{g}(\mathbf{x}) \leq \mathbf{0} & L = f(\mathbf{x}) + \boldsymbol{\mu}^T \mathbf{g}(\mathbf{x}) + \boldsymbol{\lambda}^T \mathbf{h}(\mathbf{x}) \\ & \mathbf{h}(\mathbf{x}) = \mathbf{0} & \end{array}$$

$$\begin{array}{ll} \Rightarrow & \boxed{\begin{array}{l} \dfrac{\partial L}{\partial \mathbf{x}} = \dfrac{\partial f}{\partial \mathbf{x}} + \sum \mu_i \dfrac{\partial g_i}{\partial \mathbf{x}} + \sum \lambda_i \dfrac{\partial h_i}{\partial \mathbf{x}} = \mathbf{0}^T \quad \text{(optimality)} \\ \mathbf{g} \leq \mathbf{0}, \quad \mathbf{h} = \mathbf{0} \quad \text{(feasibility)} \\ \boldsymbol{\lambda} \neq \mathbf{0}, \quad \boldsymbol{\mu} \geq \mathbf{0}, \quad \mu_i\, g_i = \mathbf{0} \quad \text{(complementarity)} \end{array}} \\ \text{and} & \end{array}$$

The SQP algorithm can be explained as follows: Firstly, an initial point must be chosen for which the Lagrangian multiplier is estimated. Then, a derivative matrix is set up, which is used in a Quadratic Programming subproblem. Next, this sub problem is solved, giving the step size for the variables $\Delta \boldsymbol{x}$ and the Lagrangian multipliers $\boldsymbol{\lambda_{k+1}}$. Subsequently, the step size is added to the previous point giving: $\boldsymbol{x_{n+1}} = \boldsymbol{x_n} + \boldsymbol{\Delta x}$. Finally, the convergence criteria are checked, being tolerance and maximum number of iteration. Depending on the criteria, the algorithm either continuous with the obtained point as new initial point, or it quits.

B-5 Phase dependency

We also carried out experiments to investigate the influence of the phase difference between the two actuators. To obtain a circular motion of the feet the vertical motion must have a phase difference of ±90 deg with respect to the horizontal motion. Therefore, in other experiments this phase difference was set to 90 deg. However, an inherent, dynamic property of a mass-damper-spring system like ours is that when it is excited at eigenfrequency the output of the system lags 90 deg with respect to its input. This would mean that the phase difference between the two actuators should be either 0 deg or 180 deg to obtain the desired circular output motion. Hence, we investigated influence of phase difference between the actuators on the output response of the system. Therefore, we carried out experiments at eigenfrequency, at constant power input, with a phase difference sweep of 0 deg - 360 deg - 0 deg. The most significant result of this sweep was the horizontal output amplitude dependency on the phase difference. However, to quantify this new experiments should be carried out to obtain more qualitative data about this dependency.

B-6 Primary 5DOF parametric model

The 1DOF parametric model is a simplification of a primary 5DOF version, shown in Figure B-2. With this model all five eigenmodes and eigenfrequencies can be obtained. The simplification from 5DOF to 1DOF introduces an error of about 5% and is based on three assumption. For FARbot it is not of great importance that the eigenfrequency is exactly what we defined, so this error is acceptable.

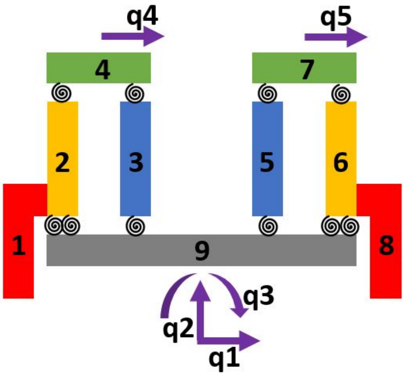

Figure B-2: An overview drawing of the 5DOF parametric model. Masses 2, 3, 5 and 6 are the identical links. Mass 4 and 7 are the motor parts and their mounts, they should be equal but are not necessarily the same in this model. Mass 1 and 8 are lumped representations of the legs and all other parts that move with the legs when they move horizontally. Mass 9 resembles the center body and all parts of the robot that do not move when the legs of the robot move horizontally. The generalized coordinates are indicated with purple arrows and exist of the 3 planar motions of the full body and the two translation DOF of the motor parts. The ten torsional springs represent the cross flexures.

Appendix C

MATLAB scripts

Here we present the two most important scripts that were written for this project. The ’`MainFile`’ calculates the eigenfrequency of FARbot, based on the set of parameters that are defined in ’`Parameters.m`’. These scripts are used by the optimization algorithm and the sensitivity analysis algorithm.

Function *MainFile* that calculates eigenfrequency

```matlab
% Parametric model of horizontal motion of  FARbot
% Johan Schonebaum
% 26-04-2019

function [EigenFreq] = MainFileFB(XS_new)
%% Obtaining all parameters
XS = XS_new;
save('XS.mat') % To be used in parameters
ParametersFB

%% Mapping kinematics
load("GeneralizedCoordinates.mat") % Load predefined generalized coordinates

theta = -asin(q(1)/(r_horFlex + L_horLink));

X1 = RotMat(CoM1_rel, theta) + CoR1;
X2 = RotMat(CoM2_rel, theta) + CoR1;
X3 = RotMat(CoM3_rel, theta) + CoR2;
X4 = [CoM4(1) + q(1); (CoM4(2) -  (r_horFlex + L_horLink)*(1-cos(theta)))];

X = [X1;theta;X2;theta;X3;theta;X4]  ;
Xd = simplify(jacobian(X,q) * dq) ;

U = ones(5,1)*theta;

%% Mass matrix
M1 = diag([m1 m1 I1 m2 m2 I2 m3 m3 I3 m4 m4]);
K1 = eye(5)*kr;
```

```

%% Kinetic and potential energy
T = 0.5 * Xd.'*M1 * Xd;
V = 0.5 * U.'*K1 * U;

%% Equations of motion
dT = jacobian(T, q).';
dV = jacobian(V, q).';
dTq = jacobian(T, dq);
ddT = jacobian(dTq, dq).'*ddq + jacobian(dTq, q).'*dq;

EoM = ddT - dT + dV;

%% Equilibrium %%
q_eq = zeros(length(q),1);
dq_eq = zeros(length(q),1);
ddq_eq = zeros(length(q),1);

%% Matrices %%
K_syms = jacobian(EoM, q);
M_syms = jacobian(EoM,ddq);

% Substitute
q=q_eq; dq=dq_eq; ddq = ddq_eq;
K = double(subs(K_syms));
M = double(subs(M_syms));

%% Eigenvectors & Eigenmodes
[¬, omega_sq] = eig(M\K);
omega_sq(omega_sq<1E-10) = 0;
EigenFreqs_rads = omega_sq.^(0.5)*ones(nDOF,1);
EigenFreq = EigenFreqs_rads/(2*pi);

end

function X_rotated = RotMat(X,a)
M = [cos(a), -sin(a); sin(a), cos(a)];
X_rotated = M*X;
end
```

Parameters script

```
% Parameters for parametric model of FARbot
% Johan Schonebaum
% 11-04-2019

%% Parameters from inputfile and optimization
load('XS.mat')

T_Flexures =   XS(1);
r_horFlex =    XS(2);
H_horFlex =    XS(3);
L_horLink =    XS(4);

V1 =           XS(30);     % Volume part 1
V2 =           XS(31);     % Volume part 2
```

```
V3 =           XS(32);     % Volume part 3
V4_p =         XS(33);     % Volume lumped part 4

I1 =         XS(34);    % Mass moment of inertia lumped part 1
I2 =         XS(35);    % Mass moment of inertia part 2
I3 =         XS(36);    % Mass moment of inertia part 3
I4_p =       XS(37);    % Mass moment of inertia part 4

%% Constants
rho = 1100;             % Density of HTM140V2
E = 3.35e9;             % Young's modulus HTM140V2
mass_stator = 1.32e-3;  % Mass of stator
% mass_pin = 0.22e-3;     % Mass of pin
I_stator = mass_stator * (10.9e-3^2 + 5e-3^2)/12;  % Approximation

CoR1 = [-15.64e-3;0]; % Center of rotation 1 wrt origin (most left)
CoR2 = [-5.21e-3; 0]; % Center of rotation 2 wrt origin

%% Part 1: lumped
m1 = V1 * rho;
CoM1 = [-18.64e-3 ; 1.45e-3]; % Center of mass wrt origin
CoM1_rel = CoM1-CoR1; % Position of mass relative to its rotation axis

%% Part 2: Link
m2 = V2 * rho;
CoM2 = [CoR1(1); 0.5 * (r_horFlex + L_horLink)];
CoM2_rel = CoM2-CoR1;  % Center of rotation of part 2 wrt origin

%% Part 3: Link
m3 = V3 * rho;
CoM3 = [CoR2(1);CoM2(2)];
CoM3_rel = CoM3-CoR2;

%% Part 4: Motor attachment
m4 = V4_p * rho + mass_stator;
I4 = I4_p + I_stator;
CoM4 = [0.25*CoR1(1) + 0.75*CoR2(1);...
        (1.5 * r_horFlex + L_horLink - 3e-3)];

%% Stiffnessess
K_theta = 5.300185 - 1.6866 + 0.885356 - 0.2094 + 0.018385; % Stiffness ...
    coefficient, eq. (16) of Jensen an Howell
I_horFlex =  T_Flexures^3 * H_horFlex / 12; % Area moment of Inertia of ...
    flexures
L_horFlex = sqrt(2*r_horFlex^2);

kr = K_theta * E * I_horFlex/ (2*L_horFlex); % Rotational stiffness of ...
    cross flexures
```

Appendix D

Kinematic designs considered for step two

In the method section of the technical paper, we chose a kinematic model for the horizontal motion mechanism in step 2 of the five step methodology. This was one of the 3 concepts that were derived. In this appendix we present the other 2 designs, that would fulfill the same kinematic requirement with solenoid actuation.

The first concept is similar to the chosen concept, however it exists of two four-bar-linkages per leg pair, see Figure D-1. The other design is slightly more complex, but it has an advantage in terms of alignment of the motor, because the stator part of the motor is fixed to the frame of the robot, see Figure D-2. For both designs, the feet move on a curve with a radius, which is biggest for the first design, which therefore moves most parallel to the sagittal plane.

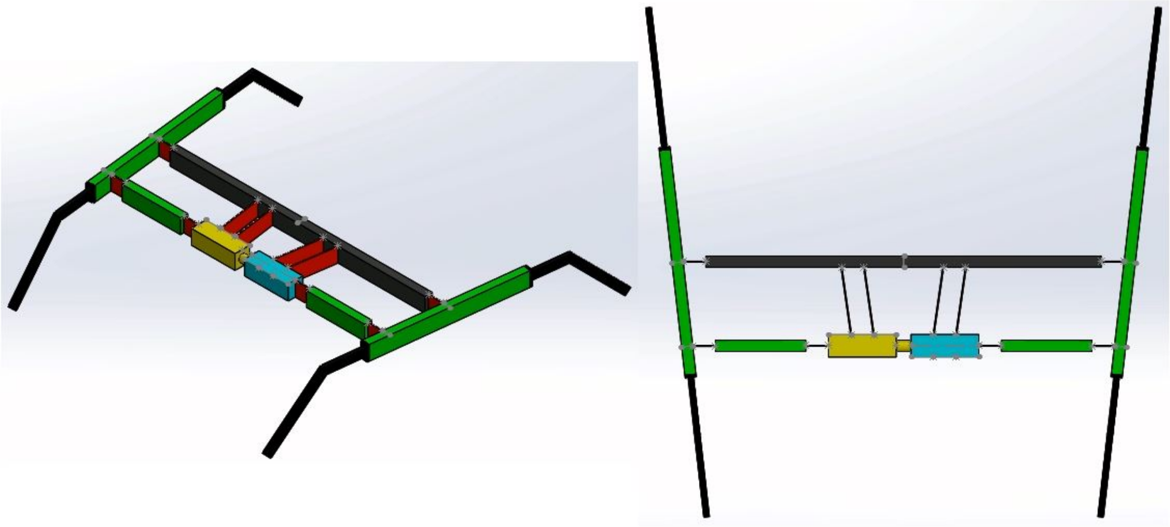

Figure D-1: This figure presents the second concept that was considered as kinematic design for FARbot. However, as it contains two four-bar-linkages per leg pair it is more complex than the chosen model, which has only one.

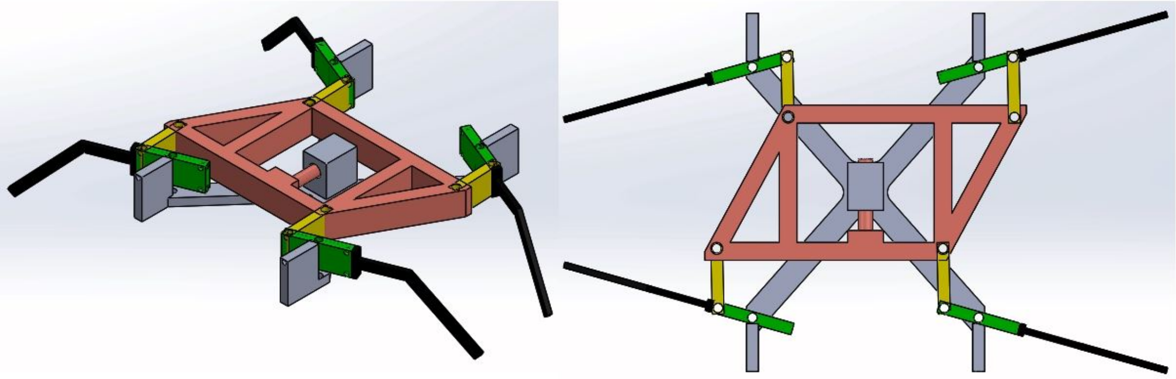

Figure D-2: This figure presents the third concept that was considered as kinematic design for FARbot. This model is slightly more complex than the chosen design, but it has the advantage the stator part of the motor is fixed to the frame of the robot. This could have been an advantage in terms of alignment as compared to the chosen model. However, it exists of much more parts than the chosen concept and was therefore not selected. Also, the alignment of the motor parts proved not to cause problems either.

Appendix E

Experiments with monolithic printing

During manufacturing of the older prototype it was observed that HTM140V2 shows promising compliant behavior for certain dimensions. This gave rise to conduct experiments with monolithically printed flexures, in order to find out if it would be feasible to manufacture FARbot monolithically. Several flexure types and mechanism parts were produced and tested for their compliant functionality, their tolerances and their robustness. With the right settings and manufacturing preparations the monolithic parts were easily produced and reproduced in little time.

The experiments show all desired compliant functionality, with great ranges of motion, see Figure E-1. Rotation angles of over 45deg are obtained in the compliant hinges, which is far more than the maximum necessary 15 deg angle in the FARbot.

Also, the tolerances mostly match the resolution of the printer, which is 25 to 30 μm for the EnvisonTEC printer that we used. This is much better than the tolerance obtained in the older prototype. The flexure thickness however, shows an approximately constant bias between the designed and the measured value. 27 flexures, with a design thickness between 0.25 and $0.35mm$ were measured, and they show an average bias of $0.12mm$ with a maximum of $0.15mm$. It should be noted however that the measurements are carried with a normal caliper with 0.05mm resolution. For more qualitative results of this measurement, equipment with higher resolution should be used.

In terms of robustness, the monolithic flexures perform well up until a minimum designed thickness of $0.30mm$, which corresponds to a measured thickness of $0.18mm$. Mechanisms that include flexure with that thickness or greater, could be dropped from a meter high without any damage. At lower thicknesses, however, the robustness of the flexures decreases rapidly. Little impact or loads already causes breaking of these thin flexures.

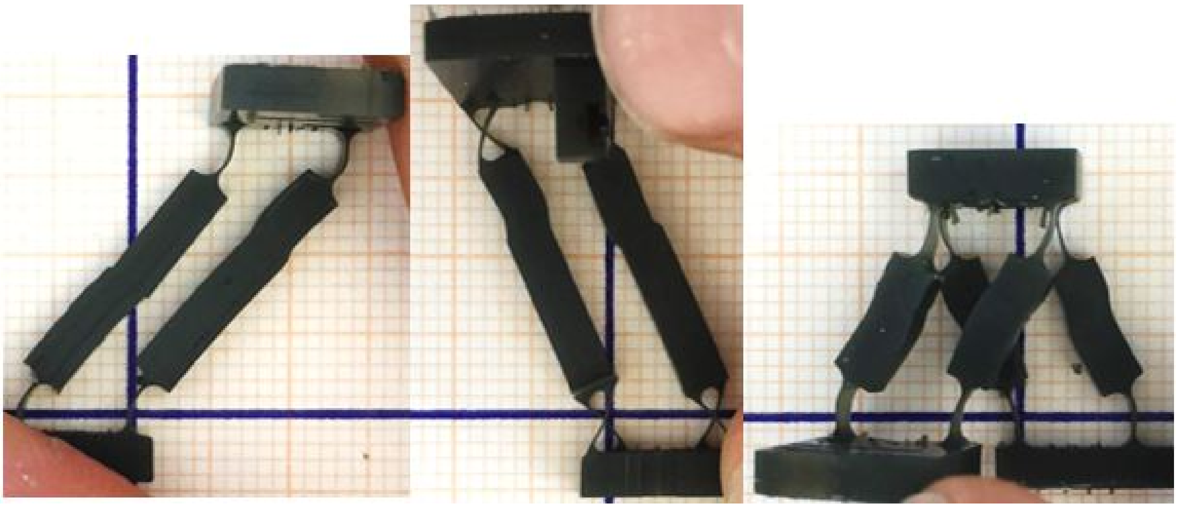

Figure E-1: This figure shows three of the monolithic experiments that were carried out.

Bibliography

[1] R. Wood, E. Steltz, and R. Fearing, “Optimal energy density piezoelectric bending actuators,” *Sensors and Actuators A: Physical*, vol. 119, no. 2, pp. 476–488, 2005.

[2] K. L. Hoffman and R. J. Wood, “Myriapod-like ambulation of a segmented microrobot,” *Autonomous Robots*, vol. 31, no. 1, pp. 103–114, 2011.

[3] R. J. Wood, S. Avadhanula, R. Sahai, E. Steltz, and R. S. Fearing, “Microrobot design using fiber reinforced composites,” *Journal of Mechanical Design*, vol. 130, no. 5, p. 052304, 2008.

[4] A. T. Baisch, O. Ozcan, B. Goldberg, D. Ithier, and R. J. Wood, “High speed locomotion for a quadrupedal microrobot,” *International Journal of Robotics Research*, vol. 33, no. 8, pp. 1063–1082, 2014.

[5] A. T. Baisch, C. Heimlich, M. Karpelson, and R. J. Wood, “Hamr3: An autonomous 1.7 g ambulatory robot,” in *Intelligent Robots and Systems (IROS), 2011 IEEE/RSJ International Conference on*, pp. 5073–5079, IEEE, 2011.